VOLUME 35 | SUPPLEMENT 2 | MARCH 2022

MODERN PATHOLOGY

ABSTRACTS (292–340)

DERMATOPATHOLOGY

2022

USCAP 111TH ANNUAL MEETING

REAL INTELLIGENCE

MARCH 19–24, 2022 LOS ANGELES, CALIFORNIA

Published by
SPRINGER NATURE
www.ModernPathology.org

USCAP Creating a Better Pathologist
AN OFFICIAL JOURNAL OF THE UNITED STATES AND CANADIAN ACADEMY OF PATHOLOGY

EDUCATION COMMITTEE

Rhonda K. Yantiss
Chair

Kristin C. Jensen
Chair, CME Subcommittee

Laura C. Collins
Chair, Interactive Microscopy Subcommittee

Yuri Fedoriw
Short Course Coordinator

Ilan Weinreb
Chair, Subcommittee for Unique Live Course Offerings

Carla L. Ellis
Chair, DEI Subcommittee

Adebowale J. Adeniran
Kimberly H. Allison
Sarah M. Dry
William C. Faquin
Karen J. Fritchie
Jennifer B. Gordetsky
Levon Katsakhyan, Pathologist-in-Training
Melinda J. Lerwill
M. Beatriz S. Lopes
Julia R. Naso, Pathologist-in-Training
Liron Pantanowitz
Carlos Parra-Herran
Rajiv M. Patel
Charles "Matt" Quick
David F. Schaeffer
Lynette M. Sholl
Olga K. Weinberg
Maria Westerhoff

ABSTRACT REVIEW BOARD

Benjamin Adam
Oyedele Adeyi
Mariam Priya Alexander
Daniela Allende
Catalina Amador
Vijayalakshmi Ananthanarayanan
Tatjana Antic
Manju Aron
Roberto Barrios
Gregory R. Bean
Govind Bhagat
Luis Zabala Blanco
Michael Bonert
Alain C. Borczuk
Tamar C. Brandler
Eric Jason Burks
Kelly J. Butnor
Sarah M. Calkins
Weibiao Cao
Wenqing (Wendy) Cao
Barbara Ann Centeno
Joanna SY Chan
Kung-Chao Chang
Hao Chen
Wei Chen
Yunn-Yi Chen
Sarah Chiang
Soo-Jin Cho
Shefali Chopra
Nicole A. Cipriani
Cecilia Clement
Claudiu Cotta
Jennifer A. Cotter
Sonika M. Dahiya
Elizabeth G. Demicco
Katie Dennis
Jasreman Dhillon
Anand S. Dighe
Bojana Djordjevic
Michelle R. Downes
Charles G. Eberhart
Andrew G. Evans
Fang Fan
Julie C. Fanburg-Smith
Gelareh Farshid
Michael Feely
Susan A. Fineberg
Dennis J. Firchau
Gregory A. Fishbein
Agnes B. Fogo
Andrew L. Folpe
Danielle Fortuna
Billie Fyfe-Kirschner
Zeina Ghorab
Giovanna A. Giannico
Anthony J. Gill
Tamar A. Giorgadze
Alessio Giubellino
Carolyn Glass
Carmen R. Gomez-Fernandez
Shunyou Gong
Purva Gopal
Abha Goyal
Christopher C. Griffith
Ian S. Hagemann
Gillian Leigh Hale
Suntrea TG Hammer
Malini Harigopal
Kammi J. Henriksen
Jonas J. Heymann
Carlo Vincent Hojilla
Aaron R. Huber
Jabed Iqbal
Shilpa Jain
Vickie Y. Jo
Ivy John
Dan Jones
Ridas Juskevicius
Meghan E. Kapp
Nora Katabi
Francesca Khani
Joseph D. Khoury
Benjamin Kipp
Veronica E. Klepeis
Christian A. Kunder
Stefano La Rosa
Stephen M. Lagana
Keith K. Lai
Goo Lee
Michael Lee
Vasiliki Leventaki
Madelyn Lew
Faqian Li
Ying Li
Chieh-Yu Lin
Mikhail Lisovsky
Lesley C. Lomo
Fang-I Lu
aDeqin Ma
Varsha Manucha
Rachel Angelica Mariani
Brock Aaron Martin
David S. McClintock
Anne M. Mills
Richard N. Mitchell
Hiroshi Miyamoto
Kristen E. Muller
Priya Nagarajan
Navneet Narula
Michiya Nishino
Maura O'Neil
Scott Roland Owens
Burcin Pehlivanoglu
Deniz Peker Barclift
Avani Anil Pendse
Andre Pinto
Susan Prendeville
Carlos N. Prieto Granada
Peter Pytel
Stephen S. Raab
Emilian V. Racila
Stanley J. Radio
Santiago Ramon Y Cajal
Kaaren K Reichard
Jordan P. Reynolds
Lisa M. Rooper
Andrew Eric Rosenberg
Ozlen Saglam
Ankur R. Sangoi
Kurt B. Schaberg
Qiuying (Judy) Shi
Wonwoo Shon
Pratibha S. Shukla
Gabriel Sica
Alexa Siddon
Anthony Sisk
Kalliopi P. Siziopikou
Stephanie Lynn Skala
Maxwell L. Smith
Isaac H. Solomon
Wei Song
Simona Stolnicu
Adrian Suarez
Paul E. Swanson
Benjamin Jack Swanson
Sara Szabo
Gary H. Tozbikian
Gulisa Turashvili
Andrew T. Turk
Efsevia Vakiani
Paul VanderLaan
Hanlin L. Wang
Stephen C. Ward
Kevin M. Waters
Jaclyn C. Watkins
Shi Wei
Hannah Y. Wen
Kwun Wah Wen
Kristy Wolniak
Deyin Xing
Ya Xu
Shaofeng N. Yan
Zhaohai Yang
Yunshin Albert Yeh
Huina Zhang
Xuchen Zhang
Bihong Zhao
Lei Zhao

To cite abstracts in this publication, please use the following format: **Author A, Author B, Author C, et al. Abstract title (abs#). In "File Title."** ***Modern Pathology*** **2022; 35 (suppl 2): page#**

292 The DNA Cytosine Deaminase APOBEC3B (A3B) is Overexpressed and Enzymatically Active in Malignant Melanomas of the Skin

Prokopios Argyris[1], Jordan Naumann[1], Kyu Young Song[1], Ioannis Koutlas[2], Alessio Giubellino[1], Reuben S Harris[1]
[1]University of Minnesota, Minneapolis, MN, [2]Malcolm Moos Health Science Tower, Minneapolis, MN

Disclosures: Prokopios Argyris: None; Jordan Naumann: None; Kyu Young Song: None; Ioannis Koutlas: None; Alessio Giubellino: None; Reuben S Harris: None

Background: The DNA cytosine deaminase A3B represents a major endogenous source of mutation in human cancer promoting tumor evolution, drug resistance and, thus, poor clinical outcomes. A3B causes C-to-T/-G base substitutions in 5'-TCA/T trinucleotide motifs. Cutaneous melanomas (CM) are characterized by increased genomic instability and mutational burden. APOBEC3-specific mutational signatures SBS2 and SBS13 are identified in acral melanomas and CM of adolescents and young adults. Notwithstanding *A3B* mRNA upregulation in CM, only a low fraction (1%) of mutational signatures detected is attributable to APOBEC3. However, UVR-induced dipyrimidine-focused C-to-T mutations could eclipse an A3B deamination signature. The role of A3B in CM development and progression is poorly understood.

Design: Immunohistochemistry approaches using our newly developed rabbit α-human A3B monoclonal antibody (5210-87-13) were implemented to assess A3B protein levels in FFPE CM (n=24) and benign nevi (n=8). A3B nuclear immunostaining was visualized and quantified using the Aperio ScanScope XT platform. Endogenous levels of A3A/B/G proteins were probed in CM cell lines (n=18) by western-blotting, while A3B deamination activity on single-stranded DNA was also assessed.

Results: Endogenous expression of A3B was detected in 15 of 18 (83%) CM cell lines. Interestingly, 10 of 18 (56%) cell lines also expressed A3G, whereas A3A expression was not observed in any cell line studied. All A3B-expressing CM cell lines exhibited prominent deaminase activity and successfully cleaved single-stranded DNA. By immunohistochemistry, CM showed marked inter- and intratumoral heterogeneity regarding A3B staining with most tumors exhibiting moderate-to-strong and diffuse, nuclear only, immunopositivity. Notably, a portion of CM demonstrating, overall, low A3B protein levels showed marked cytoplasmic immunoreactivity, consistent with A3G. In contrast, skin melanocytic nevi showed low or absent A3B nuclear positivity.

Conclusions: Herein, cell line and immunohistochemical studies combine to suggest overexpression of endogenous A3B levels in CM. Furthermore, A3B is enzymatically active. A3B-driven prolonged mutagenesis may contribute to the heightened number of genomic abnormalities and targeted therapy resistance in skin melanoma.

293 Whole Transcriptomic Analysis Reveals Unique Signatures in CD8+ Mycosis Fungoides and Type D Lymphomatoid Papulosis

Kimon Argyropoulos[1], Kelsey Zhu[2], Theodore Vougiouklakis[3], Randie Kim[3], Konstantinos Linos[4], Maria Angelica Selim[5], Rami Al-Rohil[6], Jennifer Crimmins[7], George Jour[8]
[1]Memorial Sloan Kettering Cancer Center, New York, NY, [2]NYU Langone Medical Center, New York, NY, [3]New York University School of Medicine, New York, NY, [4]Dartmouth-Hitchcock Medical Center, Lebanon, NH, [5]Duke University, Durham, NC, [6]Duke University School of Medicine, Durham, NC, [7]Virginia Commonwealth School of Medicine, Richmond, VA, [8]New York University, New York, NY

Disclosures: Kimon Argyropoulos: None; Kelsey Zhu: None; Theodore Vougiouklakis: None; Randie Kim: None; Konstantinos Linos: None; Maria Angelica Selim: None; Rami Al-Rohil: *Consultant*, Frontier Diagnostics; *Employee*, Foundation Medicine Inc.; Jennifer Crimmins: None; George Jour: None

Background: There is paucity of transcriptomic data concerning primary cutaneous CD8+ lymphoproliferative disorders. Herein we aim to investigate the transcriptomic profile of CD8+ mycosis fungoides (CD8+ MF) and type D lymphomatoid papulosis (Type D LyP), in order to better characterize them at and assess whether the two entities are biologically related.

Design: Adequate RNA was successfully extracted from formalin-fixed paraffin embedded sections derived from 7 CD4+ MF, 8 CD8+ MF and 4 type D LyP. After passing quality control, whole transcriptome sequencing (WTS) was performed. Fusion detection was performed using star-fusion (version 1.10.0). Accurate transcript quantification from RNASEQ data was performed using RSEM (version 1.3.1). DESEQ2 was used for differential gene expression (DGE) analysis, comparing CD8+ MF vs CD4+MF, CD8+ MF vs type D LyP groups, after normalization against normal skin controls.

Results: Unsupervised clustering classified CD4+ MF and CD8+ MF into two distinct groups and identified 100 genes that were differentially expressed at a significant level between both entities (Figure 1 a). CD8+ MF shows a profound down regulation of skin-homing chemokine receptors, immune signaling-related molecules or transcription factors and upregulation of long non-coding RNAs (lncRNAs) and small nuclear RNAs (snRNAs) (Figure 1a). KEGG pathway analysis showed an upregulation of pathways related to linoleic acid metabolism, as well as retinoid acid, *PPAR* and adipocytokine signaling in CD8+ MF (Figure 1b). Unsupervised clustering did not segregate CD8+ MF and Type D LyP. Nevertheless, DGE analysis identified 546 genes that were differentially expressed between both (FDR<0.01, fold change: > 1 or < -1, Figure 1c). KEGG pathway analysis showed that Wnt signaling is significantly upregulated in CD8+ MF compared to Type D LyP. A recurrent mRNA-lncRNA fusion secondary to interstitial deletion involving *RP11-367G6.3-FAM65B (*Figure 1d*)* was identified in 5 cases from 4 unique patients, including 2 type D LyP and 2 CD8+ MF patients.

Figure 1 - 293

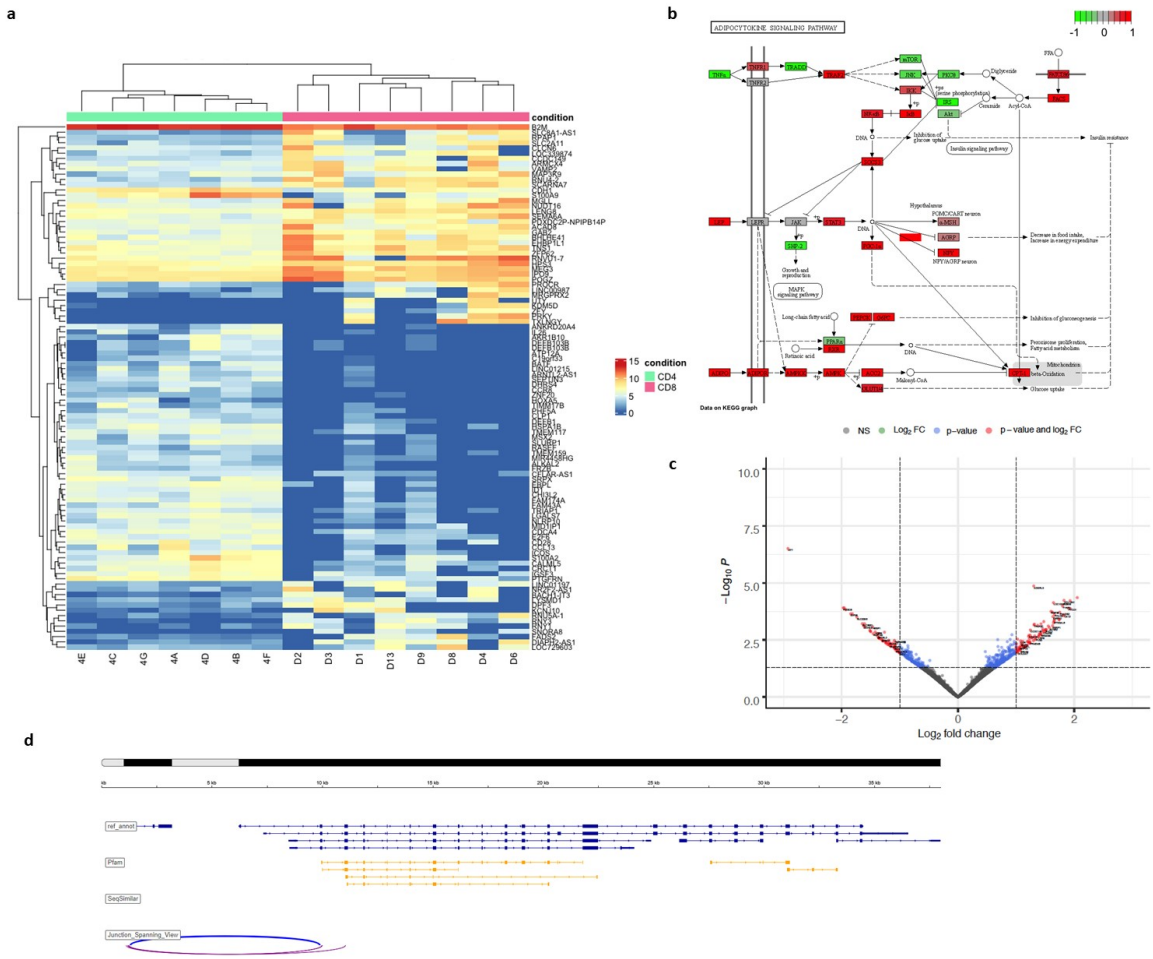

Figure legend

Figure 1.(a) Heatmap showing unsupervised clustering analysis between CD4+ and CD8+ MF specimen. **(b)** KEGG pathway displaying Adipocytokine signaling elements that are differentially expressed in CD4+ MF vs CD8+ MF. **(c)** Volcano plot displaying genes that are upregulated and downregulated in CD8+ MF vs type D LyP. With red are genes that show significant differential expression (p<0.005) with a fold change above or below. **(d)** Schematic of the interstitial deletion involving *RP11-367G6.3-FAM65B* on chromosome 6.

Conclusions: WTS shows that CD8+ MF has unique signatures compared to CD4+MF pertaining to lncRNAs and snRNAs. Type D LyP and CD8+ MF display similar genomic rearrangements, yet pathway analysis highlights different genes contributing to their pathogenesis.

294 Multi-omics Analysis of Digital Papillary Adenocarcinoma Reveals Upregulation of MAGEA4 and Infrequent Zinc Finger Genes Rearrangements

Phyu Aung[1], Pavandeep Gill[2], Zongshan Lai[1], Kelsey Zhu[3], Varshini Vasudevaraja[4], Doina Ivan[1], Priya Nagarajan[1], Woo Cheal Cho[1], Leomar Ballester[1], Jonathan Curry[1], Carlos Torres-Cabala[1], Victor Prieto[1], George Jour[5]
[1]The University of Texas MD Anderson Cancer Center, Houston, TX, [2]Royal Jubilee Hospital, Victoria, Canada, [3]NYU Langone Medical Center, New York, NY, [4]New York University Medical Center, New York, NY, [5]New York University, New York, NY

Disclosures: Phyu Aung: None; Pavandeep Gill: None; Zongshan Lai: None; Kelsey Zhu: None; Varshini Vasudevaraja: None; Doina Ivan: None; Priya Nagarajan: None; Woo Cheal Cho: None; Leomar Ballester: None; Jonathan Curry: None; Carlos Torres-Cabala: None; Victor Prieto: *Consultant*, Novartis, Orlucent; George Jour: None

Background: Digital papillary adenocarcinoma (DPAC) is a rare but aggressive cutaneous malignant sweat gland neoplasm that occurs on acral sites and mimics other benign entities leading to diagnostic dilemmas. We investigate genomic and transcriptomic signatures unique to DPAC that would help differentiate it from other benign entities and aim to unveil unique transcriptomic signatures inherent to its biology.

Design: 9 DPAC and 10 hidradenoma (HD) cases were selected (Table 1). DNA analysis used targeted 607 gene FDA validated panel (clinically validated). Customized RNA panel targeting 104 genes (FusionSeeqer) was used for fusion analysis. All pipelines used are clinically validated. Transcriptomic analysis used nCounter *Pan Cancer IO* 360™ panel (770 genes) with subsequent analysis using our own pipelines n R studio. Accurate transcript quantification (lg2FC) was performed after normalization to standard housekeeping genes. DESEQ2 was used for the gene level differential gene expression (DGE) analysis after normalization to reference group benign HDs (FDR<0.01, fold change: > 2 or < -2) with subsequent KEGG pathway analysis.

Results: DPAC cases showed very low tumor mutational burden on genomic analysis (range 0-1 mut/mb). Gene rearrangements were more frequent in HD compared to DPAC (4/4 vs 2/7, p= 0.03). Mastermind-like family of protein genes (*MAML2*) rearrangements were more frequent in HD, while DPAC showed novel zinc finger gene (*PLAG1*) rearrangements (*TRPS1-PLAG1;* n=1) (Fig 1A). Unsupervised clustering analysis and subsequent DGE analysis revealed 100 significantly differentially expressed genes between DPAC and HD. *MAGEA4, IL2, IFNG, and COL11A2* showed a significant upregulation in DPAC (lg2FC =2.6, 2.93, 2.98, 3.04, FDR range = 0.0001 to 0.00004) respectively (Fig 1B). Pathway analysis identified enrichment of JAK/STAT pathway, which is triggered by the upregulated cytokines in DPAC (Fig 1C).

Table 1: Patient demographic and clinicopathological characteristics for digital papillary adenocarcinoma (DPA) and hidradenoma (HD)

Parameters		DPAC (n=9)	HD (n=10)
Mean age, years (SD)		47.1 (11.3)	58.6 (14.9)
Sex, n (%)	Female	4 (44.4)	5 (50.0)
	Male	5 (55.6)	5 (50.0)
Race, n (%)	White	8 (88.9)	9 (90.0)
	Black	0 (0)	1 (10.0)
	Unknown	1 (11.1)	0 (0)
Anatomic site, n (%)	Hand	6	1
	Foot	3	0
	Face/scalp	0	4
	Trunk	0	2
	Back	0	1
	Upper extremity	0	1
	Lower extremity	0	1
Perineural invasion, n (%)	Absent	9 (100.0)	10 (100.0)
	Present	0 (0)	0 (0)
Lymphovascular invasion, n (%)	Absent	7 (77.8)	10 100.0)
	Present	2 (22.2)	0 (0)
Any Metastasis, n (%)	Absent	7 (77.8)	10 (100.0)
	Present	2 (22.2)	0 (0)
Regional metastasis, n (%)	Absent	8 (88.9)	10 (100.0)
	Present	1 (11.1)	0 (0)
Distant metastasis, n (%)	Absent	7 (77.8)	10 (100.0)
	Present	2 (22.2)	0 (0)
Outcome, n (%)	Dead	1 (11.1)	0 (0)
	Alive	8 (88.9)	10 (100.0)

Figure 1 - 294

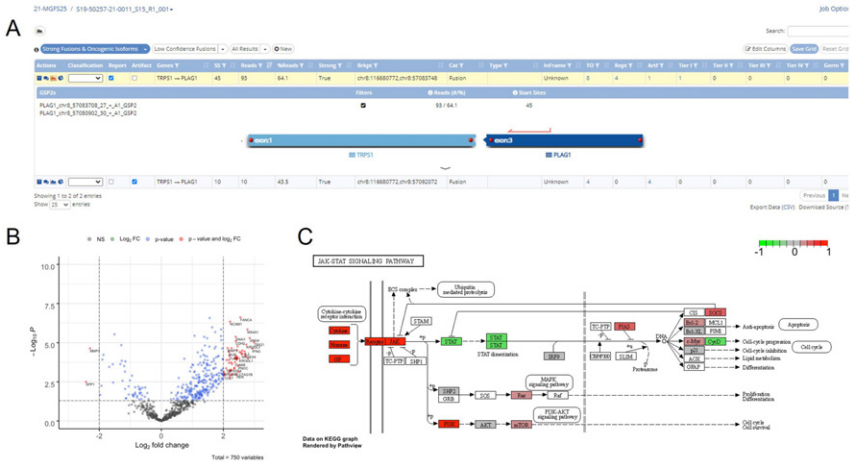

Figure 1: A. Fusion analysis showing novel zinc finger gene (*PLAG1*) rearrangements more frequent in DPAC. **B.** Summary of differential gene expression (DGE): Enhanced volcano (DPAC vs. Hidradenoma) showing a group of genes overexpressed in DPAC with a significant log2FC and *p* value. **C.** Pathway analysis shows an enrichment of JAK/STAT pathway in DPAC, triggered by *MAGEA4* and *IFNG* Overexpression.

Conclusions: While morphologically overlapping, DPAC and HD are biologically distinct. *MAGEA4* upregulation seen in DPAC could serve as potential marker for both diagnostic and therapeutic purposes, since it could be potentially targeted with adoptive T-cell therapy (ADP-A2M4). Validation of the findings on a larger cohort is underway.

295 Institutional Retrospective Review of Correlative Immunohistochemical and Molecular Mismatch Repair Staining Pattern of Sebaceous Tumors over a 10-year Period

Monica Bronte[1], Javier Arredondo Montero[1], Alba Larrea[1], Clara Cerezo[2], Yessica Rodriguez[1], Rosa Guarch[1], Marta Montes[1], Yerani Ruiz de Azúa, Gregorio Aisa[1], Alicia Córdoba[1]
[1]Complejo Hospitalario de Navarra, Pamplona, Spain, [2]Valencia, Sweden

Disclosures: Monica Bronte: None; Javier Arredondo Montero: None; Alba Larrea: None; Clara Cerezo: None; Yessica Rodriguez: None; Rosa Guarch: None; Marta Montes: None; Yerani Ruiz de Azúa: None; Gregorio Aisa: None; Alicia Córdoba: None

Background: Sebaceous skin tumors (SST) comprise into sebaceoma, sebaceous adeoma and sebaceous carcinoma. Immunohistochemistry of mismatch repair (MMR) proteins and genetic microsatellite instability testing should be performed on sebaceous neoplasms to diagnose Muir-Torre Syndrome (MTS), a variant of Lynch syndrome that combines SST and visceral malignancies. Studies have been published in the scientific literature, but on small series of patients. To the authors' knowledge, this is one of the largest series of sebaceous skin tumors in the European population.

Design: We performed a retrospective search of SST diagnosed in our institution over the last 10 years. We included only those sebaceous lesions with histological and immunohistochemical confirmation. Tumors were tested for MSH2, MSH6, MLH1, and PMS2 deficiency. We excluded hamartomatous lesions (nevus sebaceous) and lesions with an inconclusive diagnosis of sebaceous tumor.

Results: IHC stains confirmed 110 tumors (26 sebaceomas, 35 adenomas, 41 carcinomas, 8 other) in 100 patients (M:F 1.5:1). Of these, 4 patients presented more than 1 tumor at diagnosis. 8 tumors were recurring lesions in already studied patients. The average age at presentation was 74.63 ± 2.08 for all groups. Both sebaceomas and sebaceous adenomas were mostly located on the forehead and nose. The most frequent location for the carcinoma group was the eyelid. Stains for MMR proteins identified 27 patients (27%) with MMR abnormal staining pattern. The abnormal MMR staining patterns included concurrent loss of MSH2/MSH6 (15, 55.56 %), concurrent loss of MLH1/PMS2 (4, 14.81 %), and isolated loss of MSH6 (8, 29.63 %). Although other neoplasms were observed in 10 patients, only 5 had (4 adenomas, 1 carcinoma) an altered molecular study with microsatellite instability confirming MTS. One patient had clinical criteria of Lynch Syndrome, but no molecular alteration of APC and MUYTH.

Conclusions: In our series, one of the largest reported to date, 76% of SST retained expression of MMR proteins. 27% showed an absence of expression; concurrent loss of HSMH2 and HMSH6 being more frequent; 6 % associated a molecular loss of MMR genes, especially in relation to sebaceous adenomas. In patients with normal MMR protein expression on immunohistochemistry and molecularly stable, it would be interesting to consider: somatic mutations of MMR genes, and mutations in APC, MUTYH. For these reasons, MMR proteins testing should be performed on sebaceous neoplasms to exclude a diagnosis of MTS.

296 TRPS1 Expression is Frequently Seen in Mammary and Extramammary Paget Diseases, Except for Those Arising in the Perianal Skin

Woo Cheal Cho[1], Qingqing Ding[1], Wei-Lien (Billy) Wang[1], Priya Nagarajan[1], Jonathan Curry[1], Carlos Torres-Cabala[1], Doina Ivan[1], Constance Albarracin[1], Aysegul Sahin[1], Victor Prieto[1], Phyu Aung[1]
[1]The University of Texas MD Anderson Cancer Center, Houston, TX

Disclosures: Woo Cheal Cho: None; Qingqing Ding: None; Wei-Lien (Billy) Wang: None; Priya Nagarajan: None; Jonathan Curry: None; Carlos Torres-Cabala: None; Doina Ivan: None; Constance Albarracin: None; Aysegul Sahin: None; Victor Prieto: *Consultant*, Novartis; *Consultant*, Orlucent; Phyu Aung: None

Background: Trichorhinophalangeal syndrome type 1 (TRPS1) is a recently described immunohistochemical marker highly sensitive and specific for breast carcinomas, including those with triple-negative immunophenotype. Given the strong association with an underlying breast carcinoma in mammary Paget diseases (MPDs), TRPS1 expression in MPDs is anticipated. However, the status of TRPS1 expression by immunohistochemistry (IHC) in extramammary Paget diseases (EMPDs) is currently unknown. Herein, we evaluate the utility of TRPS1 as a potential discriminatory marker in distinguishing MPDs and EMPDs from their close histologic mimics in the skin.

Design: Immunohistochemical studies were performed with a rabbit polyclonal antibody against TRPS1 (Invitrogen/ThermoFischer, Waltham, MA) on selected cases of MPDs (n=16), EMPDs (n=15), squamous cell carcinoma in situ (SCCIS) with pagetoid pattern of growth (n=8), melanoma in situ (MIS) (n=7), and intraepidermal sebaceous carcinoma (SC) with pagetoid pattern of growth (n=1). The frequency, pattern, intensity, and proportion of TRPS1 expression were recorded.

Results: All MPDs were from the nipple and associated with underlying breast carcinomas (8 invasive ductal carcinoma and 8 ductal carcinoma in situ). EMPDs were found in inguinal/groin (8), perianal (6), and axillary (1) regions. All cases of SCCIS, MIS, and intraepidermal SC were from the sun-exposed skin. In our cohort (Table 1), the expression pattern of TRPS1 (Figure 1) was consistently nuclear when present. All cases of MPD strongly and diffusely expressed TRPS1, while a subset of EMPDs (6/15, 40%) lacked TRPS1 expression. Intriguingly, those EMPDs (6/6, 100%) lacking TRPS1 expression were consistently of perianal origin. All SCCISs (8/8, 100%) and intraepidermal SC (1/1, 100%) strongly and diffusely expressed TRPS1, while all MISs were devoid of TRPS1 expression.

Table 1. TRPS1 expression frequency, pattern, intensity, and proportion in selected cases of MPDs, EMPDs and other close histologic mimics

	MPD (n=16)	EMPD (n=15)	SCCIS (n=8)	MIS (n=7)	Intraepidermal SC (n=1)	Total (n=47)
TRPS1 Expression Frequency	16 (100%)	9 (60%)*	8 (100%)	0 (0%)	1 (100%)	34 (72%)
TRPS1 Expression Pattern	Nuclear (16/16, 100%)	Nuclear (9/9, 100%)	Nuclear (8/8, 100%)	N/A	Nuclear (1/1, 100%)	N/A
TRPS1 Expression Intensity and Proportion**	Strong, diffuse (16/16, 100%)	Strong, diffuse (5/9, 56%) Moderate, diffuse (3/9, 33%) Weak, patchy (1/9, 11%)	Strong, diffuse (8/8, 100%)	N/A	Strong, diffuse (1/1, 100%)	N/A

* Of 15 cases of EMPD studied, all those lacking TRPS1 expression were of perianal origin.
** Sebocytes, outer root sheath of fair follicle, inner luminal cells of eccrine glands, and matrical cells of hair follicles were used as internal controls. The proportion of TRPS1 expression was defined as: absent (<1%), focal (1-25%), patchy (26-75%), and diffuse (>75%)

Abbreviations: TRPS1, trichorhinophalangeal syndrome type 1; MPD, mammary Paget disease; EMPD, extramammary Paget disease; SCCIS, squamous cell carcinoma in situ; MIS, melanoma in situ; SC, sebaceous carcinoma; N/A, not applicable

Figure 1 - 296

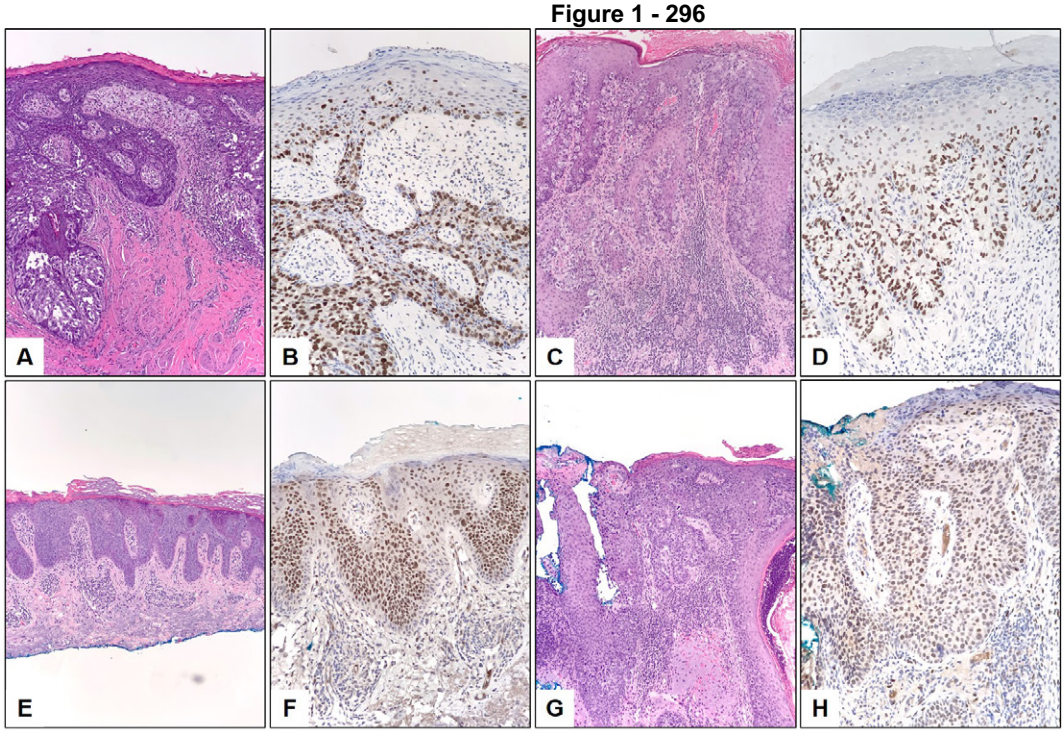

Figure 1. Representative cases of mammary (A: H&E, 10x; B: TRPS1, 20x) and extramammary Paget (C: H&E, 10x; D: TRPS1, 20x) diseases, squamous cell carcinoma in situ with pagetoid pattern of growth (E: H&E, 10x; F: TRPS1, 20x), and intraepidermal sebaceous carcinoma (G: H&E, 10x; H: TRPS1, 20x) showing diffuse and strong expression of TRPS1.

Abbreviation: H&E, hematoxylin and eosin; TRPS1, trichorhinophalangeal syndrome type 1

Conclusions: To our knowledge, this is the first study to demonstrate TRPS1 expression in MPDs, EMPDs, and their close histologic mimics, including SCCISs with pagetoid pattern of growth. Our results indicate TRPS1 is helpful to distinguish MPDs/EMPDs from MISs; however, additional IHC markers besides TRPS1 are still needed to differentiate those from SCCISs or intraepidermal SCs. Moreover, lack of TRPS1 immunoreactivity in EMPDs of perianal origin suggests this subset of EMPDs may be derived from different cell types of origin. Further studies with a larger cohort are needed to further confirm this impression.

297 Clinicopathological and Molecular Features of Penile Melanoma

Kristine Cornejo[1], Amrita Goyal[2], Aida Valencia Guerrero[3], Michael Astudillo[4], Dora Dias-Santagata[1], Mai Hoang[5]
[1]Massachusetts General Hospital, Boston, MA, [2]Minneapolis, MN, [3]Vanderbilt Medical Center, Nashville, TN, [4]Mass General Brigham, Boston, MA, [5]Massachusetts General Hospital, Harvard Medical School, Boston, MA

Disclosures: Kristine Cornejo: None; Amrita Goyal: None; Aida Valencia Guerrero: None; Michael Astudillo: None; Dora Dias-Santagata: None; Mai Hoang: None

Background: Mucosal melanomas (MM) are rare and display different molecular alterations from cutaneous melanomas (CM). MMs typically present with advanced disease and are difficult to stage as there are no validated staging systems. Penile melanomas (PM) including those of the distal urethra are an exceedingly rare subtype of MM and our aim is to review its clinicopathologic features and molecular profile as well as determine whether prognostic parameters used in the evaluation of CM may also correlate with outcome in PM.

Design: We reviewed the clinicopathologic features and performed molecular profiling using next-generation sequencing of genomic DNA in 7 PMs, by employing the Anchored Multiplex PCR (AMP)-based SNaPshot platform to examine alterations across 97 cancer genes. Given the rarity of PMs, we reviewed the English literature and included cases with a reported depth of invasion and follow-up data and additionally used the Surveillance, Epidemiology, and End Results (SEER) database. Statistical analysis was performed evaluating prognostic parameters using Log-Rank test and Kaplan Meier survival curves.

Results: The clinicopathologic and mutation profiles are summarized in Table 1 and Figures 1-2. The patient ages ranged from 46-78 (mean: 60.9) years with involvement on the glans (n=5; 71%) and distal urethra (n=2; 29%). Tumor depth ranged from 1.6-10 (mean: 4.6) mm. Six patients underwent partial penectomy and sentinel lymph node (LN) biopsy, respectively. Six patients had metastatic disease at diagnosis and 3 died of disease with a mean follow-up period of 30.9 (2-72) months.

Five of 7 (71%) cases identified 15 molecular alterations within *KIT* (n=2), *CDKN2A* (n=2), *NF1* (n=2), *PTEN* (n=2), *APC* (n=2), *NRAS* (n=1), *MAP3K1* (n=1), *CDH1* (n=1), *MSH6* (n=1), and *TERT* (n=1). Two cases were not found to harbor genetic aberrations.

A total of 124 PMs (our cohort [n=7]+literature review [n=75]+SEER data [n=42]) were analyzed for prognostic parameters and the overall survival was significantly worse in patients with LN metastasis (P=0.0432) and greater depth of invasion (P=0.0003). Presence of ulceration was not found to correlate with outcome (P=0.12).

Case #	Age (y)	Site	Tumor Size (mm)	Depth (mm)	Mitosis (mm2)	LVI/PNI	Ulceration/ Regression	TILs	RGP/VGP	Cell Type	Microsatellites	Precursor Nevus	Circumcised
1	61	Urethra	21	2.0	3	+/+	-/-	Non-brisk	+/+	Epithelioid	Absent	No	No
2	61	Glans	---	8.0	13	+/-	+/-	Absent	+/+	Epithelioid	Absent	No	Yes
3	68	Glans	32	4.0	36	-/-	-/-	Absent	+/+	Epithelioid	Absent	No	No
4	57	Glans	50	10.0	36	+/+	+/-	Non-brisk	+/+	Epithelioid	Present	No	Yes
5	78	Glans	7	2.9	6	+/-	+/-	Non-brisk	+/+	Epithelioid	Absent	No	No
6	55	Urethra	5	3.5	4	-/-	-/-	Absent	-/+	Epithelioid	Absent	No	---
7	46	Glans	50	1.6	14	-/-	-/-	Non-brisk	+/+	Epithelioid Spindled	Absent	No	Yes

Case #	Procedure	Margin Status	Involvement at Diagnosis	Pathologic Stage (Cutaneous Staging)	Recurrence	Follow-Up (m)
1	Partial Penectomy + Adrenalectomy	Positive	Metastasis to Adrenal Gland	pT2aNxM1c	Metastasis to inguinal/pelvic LN, small and large bowel; pancreas, liver, lung, abdominal/thigh muscle	DOD 24
2	Penile Biopsy + SLNB	Negative	Metastasis to Inguinal LN	pT4bN1	Metastasis to LN, liver, bone, brain	DOD 57
3	Partial Penectomy + SLNB	Negative	Metastasis to Inguinal LN	pT3aN1	Metastasis to LN, liver, lungs	DOD 23
4	Partial Penectomy + SLNB	Negative	Metastasis to Inguinal LN	pT4bN2c	No other metastasis or recurrence	AWOD 18
5	Partial Penectomy + SLNB	Negative	Metastasis to Inguinal LN	pT3bN1	Local recurrence	AWOD 20
6	Partial Penectomy + SLNB	Positive	None	pT3aN0	No metastasis or recurrence	AWOD 2
7	Partial Penectomy + SLNB	Positive	Metastasis to Inguinal LN	pT2aN1	Local recurrence and in-transit metastasis (penis/scrotum), inguinal LN	AWOD 72

Figure 1 - 297

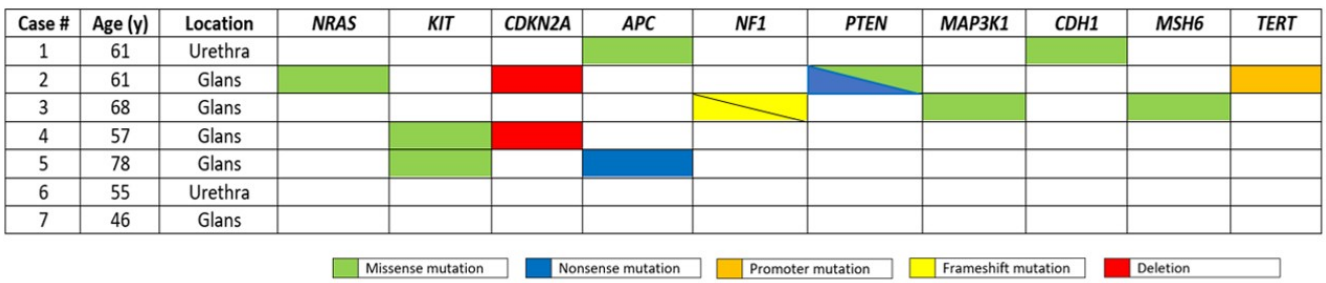

Figure 2 – 297

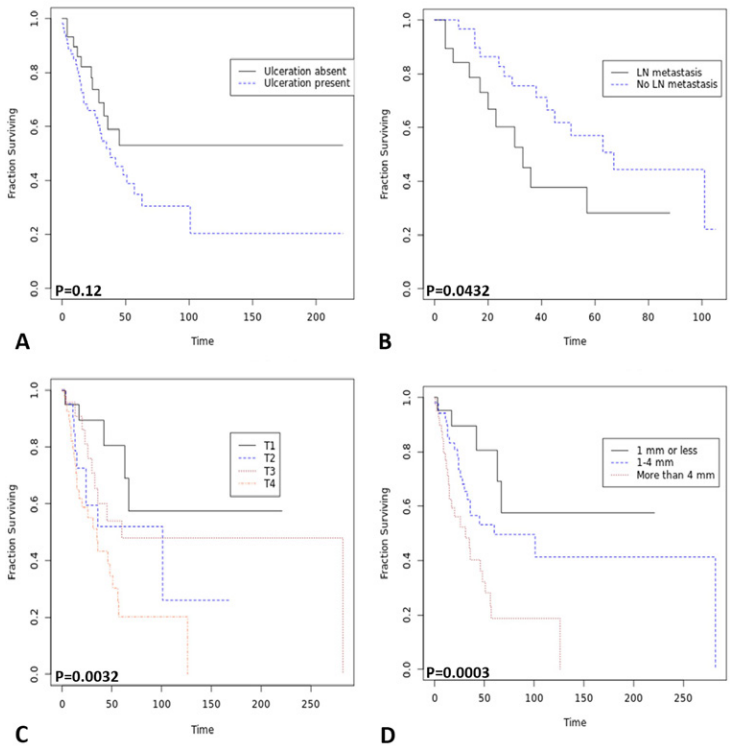

Conclusions: PMs most commonly involve the glans and present at an advanced stage with locoregional disease. PMs harbor heterogenous molecular alterations that are more commonly identified in MMs, and targeted therapies may potentially improve outcome in these patients. Prognostic parameters used in staging of CMs may also be used in PMs.

298 Histopathologic Characterization of Clinically Regressing Infantile Myofibromas

Carina Dehner[1], Louis Dehner[1], Leigh Compton[2]
[1]Washington University School of Medicine, St. Louis, MO, [2]Washington University in St. Louis, St. Louis, MO

Disclosures: Carina Dehner: None; Louis Dehner: None; Leigh Compton: None

Background: Myofibromas are uncommon mesenchymal neoplasms that may occur as a single lesion or as multifocal disease in the setting of infantile myofibromatosis. While organ involvement is a poor prognostic factor, solitary and multicentric lesions without organ involvement are usually indolent. Spontaneous regression of myofibromas is an established clinical phenomenon, particularly in skin and soft tissue lesions, but the histopathologic features of regression have not been well established. Herein, we report a series of myofibromas with distinct histopathology compatible with involution given two lesions were excised in the context of clinically apparent regression.

Design: Departmental archives were queried for cases of myofibromas. A total of 143 cases were screened and slides for 61 cases were re-reviewed. Demographic information, tumor site, tumor size, body site, patient age and gender, organ involvement, histologic description including histological features of regression and clinical follow up including clinical and radiographic features of regression were collected.

Results: Clinical chart review of 61 cases resulted in two index cases of myofibroma with clinical evidence of regression based on clinical exam and/or imaging. On histology both cases showed peripheral nodular proliferations of vessels surrounded by plump spindle cells. Centrally, edematous stroma with decreased cellularity and abundant lipofuscin-laden macrophages were present.

Re-review of slides of the remaining 59 cases resulted in additional 6 cases with similar histological features. Central necrosis and/or calcification were commonly seen. Median age was 1.75 years (639 days; range: 14 days – 17 years), with an equal gender distribution (4 female, 4 male). Both index cases had more than one lesion, 3 cases presented with solitary lesion and 3 were lost for follow-up. There was a wide anatomic distribution involving the back (3/8), thigh (2/8), plantar foot (1/8), cheek (1/8) and chest wall (1/8). None of the patients had evidence of organ involvement or other pertinent past medical history. One of the index cases was later found to suffer from Koolen-de Vries syndrome.

Conclusions: Herein we define the histologic features of clinically regressing or regressed myofibromas and subsequently identified these features within a larger cohort of cases. Recognition of these features, particularly in the setting of a completely regressed lesion and multifocal disease, is of histopathologic diagnostic and clinical utility.

299 Clinical, Morphologic and Molecular Characteristics of Cutaneous Leiomyomas; A Tool to Recognize Hereditary Leiomyomatosis and Renal Cell Cancer

Sabina Desar[1], Edward Cowen[2], Chyi-Chia Lee[3], W Linehan[3], Maria Merino[4]
[1]National Cancer Institute, National Institutes of Health, Bethesda, MD, [2]Clinical Center, National Institutes of Health, Bethesda, MD, [3]National Institutes of Health, Bethesda, MD, [4]National Cancer Institute, Bethesda, MD

Disclosures: Sabina Desar: None; Edward Cowen: None; Chyi-Chia Lee: None; W Linehan: None; Maria Merino: None

Background: Hereditary leiomyomatosis and renal cell cancer (HLRCC) is an autosomal dominant disorder characterized by multiple cutaneous and uterine leiomyomas and aggressive kidney cancer. It results from germline heterozygous mutation of fumarate hydratase (FH), a tumor suppressor gene. HLRCC related renal cancer has characteristic morphologic features that have also been identified in the cutaneous leiomyomata lesions, occasionally leading to misdiagnosis of leiomyosarcoma. Cutaneous leiomyomas in the setting of HLRCC can be large size and are often multiple in number; however, metastasis has not been identified.

Design: We studied the morphologic, molecular and IHC characteristics of 46 biopsies of cutaneous leiomyoma (diagnosed between 2001-2021) in HLRCC patients identified from our Laboratory of Pathology files. The following clinical and pathologic features were evaluated: age, sex, tumor site, tumor size, cellularity, pleomorphism, necrosis and mitosis. IHC for Fumarate Hydratase (FH) and 2-Succinocysteine (2SC) were performed. Tru-Sight Oncology 500 gene panel was performed on several cases.

Results: 46 biopsies obtained from 35 patients were evaluated. Of these, 24 (68.6 %) were male and 11 (31.4%) were female. The age range was 18-76 years and median age was 44 years. The most common site was upper extremities (52.2%); followed by trunk (32.6 %), lower extremities (13.0%) and head and neck (2.2%). Individual lesions ranged in size from 0.2- 2.5 centimeters. Fourteen out of forty-six biopsies demonstrated mild or greater atypia. Three out of forty-six cases showed moderate increase in cellularity. Three cases showed mitotic figures; however, <1/10 high power field. Necrosis was not identified in any cases. Nine cases showed HLRCC like nuclear changes. Cases were stained for FH and 2SC. All the cases were immunoreactive for 2SC and negative for FH expression. Tru-Sight Oncology 500 gene panel showed mutation of the FH gene in all cases studied.

Figure 1 - 299

Conclusions: This is one of the largest studies to date of characterizing the histologic features of cutaneous leiomyomas in HLRCC. HLRCC-associated cutaneous leiomyomas often show minimal atypia and rare mitotic figures; however significant atypia, pleomorphism and mitosis >1/10 hpf can rarely be present. None of the cases showed evidence of sarcomatous changes or malignancy; and none cases has metastasized. Multiple skin leiomyomas in any patient should prompt for germline testing for fumarate hydratase mutation. The combination of FH and 2-SC immunostains are very helpful in such cases. Identification of skin lesion can be helpful in identifying patients with HLRCC syndrome and renal cancer.

300 EphB2 is Involved in Dermal Fibrosis during Systemic Sclerosis

Erika Egal[1], Quinian Johanson[1], Danald Severin Kamdem[1], Ching-Chu Yang[1], Mark Henkemeyer[2], Troy Jaskowski[3], Anne Tebbo[1], My Helms[1], Tracy French[1], Patrice Mimche[1]
[1]The University of Utah, Salt Lake City, UT, [2]The University of Texas, Dallas, TX, [3]ARUP Laboratories, University of Utah, Salt Lake City, UT

Disclosures: Erika Egal: None; Quinian Johanson: None; Danald Severin Kamdem: None; Ching-Chu Yang: None; Mark Henkemeyer: None; Troy Jaskowski: None; Anne Tebbo: None; My Helms: None; Tracy French: None; Patrice Mimche: None

Background: Systemic sclerosis (SSc) is an autoimmune disease characterized by fibrosis of the skin and internal organs. We recently showed that the receptor tyrosine kinase EphB2 is involved in liver and kidney fibrosis. We are showing that EphB2 is activated and highly expressed in skin biopsies of patients with SSc. We further showed that EphB2 is required for TGFβ-mediated dermal fibroblast-to-myofibroblast conversion. EphB2 is a critical promoter of skin fibrosis in mice because *EphB2-/-* mice exhibit a drastic reduction of bleomycin-induced fibrosis compared to littermates *in vivo*. Conditional deletion of *EphB2* in skin fibroblasts conferred protection from bleomycin-induced dermal fibrosis in mice. Our study unveils novel findings regarding the potential implication of EphB2 signaling during SSc in both humans and mice.

Design: The study received approval from the institutional review board of University of Utah (IRB #38705).Immunofluorescence confocal microscopy was used to detect, activated “p-EphB1/B2” and αSMA in skin biopsy of healthy volunteers and patients with SSc. The regulation of EphB2 expression on normal and scleroderma human dermal fibroblasts was evaluated by western blot, qPCR, hydroxyproline assay, and immunofluorescence. The Bleomycin-induced skin fibrosis EpHB2 (-/-),Cre-flox with specific deletion of EphB2 in fibroblast, and TSK 1+ mice model were used for *in vivo* studies.

Results: We showed that p-EpHB2 was elevated in the skin of patients with SSc. Our *in vitro* studies demonstrated that EphB2 is required for TGFβ1-mediated dermal fibroblast-to-myofibroblasts transition HDF) and that HDF and SSc-dermal fibroblasts upregulate EphB2 when stimulated with TGF-β1 for 24h. Skin fibrosis was attenuated in the absence of EphB2 and in conditional deletion of EphB2 in fibroblasts *in vivo*. In the tight skin model (TSK1+) of dermal fibrosis, EphB2 heterozygous mice also presented reduced dermal thickness and fibrosis compared to littermate controls.

Figure 1 - 300

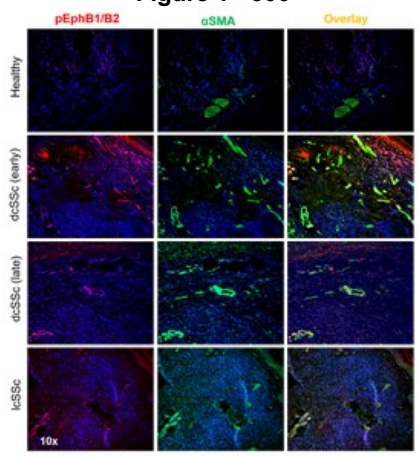

Figure 1. Expression of activated “phosphoEphB1/B2” proteins in the skin of patients with various stage of Scleroderma. Immunofluorescence staining procedure was used to detect proteins expression of phosphoEphB1+EphB2$^{Y594/Y604}$ in human skin specimen of healthy and patients with various manifestations of limited or diffuse cutaneous SSc (lcSSc or dcSSc; early < 2 years disease duration and Late > 7 years disease duration).

Figure 2 - 300

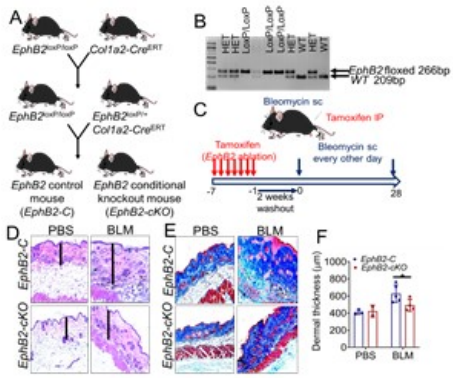

Figure 2. Bleomycin-induced skin fibrosis is dependent on EphB2 in fibroblasts. reduced in mice lacking *EphB2*. (**A**) Schematic of the generation of *EphB2-cKO* mice. (**B**) Representative genotyping showing the WT band (209 bp) , the heterozygote (HET), and the homozygote EphB2 floxed band (266 bp). (**C**) Schematic showing mice subjected to tamoxifen treatment followed by the bleomycin-induced dermal fibrosis model. (**D**) H&E staining of PBS and Bleomycin-treated *EphB2-C* and *EphB2-cKO* mice (bold line indicates dermal thickness). (**E**) Masson-trichrome staining of PBS and Bleomycin-treated *EphB2-C* and *EphB2-cKO* mice. (**F**) Quantification of dermal thickness of PBS and Bleomycin-treated *EphB2-C* and *EphB2-cKO* mice. Data represent Mean±SD. *p<0.05

Conclusions: In conclusion, EphB2 was activated and highly expressed in the skin of patients with SSc relative to healthy subjects and partially co-localized with αSMA. Skin fibrosis is reduced in EphB2-deficient mice following bleomycin treatment. Fibroblast-specific deletion of EphB2receptor reduces dermal fibrosis in bleomycin mouse models. Our data suggest that EphB2 activation may contribute to skin fibrosis. Further studies to delineate the fibrotic role of this molecule may have potential therapeutic implications in SSc.

301 Proliferating Pilar Tumors are Characterized by Recurrent Chromosome 15q Gains and Chromosome 6q and 6p22.2 Losses

Grant Fischer[1], Neal Lindeman[2], Eleanor Russell-Goldman[3]
[1]Brigham and Women's Hospital, MA, [2]Harvard Medical School, Brigham and Women's Hospital, Boston, MA, [3]Brigham and Women's Hospital, Harvard Medical School, Boston, MA

Disclosures: Grant Fischer: None; Neal Lindeman: None; Eleanor Russell-Goldman: None

Background: Proliferating pilar tumors (PPTs), also known as proliferating trichilemmal cysts, are rare benign neoplasms of external root sheath derivation, which most commonly occur on the scalp of elderly women. PPTs are characterized by a lobular proliferation of squamous epithelium with prominent trichilemmal-type keratinization. These tumors infrequently undergo malignant transformation resulting in high recurrence rates and metastatic potential. There is a paucity of data on the molecular pathogenesis of PPTs. Herein, we describe the use of a next generation sequencing (NGS) platform to provide the most comprehensive molecular genetic analysis of PPTs to date.

Design: This study includes 5 PPT cases. DNA was extracted from formalin-fixed paraffin-embedded tissue and analyzed by a targeted massively parallel sequencing platform using a solution-phase Agilent SureSelect hybrid capture kit and an Illumina HiSeq 2500 sequencer. The platform interrogates possible alterations in the complete exonic DNA sequences of 447 cancer-related genes including substitutions, insertions, and deletions. Additionally, 191 intronic regions across 60 genes are analyzed for the detection of structural rearrangements. To assess copy number variations, regions harboring single nucleotide polymorphisms (SNPs), spaced approximately every 4 MB across the genome, are captured and sequenced.

Results: Broad low copy number gains of chromosome 15q and concurrent single copy losses of chromosome 6q were seen in 4 of 5 (80%) cases. In addition, single copy losses of 6p22.2 were also present in each of these 4 cases. No other significant recurrent shared alterations were found among cases. One case harbored a single copy loss of *TP53* and showed a concurrent missense mutation [c.832C>T (p.P278S), exon 8], suggesting biallelic loss of *TP53* in this case, in addition to the chromosomal alterations noted above.

Conclusions: Recurrent chromosome 15q gains with losses of chromosome 6q and 6p22.2 in 4 of 5 PPT cases analyzed by NGS suggest a significant role for chromosomal aberrations in the pathogenesis of PPTs.

302 Characterizing the Clinicopathologic and Molecular Landscape of Acral Lentiginous Melanoma: A Retrospective Review of 331 Patients

Pavandeep Gill[1], Denai Milton[2], Leomar Ballester[2], Woo Cheal Cho[2], Priya Nagarajan[2], Jonathan Curry[2], Doina Ivan[2], Victor Prieto[2], Michael Davies[2], Carlos Torres-Cabala[2], Phyu Aung[2]
[1]Royal Jubilee Hospital, Victoria, Canada, [2]The University of Texas MD Anderson Cancer Center, Houston, TX

Disclosures: Pavandeep Gill: None; Denai Milton: None; Leomar Ballester: None; Woo Cheal Cho: None; Priya Nagarajan: None; Jonathan Curry: None; Doina Ivan: None; Victor Prieto: None; Michael Davies: None; Carlos Torres-Cabala: None; Phyu Aung: None

Background: Acral lentiginous melanoma (ALM) is a rare, distinct subtype of cutaneous melanoma that is typically associated with a delayed diagnosis and worse prognosis than non-acral cutaneous melanomas. We performed a retrospective analysis of ALM patients (pts) that underwent molecular testing at our institution to characterize the clinicopathologic and molecular landscape of this melanoma subtype.

Design: We identified pts with ALM who underwent mutational testing between 1990 and 2020 at our tertiary cancer center. Platforms for testing included next generation sequencing and polymerase chain reaction studies. We collected demographic,

clinicopathologic, follow-up, and molecular data for all pts. Associations between demographic and clinicopathologic measures were evaluated using Fisher's exact tests. The Kaplan-Meier method was used to estimate overall survival (OS) and Cox proportional hazards regression models were performed to identify factors associated with OS.

Results: For this cohort of 331 ALM pts, 55% were male, the median age was 62.7 years (range: 13.9-89.6 years), and ethnicity included Caucasian (72%), Hispanic (17%), Black (6%), and Asian (4%). The majority of primary tumors were located on the lower extremity (84%) and had high-risk features, with 69% Clark level IV, 44% with Breslow thickness (BT) > 4 mm, and 61% ulcerated. Most pts were diagnosed with stage III disease (69%), including 48% with positive sentinel lymph nodes (LN). 7%, 22%, and 2% of pts were at stage I, II, and V, respectively. 24% of pts had brain metastases over the course of disease and the majority of pts (62%) died. The most common mutations were in *BRAF* (35%), *KIT* (25%), and *NRAS/HRAS/KRAS* (35%). Significant associations were seen for *KIT* mutations with sex (p=0.010); *RAS* mutations with ethnicity (p=0.046) and stage (p=0.003); *BRAF* mutations with ulceration (p=0.049); and presence of lymphovascular invasion (LVI) with positive LN (p<0.001). On univariate analysis, OS was associated with stage, LN status, Clark level, BT, mitotic figure count, ulceration, LVI, and brain metastases. Stage, LN status, LVI, and brain metastases remained significantly associated with OS in multivariable analysis (Table 1).

Table 1: Summary of Overall Survival

	Univariate		Multivariable	
Measure	**Hazard Ratio (95% CI)**	**p-value**	**Hazard Ratio (95% CI)**	**p-value**
Stage				
II vs. I	2.42 (1.18, 4.98)	**0.016**	2.45 (1.00, 6.01)	**0.050**
III vs. I	3.07 (1.55, 6.08)	**0.001**	2.99 (0.79, 11.33)	0.11
LN status at diagnosis				
Sentinel vs. None	1.25 (0.90, 1.75)	0.19	0.62 (0.20, 1.92)	0.41
Enlarged vs. None	2.78 (1.70, 4.54)	**< 0.001**	4.43 (1.24, 15.77)	**0.022**
Regional vs. None	3.12 (1.89, 5.15)	**< 0.001**	0.74 (0.20, 2.70)	0.65
Sentinel/Regional vs. None	2.29 (1.31, 3.99)	**0.004**	1.06 (0.28, 3.95)	0.93
Total number of LN at diagnosis	1.13 (1.08, 1.19)	**< 0.001**	1.00 (0.91, 1.10)	0.97
Clark level				
IV vs. II/III	1.77 (0.93, 3.38)	0.08	1.12 (0.46, 2.70)	0.81
V vs. II/III	2.89 (1.46, 5.71)	**0.002**	1.64 (0.63, 4.31)	0.31
Breslow thickness				
1.01-2 mm vs. ≤ 1 mm	1.56 (0.73, 3.36)	0.25	1.05 (0.40, 2.76)	0.93
2.01-4 mm vs. ≤ 1 mm	1.97 (0.94, 4.11)	0.07	0.86 (0.32, 2.29)	0.76
> 4 mm vs. ≤ 1 mm	2.51 (1.22, 5.18)	**0.013**	0.79 (0.28, 2.20)	0.65
Mitotic figures				
1-4/mm^2 vs. < 1/mm^2	1.60 (0.95, 2.69)	0.08	1.18 (0.61, 2.31)	0.62
5-9/mm^2 vs. < 1/mm^2	2.19 (1.28, 3.74)	**0.004**	0.98 (0.47, 2.03)	0.96
10-20/mm^2 vs. < 1/mm^2	2.00 (1.12, 3.56)	**0.019**	0.71 (0.31, 1.63)	0.42
> 20/mm^2 vs. < 1/mm^2	3.80 (1.87, 7.73)	**< 0.001**	1.80 (0.68, 4.74)	0.24
Ulceration				
Present vs. Absent	1.43 (1.06, 1.92)	**0.018**	1.42 (0.94, 2.14)	0.10
Vascular invasion				
Present vs. Absent	1.80 (1.33, 2.46)	**< 0.001**	1.47 (1.01, 2.14)	**0.042**
Presence of Brain metastases[a]	7.65 (5.65, 10.35)	**< 0.001**	10.27 (7.05, 14.97)	**< 0.001**

[a] Included in the model as a time-dependent covariate.

Abbreviation: CI = confidence interval; LN = lymph node.

Conclusions: Our study in a select cohort of ALM pts enhances our current knowledge of the clinicopathologic and genetic landscape of ALM and offers new insights about associations between genetic alterations and clinicopathologic parameters, potentially useful for therapy and prognosis.

303 Cutaneous Deep Fungal Infections: Retrospective Review at a Tertiary Care Cancer Center

Pavandeep Gill[1], Teny John[2], Jeffrey Tarrand[2], Xinyang Jiang[2], Jing Ning[2], Phyu Aung[2], Woo Cheal Cho[2], Jonathan Curry[2], Carlos Torres-Cabala[2], Doina Ivan[2], Victor Prieto[2], Priya Nagarajan[2]
[1]Royal Jubilee Hospital, Victoria, Canada, [2]The University of Texas MD Anderson Cancer Center, Houston, TX

Disclosures: Pavandeep Gill: None; Teny John: None; Jeffrey Tarrand: None; Xinyang Jiang: None; Jing Ning: None; Phyu Aung: None; Woo Cheal Cho: None; Jonathan Curry: None; Carlos Torres-Cabala: None; Doina Ivan: None; Victor Prieto: *Consultant*, Novartis, Orlucent; Priya Nagarajan: None

Background: Cutaneous deep fungal infections (CDFI) are frequent and often fatal in immunocompromised patients (pts), necessitating timely recognition and management. We retrospectively reviewed histopathologically-proven CDFI cases at a major cancer center to identify organism-specific histopathologic features and enhance early detection of subtle infections.

Design: Demographic, clinicopathologic, microbiology culture, and follow-up data were collected for all histopathologically-proven CDFI cases received from 06/2016 and 06/2020.

Results: 61 pts were identified with male to female ratio of 3:2; median age of 60 years. Most were white (n=40) with predominance of O+ blood type (n=25). 85% (52/61) pts died (median time to death from biopsy was 26.5 days (d); 46% died within 30d). Hematologic malignancy was the most common underlying disease (n=58), of which acute myelogenous leukemia was most frequent (n=32). 21 pts had prior hematopoietic stem cell transplant and 32 pts had relapsed cancer. Skin lesions were often multiple (61%) but localized to one anatomic region (57%), usually the lower extremity (28%). Skin was the first site of infection in 87% of pts, with acute onset (≤1 week) in 66% and most (57%) were painful (Table 1).

Fungal organisms were easily seen on H&E-stained sections at 200× in 77% (47/61) of pts, including yeasts in 21% and hyphae in 79%, with no inflammation in 64%. Concurrent microbiology cultures were done in 59 pts and only 70% were positive. Growth was initially noted within 7d in 66% of pts; however, organism identification took an extra 2-4 weeks.

In 13 pts with yeasts, *Candida tropicalis* was most frequent (n=7), of which pseudohyphae were seen in GMS stain in 4 pts (Figure 1); culture failed in 1 case. In the 47 pts in which fungal hyphae were identified, *Fusarium sp.* was the most frequent (n=23) and chlamydospores were identified in 70% (16/23). Of 12 pts with mucormycosis infection, culture failed in 7 pts (confirmed by *Rhizopus* immunohistochemistry). Angiotropism, neurotropism and epidermotropism were noted in 20, 9 and 10 cases of *Fusarium sp.* and 8, 7 and 5 cases of mucormycosis infection, respectively. Gram stain showed rare yeast forms in 43% (10/23) of *Fusarium sp.* infections (Figure 2).

Table 1. Demographic and clinical features

Underlying malignancy		Anatomic site		Number of lesions		Duration (weeks)		Clinical appearance		Symptoms		Dissemination	
AML	32	Multiple regions	26	Multiple	37	≤ 1	40	Macules & papules	2	Asymptomatic	24	Present	35
ALL	8	Lower extremity	17			2-4	16	Patches & plaques	15				
Lymphoma	8	Upper extremity	11			> 4	4	Papules & nodules	19	Pain/ tenderness	35		
MDS/MPD	7	Trunk	4	Single	24	NA	1	Ulcer	22			Absent	26
Multiple myeloma	3	Head & neck	3					Soft tissue swelling	3	NA	2		
Solid tumors	3												

Figure 1 - 303

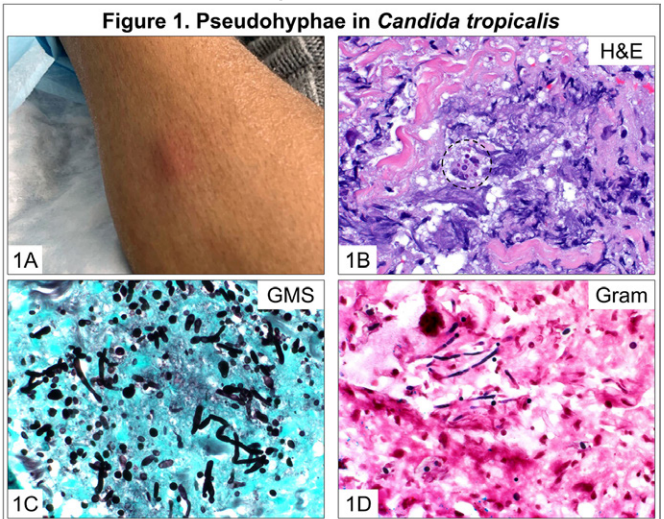

1A. Single erythematous subcutaneous nodule in left forearm. **1B.** Rare yeast forms (dashed circle) within an area of dermal necrosis (H&E, 600×) **1C.** Numerous yeasts and scattered thin hyphae in a background of necrosis. (GMS, 600×) **1D.** Scattered gram-positive yeasts admixed with rare gram-variable thin septate hyphae (Gram 600×).

Figure 2 - 303

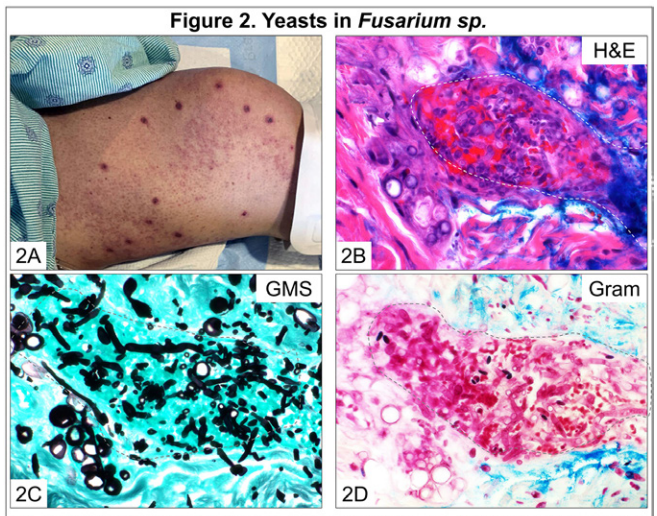

2A. Multiple erythematous/ violaceous papules on left leg. **2B.** Numerous septate hyphae and chlamydospores (H&E, 600×). **2C.** Numerous septate hyphae and chlamydospores (GMS, 600×). **2D.** Numerous gram negative septate hyphae and chlamydospores and rare gram-positive yeasts (Gram 600×). 2B-2D: Dashed line: vessel wall.

Conclusions: We show that histopathological analyses may identify fungal organisms even when cultures are negative. Presence of hyphae in yeast infection is most common among *Candida tropicalis*, while presence of rare yeast forms is most common among *Fusarium sp*. infection.

304 Histological and Immunohistochemical Features of Acquired Cold Urticaria in Experimentally Induced Hives: a Series of Eleven Cases

Maria Monica Gonzalez Farre[1], Nasser Porras[1], Evelyn Andrades López[2], Ana Isabel Alvarez Mancha[1], Adrian Puche[3], Belen Lloveras[1], Carlos Barranco[1], Ana Arnau[4]

[1]Hospital del Mar, Barcelona, Spain, [2]IMIM-Hospital del Mar, Barcelona, Spain, [3]Hospital del Mar-Parc de Salut Mar, Barcelona, Spain, [4]Hospital del Mar-Parc de Salut Mar, San Cugat del Valles, Spain

Disclosures: Maria Monica Gonzalez Farre: None; Nasser Porras: None; Evelyn Andrades López: None; Ana Isabel Alvarez Mancha: None; Adrian Puche: None; Belen Lloveras: None; Carlos Barranco: None; Ana Arnau: *Grant or Research Support*, Uriach, Novartis; *Speaker*, Avene; *Advisory Board Member*, Themo Fisher, Sanofi; *Primary Investigator*, Amgen, Astra; *Consultant*, Almirall; *Grant or Research Support*, Feder Carlos III; *Speaker*, Menarini

Background: Cold urticaria (CoU) is an inducible condition characterized by hive eruption upon skin exposure to cold. It results from vascular dilatation and fluid leakage into the skin in response to molecules released from mast cells. Previous studies have shown that in chronic spontaneous urticaria (CSU) there is PAF receptor (PAF-R) overexpression in the epidermis, endothelium, nerves and T cells. The objective of this study is to characterize, for the first time, the histological and immunohistochemical features of CoU experimentally induced hives

Design: Histopathological features of experimentally induced hives were evaluated in 11 CoU patients by 4 independent observers. Biopsies were taken from hives induced at 4°C for 1-5 minutes. Data related to the epidermal and dermal changes and the type and distribution of inflammatory infiltrates were collected. C-KIT, PAF-R and PAF-R/CD43 immunohistochemistry was performed

Results: Six men and 5 women (mean age, 44) were included. The epidermis was preserved in 7/11 cases, while light atrophy was observed in 4/11. All instances showed a variable degree of dermal edema and perivascular and interstitial lympho-histiocytic inflammatory infiltrates. The infiltrate density was mild (4/11) or moderate (7/11). At times, lymphohistiocytic cells were accompanied by neutrophils (2/11) and/or eosinophils (9/11). Increased C-KIT expression in mast cells was observed in comparison to healthy skin from controls. PAF-R was expressed in the epidermis in a patchy pattern reminiscent of that seen in CSU, whereas PAF-R positivity in sebaceous and eccrine glands and pilosebaceous units was like that observed in normal

skin. PAF-R overexpression was not identified in the endothelium, nerves or T cells. CD43 revealed that lymphocytic infiltrates were composed mostly of T cells

Conclusions: This is the first series studying the histology of CoU experimentally induced hives. Dermal edema and characteristic inflammatory infiltrates were homogenously found. C-KIT expression in CoU is the result of mast cell activation, which suggests that C-KIT inhibition could be a potential therapeutic target. In contrast to what happens in CSU, no PAF-overexpression was seen in the endothelium, nerves or T cells, suggesting that CoU might be a distinct entity displaying pathological features unlike those of CSU. Since T cells were the main component of the inflammatory infiltrate, therapies addressed to blocking T cells could be useful in treating cases refractory to first-line treatments

305 Accuracy of Preferentially Expressed Antigen in Melanoma (PRAME) Expression in Diagnosis of Melanoma: A Systematic Review and Meta-Analysis

Abhinav Grover, Medical College of Wisconsin Affiliated Hospitals, Milwaukee, WI

Disclosures: Abhinav Grover: None

Background: Preferentially Expressed Antigen in Melanoma (PRAME) expression (diffuse nuclear reactivity) was first evaluated as an immunohistochemical marker to differentiate melanoma from benign and atypical melanocytic tumors in 2018. Recently, a growing body of evidence has been amassed on evaluation of PRAME in the diagnosis of melanoma. We conducted this meta-analysis to study the pooled rates of performance of diffuse nuclear positive PRAME immunostaining in the diagnosis of melanoma and its differentiation from benign lesions.

Design: Multiple databases were searched (from inception to September 2021) and studies that reported on the performance of PRAME in the diagnosis of melanoma on immunohistochemistry were selected. A random effects model was used, and pooled accuracy were calculated. Publication bias was assessed using a funnel plot.

Results: Thirteen studies evaluating PRAME immunostaining in a total of 1601 patients were included in our final analysis. Two studies evaluated the role of PRAME in conjunctival melanoma, one study looked at oral melanoma, acral melanoma and metastatic melanoma each and the rest of the studies included different types of melanomas. The pooled diagnostic accuracy of PRAME based on random effects model was 88.2 % (95% confidence interval = 82-92) with a heterogeneity (I-squared) of 86.11. The publication bias was acceptable based on funnel plot analysis of standard errors. The sensitivity ranged from 67-100 % and specificity was 95-100 %.

Figure 1 - 305

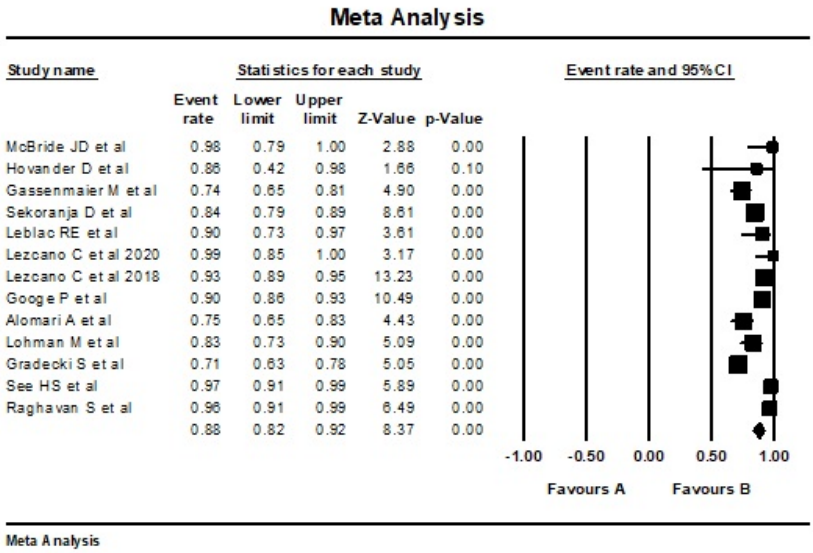

Figure 2 – 305

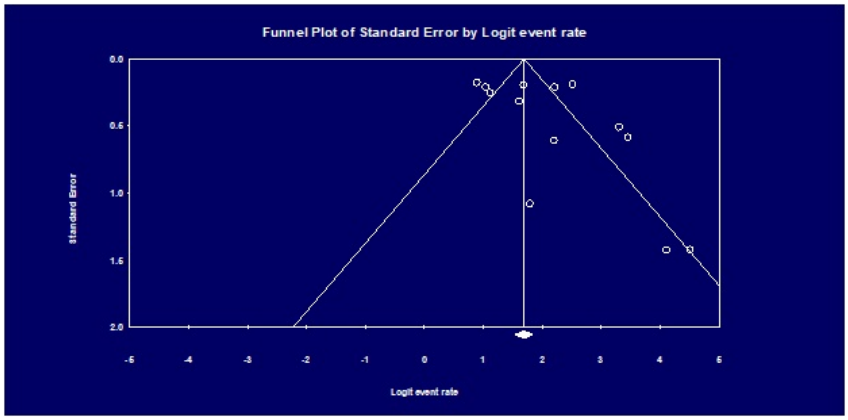

Conclusions: Based on our meta-analysis, PRAME achieved high accuracy in diagnosis of melanoma and can be an important tool to aid in the diagnosis of melanoma for dermatopathologists.

306 Skin Adnexal Tumors Have Variable Tumor Mutation Burdens and Heterogenous Association with UV Mutation Signature: A Discovery Study

Ruifeng (Ray) Guo[1], Zachary Fogarty[1], Aditya Bhagwate[1], Katelyn Reed[1], Jaime Davila[1], Chen Wang[1]
[1]Mayo Clinic, Rochester, MN

Disclosures: Ruifeng (Ray) Guo: None; Zachary Fogarty: None; Aditya Bhagwate: None; Katelyn Reed: None; Jaime Davila: None; Chen Wang: None

Background: Skin adnexal tumors from pilosebaceous, sweat gland and sweat duct origins are poorly understood regarding their molecular oncogenesis, which lead to difficulty for accurate diagnosis, classification and ambiguity in clinical guidance. In this study we comprehensively studied the mutation profiles of representative skin adnexal tumors with the goal of the first exploratory investigation in this aspect.

Design: The cohort consists of 24 cases including: malignant eccrine (n=10) encompassing cases of definitive porocarcinoma and spiradenocarcinoma; malignant apocrine (n= 5); trichoblastoma (n=3); microcystic adnexal carcinoma (MAC) (n=2); common skin cancer (n=2) and common benign adnexal tumor (n=2). All cases underwent tumor mutation burden (TMB) and mutation signature analysis through QIAseq Tumor Mutational Burden Panels (Qiagen) covering 486 genes. The variant calling was performed using Qiagen GeneGlobe web-based tools. Germline variants with a dbSNP rsID and variants with low UMI depth (<20) were removed.

Results: TMB ranged 64-4737 alterations in these tumors. UV signature were mainly observed in surface tumors and tumors of follicular origin, including basal cell carcinoma with follicular differentiation (1/1), squamous cell carcinoma with clear cell feature (1/1), desmoplastic trichoepithelioma (1/1), and trichoblastoma (2/3). 1/2 MAC showed UV signature, absent in the other case with evident clear cell change. Tumors of eccrine origin showed much less UV signature, only observed in 2/10 malignant cases and negative in the syringoma (0/1); both eccrine carcinomas with high TMB and UV signature demonstrated prominent squamous component including one squamoid eccrine ductal carcinoma. Tumors of apocrine origin showed distinct patterns. The 2 cases of genital location (vulva and scrotum) had predominantly apocrine ductal carcinoma in situ and both demonstrated UV signature, with the vulvar case showing significant high TMB. UV signature was absent in the rest of 3 cases from scalp, trunk and axilla.

Conclusions: Our study indicates skin adnexal tumors of hair follicle origins share similar high TMB and UV signature as the surface tumors. However, the tumors of sweat gland and sweat duct origins tend to lack these mutation profiles except a small subset with distinct histomorphology or tumor locations. These findings emphasize the different molecular mechanisms underlying tumorigenesis of skin tumors that have potential influence in precision diagnosis and clinical management.

307 Transcriptomic Analysis of Digital Papillary Adenocarcinoma, Hidradenoma and Hidradenocarcinoma Reveals Similar Gene Expression Pathway, Low Tumor Mutation Burden and Recurrent CRTC1-MAML2 Translocation in Hidradenoma

Ruifeng (Ray) Guo[1], Asha Nair[1], Rosalind Sharain[2], Hong Jiang[3], Katelyn Reed[1], Kevin Halling[1]
[1]Mayo Clinic, Rochester, MN, [2]NorthShore University HealthSystem, Arlington Heights, IL, [3]University of Virginia School of Medicine, Rochester, MD

Disclosures: Ruifeng (Ray) Guo: None; Asha Nair: None; Rosalind Sharain: None; Hong Jiang: None; Katelyn Reed: None; Kevin Halling: None

Background: Skin adnexal tumors of sweat gland and sweat duct origins are challenging for accurate histological classification. The distinction can be critical especially when the tumor occurs on distal extremities, with digital papillary adenocarcinoma (DPA) and hidradenoma as the most common differential diagnoses. Because of the morphological ambiguity, we systemically studied the transcriptomes of these tumors with the goal of further understanding their molecular characteristics and their potential clinical utility.

Design: DPA (n=7), benign hidradenoma (n=7), hidradenoma with atypia (n=2), and hidradenocarcinoma (n=5) underwent whole transcriptome RNA sequencing. Adjacent normal skin tissue (n=7) was used as normal control, and one case of basal cell carcinoma with features mimicking hidradenoma was used as high tumor mutation burden control. Gene Set Enrichment Analysis (GSEA) for gene expression, gene rearrangement and tumor mutation burden (TMB) were investigated. An additional 14 cases of clear cell nodular hidradenoma underwent fluorescence in situ hybridization (FISH) testing with MAML2 gene break-apart probe.

Results: RNA sequencing revealed recurrent gene translocations in 5/7 cases of benign/atypical hidradenoma, including CRTC1-MAML2 (n=2), YAP1-MAML2 (n=2) and YAP1-NUTM1 (n=1). Among them, the 3 cases with YAP1-MAML2 or YAP1-NUTM1 translocations showed poroid cytomorphology. In contrast, the 2 cases of hidradenoma with CRTC1-MAML2 translocations demonstrated non-poroid clear cell nodular features. Additionally, 13/14 cases meeting strict diagnostic criteria for clear cell nodular hidradenoma showed positive MAML2 FISH results . In contrast, none of the hidradenocarcinoma or DPA showed gene rearrangement. TMB analysis showed a low mutation burden in all cases without UV signature, ranging from 0-2.4 mutations/Mb. GSEA demonstrated a significantly dysregulated cell cycle pathways in hidradenocarcinoma and DPA in contrast to benign hidradenoma, with hidradenocarcinoma and DPA sharing over 60% commonly dysregulated genes.

Conclusions: DPA, hidradenoma and hidradenocarcinoma are characterized by dysregulated cell cycle pathways (enriched in malignant cases) and low tumor mutation burden. In addition, CRTC1-MAML2 translocation is common in benign hidradenoma. These findings are distinct from common skin cancers and have potential for more accurate pathological diagnoses.

308 Spitz Melanocytic Tumors with Heterozygous Loss of CDKN2A Gene and Complete Loss of p16 Protein Expression: A Clinical and Pathological Study

Clarissa Jordan[1], Katherine Geiersbach[1], Linda Hasadsri[1], Ruifeng (Ray) Guo[1]
[1]Mayo Clinic, Rochester, MN

Disclosures: Clarissa Jordan: None; Katherine Geiersbach: None; Linda Hasadsri: None; Ruifeng (Ray) Guo: None

Background: The stratification of atypical and malignant Spitzoid lesions on histopathology is not always straightforward, and molecular and cytogenetic studies are often used to aid diagnosis. Among the molecular abnormalities observed in Spitzoid melanoma is homozygous loss of the CDKN2A gene locus on chromosome 9, which encodes expression of p16 and is a known indicator of poor prognosis. While monosomy 9 or heterozygous loss of CDKN2A gene has not been regarded as a diagnostic evidence for melanoma, cases with such changes and subsequent complete loss of p16 expression have not been well-studied.

Design: We systemically reviewed the cytogenetic reports of 545 cases of diagnostically challenging melanocytic tumors that underwent Single Nucleotide Polymorphism microarray (SNP array, OncoScan) test in archive. Cases (n=21) with spitzoid morphology and heterozygous deletion of CDKN2A gene were identified; among them, 11 cases demonstrated loss of p16 immunohistochemical stain in all or nearly all melanocytes. Further pathological review and clinical follow-up were pursued in these cases.

Results: The 11 cases arose in 2 males and 9 females ranging from 9 to 54 years of age. Histopathologic examination in all cases showed a dermal-based melanocytic proliferation, including cells with epithelioid cytomorphology resembling those of a Spitz

nevus. However, the presence of mitotic figures and cells with definitive cytologic atypia raised the question for a malignant process or a borderline melanocytic tumor. Among them, 4 cases had single abnormality of heterozygous 9p21 deletion or monosomy 9, with 3 of these 4 cases diagnosed as Spitz melanoma, including a case with positive sentinel lymph node. Of the remaining 7 cases, 3 had additional small chromosomal changes of uncertain significance, and 4 had additional multiple abnormalities, with 5 of these 7 cases eventually diagnosed as Spitz melanoma.

Figure 1 - 308

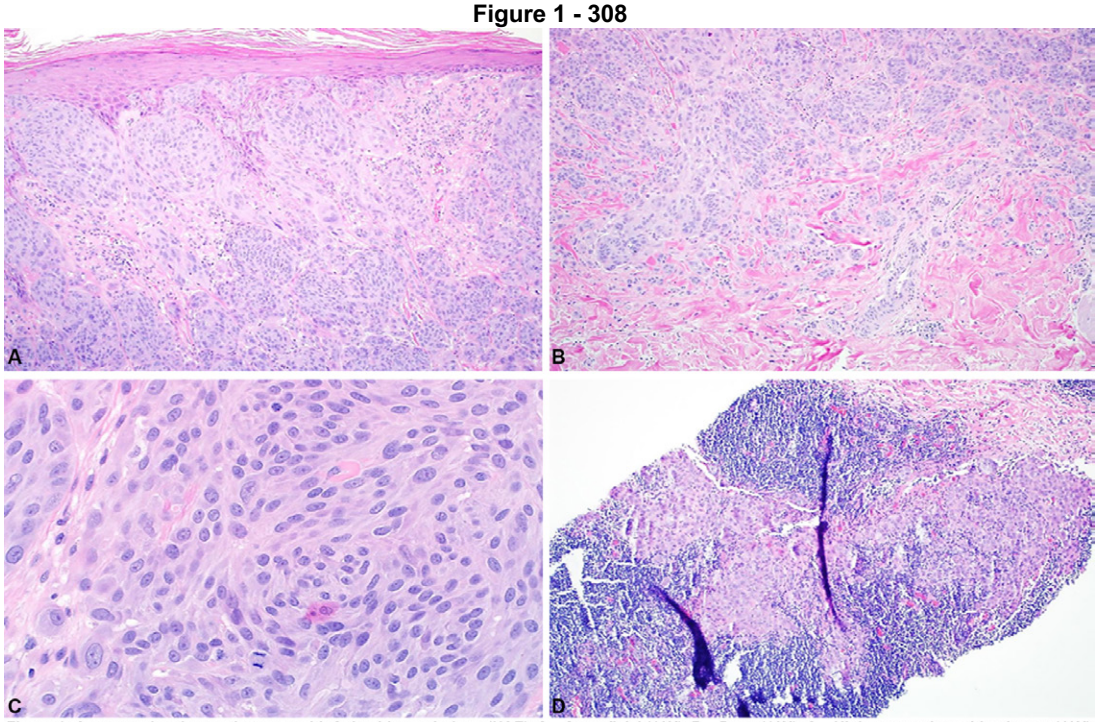

Figure 1: Compound melanocytic tumor with Spitzoid morphology (H&E). A – Superficial (10X), B – Deep (10X), C – High-power view with mitoses (40X). D – Sentinel lymph node with metastasis.

Conclusions: In patients with heterozygous loss of chromosome 9 and absent p16 expression by immunohistochemistry, we hypothesize a second-hit mechanism affects the remaining copy of CDKN2A, causing defective expression. Further studies will investigate the methylation status of CDKN2A in these cases to attempt to elucidate the mechanism of the second hit to p16 expression. Although most cases with this phenomenon were diagnosed as Spitz melanoma in our practice, its prognostic value needs to be further investigated with longer follow-up.

309 Complete and Heterogeneous Loss of H3K27 Trimethylation in Merkel Cell Carcinoma

Andrea Krajisnik[1], Neda Rezaee[1], Bonnie Balzer[1], David Frishberg[2], Wonwoo Shon[1]
[1]Cedars-Sinai Medical Center, Los Angeles, CA, [2]Cedars-Sinai Medical Center, West Hollywood, CA

Disclosures: Andrea Krajisnik: None; Neda Rezaee: None; Bonnie Balzer: *Consultant*, Core Diagnostics, Castle Biosciences, PathologyWatch; David Frishberg: None; Wonwoo Shon: None

Background: H3K27 trimethylation (H3K27me3) is a well-known epigenetic gene silencer that can inhibit transcription. Previous studies have documented the loss of H3K27me3 expression in Merkel cell carcinoma (MCC). However, little information exists about the exact relationship between H3K27me3 expression and Merkel cell polyomavirus (MCPyV) status; previously, two independent studies showed opposite results. For this reason, we investigated H3K27me3 expression in a series of well-characterized MCC with the goal of better establishing the relationship of H3K27me3 expression to MCPyV status.

Design: Formalin-fixed, paraffin-embedded whole and tissue microarray sections from 31 MCC were retrieved from our archives and examined by H3K27me3 immunohistochemistry. 'Intact' H3K27me3 was defined as a dark brown nuclear staining pattern and was further semiquantified based on intensity and proportion. Clinical and follow-up information was also obtained from chart review. For statistical analysis, characteristics were compared between groups with Fisher's exact or Wilcoxon-Mann-Whitney test,

where appropriate. Survival was compared between groups with log-rank tests and was illustrated with Kaplan-Meier curves. P-values less than 0.05 were considered statistically significant.

Results: Overall, 18/31 (58%) MCC showed loss of H3K27me3 staining (complete: 14 cases and heterogenous: 4 cases). There was a trend toward loss of H3K27me3 staining in MCPyV-negative MCC, but it did not reach statistical significance (p=0.07). While 5-year estimated overall survival was significantly improved in MCPyV-positive MCC (p = 0.023), no correlation with the outcome was seen for any other clinicopathologic findings, including H3K27me3 status.

Conclusions: This study confirmed complete or heterogeneous loss of H3K27me3 expression in both MCPyV-positive and negative MCC. However, we have not been able to identify a significant correlation between H3K27me3 expression and clinicopathologic variables, including MCPyV status. Because our study is retrospective with a relatively small sample size, we note that any correlations, or lack thereof, are preliminary at this point. Further larger studies will surely provide deeper insights and should help to determine the value of H3K27me3 as a biomarker for MCC.

310 PD-L1 Expression by Tumor-Associated Macrophages (TAMs) of M2 Subtype is Associated with Overall Survival in Acral Lentiginous Melanoma of Different Ethnicities

Rossana Lazcano[1], Sharia Hernandez[1], Jay Mehta[2], Woo Cheal Cho[1], Edwin Parra[1], Luisa Solis Soto[1], Sandro Casavilca Zambrano[3], Miluska Castillo[4], Carlos Castaneda[3], Priya Nagarajan[1], Jonathan Curry[1], Ignacio Wistuba[1], Victor Prieto[1], Phyu Aung[1], Carlos Torres-Cabala[1]

[1]The University of Texas MD Anderson Cancer Center, Houston, TX, [2]Rice University, Houston, TX, [3]Instituto Nacional de Enfermedades Neoplásicas, Lima, Peru, [4]mz a lt 26 urb Kama II et, San Martin de Porres, Lima, Peru

Disclosures: Rossana Lazcano: None; Sharia Hernandez: None; Jay Mehta: None; Woo Cheal Cho: None; Edwin Parra: None; Luisa Solis Soto: None; Sandro Casavilca Zambrano: None; Miluska Castillo: None; Carlos Castaneda: None; Priya Nagarajan: None; Jonathan Curry: None; Ignacio Wistuba: None; Victor Prieto: None; Phyu Aung: None; Carlos Torres-Cabala: None

Background: Acral lentiginous melanoma (ALM) is a rare subtype of cutaneous melanoma (CM) that arises in acral skin and is proportionally more frequent in Hispanic, Asian, and African populations. Tumor-associated macrophage (TAM) polarization to M1 (antitumoral) or M2 (immunosuppressive) subtype modulates immune response in many tumors. To date, the relationship between the two subtypes and clinicopathologic characteristics in ALM patients of different ethnicities has not been explored. This approach may help determine if specific TAM subsets can be targeted for individualized therapies.

Design: We evaluated 22 formalin-fixed paraffin-embedded primary ALM samples corresponding to 17 Hispanic (Peruvian cohort) and 5 Caucasian (US cohort) patients, respectively. (Table 1). A macrophage panel for multiplexed immunofluorescence (mIF), including CD68 (total TAMs); CD86, MRP8-14 (M1 TAMs); CD163, CD206, Arg1 (M2 TAMs); PD-L1, SOX-10 and DAPI, was validated and applied to the samples. Five intratumoral areas were selected from scanned images and analyzed using Inform software (v2.4.8). Cell densities were correlated with clinicopathologic characteristics and outcome.

Results: M2 TAMs were present in all cases with a median density of 48 cells/mm^2 (range 24-260). In contrast, M1 TAMs were detected in 7/22 cases (31.8%) with a median of 0 cells/mm^2 (range 0-4). M2 TAMs had higher density in Caucasians compared to Hispanic patients (p=0.0137). PD-L1-positive total TAMs and M2 TAMs were higher in tumors with regression (p=0.036). Overall survival (OS) was longer in patients with PD-L1-negative total TAMs and M2 TAMs compared to those with PDL1-positive TAMs (p=0.003). A trend for better OS was detected in immunotherapy treated Caucasian patients (p=0.062) (Figures 1 and 2).

Table 1. Clinicopathologic characteristics of acral lentiginous melanoma patients of different ethnicities.

Characteristics	Hispanics N (%) 17 (77)	Caucasians N (%) 5 (23)	Total N (%) 22 (100)
Median Age (Range)	69 (37 – 92)		
Sex			
Male	9 (41)	3 (14)	12 (55)
Female	8 (36)	2 (9)	10 (45)
Clinical Stage			
Stage I	2 (9)	0 (0)	2 (9)
Stage II	8 (36)	2 (9)	10 (45)
Stage III	7 (32)	3 (14)	10 (45)
Clark Level			
Level IV	9 (41)	4 (18)	13 (59)
Level V	8 (36)	1 (5)	9 (41)
Breslow Thickness			
1.01 – 2	6 (27)	0 (0)	6 (27)
2.01 – 4	2 (9)	3 (14)	5 (23)
> 4	9 (41)	2 (9)	11 (50)
Ulceration			
Yes	9 (41)	3 (14)	12 (55)
No	8 (36)	2 (9)	10 (45)
Regression			
Yes	8 (36)	0 (0)	8 (36)
No	9 (41)	5 (23)	14 (64)
TILs*			
Non-brisk	17(77)	5(23)	22 (100)
Brisk	0 (0)	0 (0)	0 (0)
Vascular Invasion			
Yes	2 (9)	2 (9)	4 (18)
No	14 (64)	2 (9)	16 (73)
Not ruled out	1 (5)	1 (5)	2 (9)
Perineural Invasion			
Yes	3 (14)	2 (9)	5 (23)
No	14 (64)	2 (9)	16 (73)
Not ruled out	0 (0)	1 (5)	1 (5)
Mitosis			
<1 x 10 HPF	4 (18)	0 (0)	4 (18)
1-4 x 10 HPF	4 (18)	3 (14)	7 (32)
5-9 x 10 HPF	6 (27)	1 (5)	7 (32)
10-20 x 10 HPF	3 (14)	1 (5)	4 (18)
Median Survival Since Dx (m) (Range)	10.5 (0.50 – 64)		

***TILS**: Tumor-infiltrating Lymphocytes

Figure 1 - 310

Figure 1. A. M2 Tumor associated macrophages (TAMs) are more abundant in Caucasians compared to Hispanic patients. **B, C.** Total and M2 TAMs expressing PD-L1 are higher in tumors with regression compared to tumors with no regression. **D.** In our series, Caucasian patients showed a trend for better overall survival (OS) compared to Hispanic patients; however, immunotherapy may account for this finding. **E.** Patients with tumors with TAMs expressing PD-L1 have a worse OS compared to those with TAMs lacking PD-L1 expression.

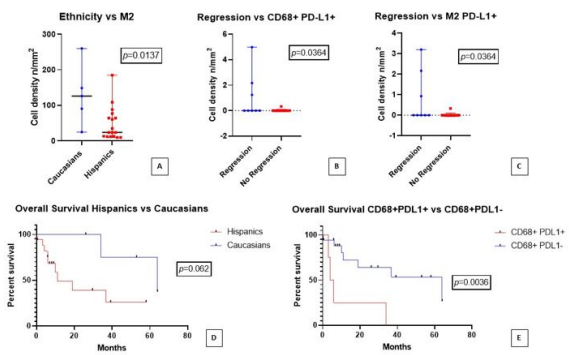

Figure 2 - 310

Figure 2. A, B. Acral lentiginous melanoma (ALM) with regression and numerous M2 macrophages expressing PD-L1. **C, D.** ALM without evidence of regression in which a low density of M2 macrophages expressing PD-L1 is noted (multiplex immunofluorescence, mIF).

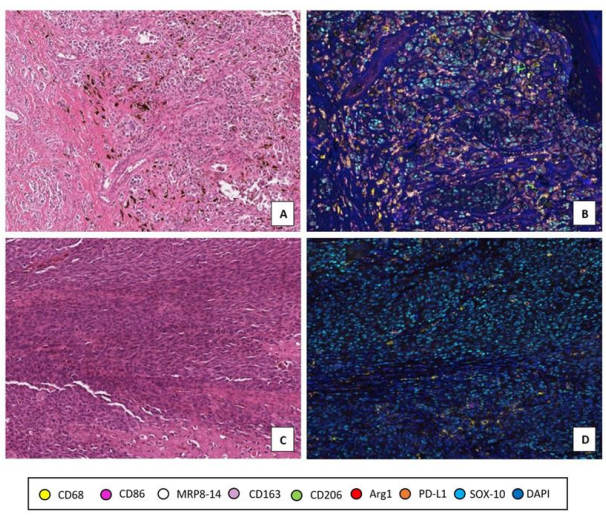

Conclusions: TAMs of M2 subtype predominate in ALM, which may account for their overall aggressive behavior of this melanoma. M2 TAMs appear to be more numerous in Caucasians than Hispanics. Expression of PD-L1 by total TAMs and M2

TAMs correlates with regression and worse OS in our series of predominantly immunotherapy-naïve patients. Further investigation of TAMs in larger cohorts of ALM is warranted.

311 Approaching the Cellular Origin of Merkel Cell Polyomavirus (MCPyV) Associated Merkel Cell Carcinomas: Effects of MCPyV Gene Expression in Epithelial and Lymphoid Cells

Amanda Macamo[1], Dan Liu[2], Martina Farber[3], Ernst-Jan Speel[2], Véronique Winnepenninckx[2], Emil Chteinberg[4], Faisal Klufah[2], Axel zur Hausen[2]
[1]University Maastricht, Maastricht, Netherlands, [2]Maastricht UMC+, Maastricht, Netherlands, [3]University of Amsterdam, Amsterdam, Netherlands, [4]University Medical Center Ulm, Ulm, Germany

Disclosures: Amanda Macamo: None; Dan Liu: None; Martina Farber: None; Ernst-Jan Speel: *Grant or Research Support*, Bayer; *Advisory Board Member*, Lilly, AstraZeneca, Amgen, Novartis; Véronique Winnepenninckx: None; Emil Chteinberg: None; Faisal Klufah: None; Axel zur Hausen: None

Background: Merkel cell carcinoma (MCC) is a rare but very aggressive non-melanoma skin cancer. The etiopathogenesis of approximately 80% of MCC is closely linked to the Merkel cell polyomavirus (MCPyV) and the etiopathogenesis of the remaining 20% is closely linked to UV-damage. MCPyV is clonally integrated into the DNA of the MCC genome and reveals tumor-specific mutations of the large T antigen (LT). Although there is much accumulating evidence of how MCPyV adds to the etiopathogenesis of MCC, the cell of origin of MCC remains elusive. These days it is generally accepted that the Merkel cell is not the cell of origin of MCC. Alternatively, e.g., epithelial (stem) cells or early B cells have been proposed. MCPyV T antigens have been shown to interact with cellular genes vastly.

Design: We stably introduced the MCPyV oncogenes sT and LT antigens in a MCPyV-negative epithelial cell line MCC13 and the MCPyV-negative acute lymphatic leukemia B-cell line REH and analyzed and compared the gene expression changes after induction of sT and LT expression. In addition, we compared the obtained expression patterns with gene expression patterns of 14 primary MCCs. We assessed the MCPyV effects using gene ontology analysis to analyze the functional association of MCPyV-T antigens expressed in MCC13 and REH cell lines with neurological terms. Pathway enrichment analysis was used to visualize molecular networks with the integrated gene expression profiles.

Results: In the lymphoid background, MCPyV T antigens' global effects are higher than the epithelial background. This effect is mainly attributed to the higher downregulation of genes caused by the sT antigen. Genes upregulated in the presence of MCPyV sT antigen were associated with neurological gene ontologies in both cell lines, and essential genes in neuronal development were enriched in pathways that have been implicated in human cancers e.g., axon guidance. We then assessed the expression of the significant genes involved in these pathways in the primary MCC cell lines and tumors, of which all genes were highly expressed.

Conclusions: The expression of MCPyV T antigens in epithelial and lymphoid background affects neurological gene ontologies in both backgrounds. However, more effects are seen by sT antigen expression in the lymphoid background. These novel cell lines represent an important innovative tool for studying the origin of MCPyV-associated MCCs and underlying MCPyV-associated molecular changes.

312 PRAME Expression in Melanocytic Neoplasms of Special Sites

Joseph Maniaci[1], Shyam Raghavan[2]
[1]University of Virginia, Charlottesville, VA, [2]University of Virginia School of Medicine, Charlottesville, VA

Disclosures: Joseph Maniaci: None; Shyam Raghavan: None

Background: The differentiation of melanocytic lesions can present a fair challenge, especially for the subset of nevi occurring at special sites (breast, ear, acral skin, the genitalia, and the scalp). Benign special site nevi are permitted a greater degree of abnormal cytology and growth patterns due to variations in the tissue microanatomy. Special site nevi may harbor both confluence of melanocytes and pagetoid spread at the center of the lesion, which would not be permitted in benign nevi at ordinary sites. Pathologists must orient themselves to the more liberal thresholds delineating the malignant from the benign in these specific areas.

PRAME (PReferentially expressed Antigen in MElanoma) is an antigen that was first identified in tumor-reactive T-cell clones in

patients with malignant melanoma. Significant work has been done showing its utility in distinguishing melanoma from benign melanocytic lesions [Lezcano C, et al., PRAME Expression in Melanocytic Tumors. PMID: 30045064]. However, its expression pattern in nevi of special sites has yet to be elucidated. Herein, we present data characterizing PRAME expression in these challenging lesions.

Design: We performed a retrospective case review at our institution and collected a panel of 35 special site nevi which were previously diagnosed as benign by a trained dermatopathologist. Site breakdown was as follows: acral surfaces (1), axilla (8), breast (16), labial (2), peri-umbilical (7), vulvar (1). H&E slides were examined to verify the diagnosis of special-site nevus. In addition, 10 melanoma and 10 melanoma in situ were collected to serve as positive controls. For all cases, sections were prepared and stained with a PRAME antibody and expression was graded by a trained dermatopathologist using the criteria established by Lezcano et al.

Results: Of our 35 cases, 19 (54%) cases had no staining (0+) for PRAME, 12 cases (34%) demonstrated 1+ PRAME expression, and 4 cases (11%) demonstrated 2+ PRAME expression. No cases showed 3+ or 4+ expression. All cases of melanoma-in-situ and melanoma showed 4+ expression.

Conclusions: Due to their atypical features, special site nevi can be challenging to assess. In this study, we have shown PRAME expression to be a reliable marker to distinguish benign from malignant. 100% of benign special site nevi demonstrated 2+ expression or less, with nearly 54% demonstrating no expression at all, highlighting the utility of PRAME staining for the differentiation of melanocytic neoplasms at special sites.

313 UV Mutational Signature Analysis by Next-Generation Sequencing Suggests Origin from Occult Cutaneous Primaries with Implications for Clinical Management

Douglas Mata[1], Zoe Fleischmann[2], Julie Tse[3], Douglas Lin[1], Matthew Hiemenz[1], Donna Ferguson[4], Tyler Janovitz[1], Jonathan Killian[1], Iain Speece[1], Matthew Margolis[1], Mirna Lechpammer[1], Vamsi Parimi[2], Garrett Frampton[5], Erik Williams[6], Richard Huang[7], Jeffrey Ross[8], Mia Levy[3], Geoffrey Oxnard[1], Ethan Sokol[1], Brennan Decker[1]
[1]Foundation Medicine, Inc., Cambridge, MA, [2]Foundation Medicine, Inc., RTP, NC, [3]Foundation Medicine, Inc., Boston, MA, [4]Foundation Medicine, Inc., Raleigh, NC, [5]Foundation Medicine, Inc., [6]University of California San Francisco, San Francisco, CA, [7]Foundation Medicine, Inc., Cary, NC, [8]SUNY Upstate Medical University, Syracuse, NY

Disclosures: Douglas Mata: *Employee*, Foundation Medicine, Inc.; *Speaker*, Astellas Pharma, Inc.; Zoe Fleischmann: None; Julie Tse: *Employee*, Foundation Medicine, Inc.; Douglas Lin: *Employee*, Foundation Medicine, Inc.; *Stock Ownership*, Roche; Matthew Hiemenz: *Employee*, Foundation Medicine / Roche; Donna Ferguson: None; Tyler Janovitz: *Employee*, Foundation Medicine; *Employee*, Roche; Jonathan Killian: *Employee*, Foundation Medicine; Iain Speece: None; Matthew Margolis: None; Mirna Lechpammer: *Employee*, Foundation Medicine, Inc; Vamsi Parimi: *Employee*, Foundation Medicine Inc.; Garrett Frampton: None; Erik Williams: *Employee*, Foundation Medicine, Inc.; Richard Huang: *Employee*, Foundation Medicine; *Employee*, Roche; Jeffrey Ross: *Employee*, Foundation Medicine; Mia Levy: None; Geoffrey Oxnard: *Employee*, Foundation Medicine; *Stock Ownership*, Roche; Ethan Sokol: *Employee*, Foundation Medicine; *Stock Ownership*, Roche; Brennan Decker: *Employee*, Foundation Medicine; *Stock Ownership*, Roche

Background: Ultraviolet (UV) radiation exposure causes a characteristic mutational pattern (Cosmic signature 7) associated with elevated tumor mutational burden (TMB) and suggests cutaneous origin in cancers of uncertain primary site. We examined the frequency of UV signatures in a pan-cancer next-generation sequencing (NGS) database.

Design: Retrospective cohort study of solid tumors tested using a hybrid-capture NGS panel during routine clinical care. Signature calling was performed using non-negative matrix factorization fitted to the COSMIC database (v2-March 2015) and included all predicted somatic point mutations with unknown functional status. At least 10 mutations were required for signature analysis.

Results: Among 295,149 cases, 22.0% (65,030/295,149) had sufficient mutations for signature analysis, of which 11.1% (7,212/65,030) exhibited UV signatures (median TMB, 31.3 mut/Mb). In all, 54.6% (3,939/7,212) were submitted as tumors of cutaneous origin (including 2,730 melanomas, 754 squamous cell carcinomas [SCCs], 172 basal-cell carcinomas, 142 Merkel-cell carcinomas, 79 angiosarcomas, 35 adnexal carcinomas, and 27 other mesenchymal neoplasms), thus detection of a UV signature supported the diagnosis. Also, 35.3% (2,543/7,212) were submitted as tumors without a specified primary site (including 1,984 melanomas; 208 SCCs; 142 carcinomas, NOS; 66 neuroendocrine carcinomas; 27 adenocarcinomas; 5 sarcomas; and 111 other tumors), thus detection of a UV signature raised the possibility of cutaneous origin and a more precise tumor classification. Last, 10.1% (730/7,212) were submitted as tumors of extra-cutaneous origin, thus detection of a UV signature raised the possibility of an occult cutaneous primary and suggested the potential for reclassification upon further clinicopathologic evaluation. Potentially

misclassified cases included 150 lung SCCs, 143 non-squamous lung cancers, 78 salivary gland cancers, 35 breast carcinomas, 29 malignant peripheral nerve sheath tumors, 17 urothelial carcinomas, 3 clear-cell sarcomas, and 275 other tumors.

Conclusions: NGS-based UV mutational signature analysis can refine the primary site in cancers of uncertain origin and suggest alternative diagnoses in tumors initially classified as extra-cutaneous, thus providing a complementary tool to the standard histological and immunohistochemical workup with important implications for clinical management.

314 p16 and BRAF V600E Immunohistochemical Staining to Predict Chromosomal Abnormalities in Spitzoid Melanocytic Lesions and their Superiority to PRAME

John McAfee[1], Xuefei Jia[2], Elizabeth Azzato[3], Caroline Astbury[1], Shira Ronen[1], Steven Billings[4], Jennifer Ko[1]
[1]Cleveland Clinic, Cleveland, OH, [2]Cleveland Clinic Quantitative Health Sciences, Cleveland, OH, [3]Cleveland Clinic Foundation, Cleveland, OH, [4]Cleveland Clinic, Lerner College of Medicine, Cleveland, OH

Disclosures: John McAfee: None; Xuefei Jia: None; Elizabeth Azzato: None; Caroline Astbury: None; Shira Ronen: None; Steven Billings: None; Jennifer Ko: None

Background: Spitzoid melanocytic neoplasms are often diagnostically challenging and require ancillary testing including immunohistochemistry (IHC) and fluorescence *in situ* hybridization (FISH). The *BRAF* V600E mutation rules out Spitz tumors, and p16 loss can be seen in high risk or malignant Spitz tumors, as well as melanoma. FISH can be technically challenging to perform and interpret, and is not universally available. The ability to predict chromosomal abnormalities with IHC could help better select cases where FISH may or may not be required.

Design: All spitzoid neoplasms tested by FISH for aberrations in 6q23, 6p25, 8q24, 9p21, and 11q13 at our institution (2013-2021) were reviewed. IHC results for p16, BRAF V600E, and PRAME expression were examined and correlated with FISH findings.

Results: Results are summarized in Table 1. We identified 163 cases. There was a 2:1 female predominance. The average age at diagnosis was 30 years. Fifty-seven cases (35%) showed chromosomal abnormalities by FISH. Absolute gain of 6p25 (*RREB1* > 2) was the most common abnormality. The majority of FISH-negative lesions were called atypical Spitz tumors (68/106, 64%) while the majority of FISH-positive lesions were called spitzoid melanoma (48/57, 84%). Among cases that were stained, p16 was lost in 53/123 cases (44%), mutant BRAF V600E was expressed in 12/77 (16%), and PRAME was expressed in 7/37 cases (24%). Loss of p16 expression was significantly associated with FISH abnormalities ($p < 0.001$, Fisher's exact test). 6/53 cases with p16 loss had retained 9p21; the rest showed homozygous loss. BRAF V600E and PRAME expression were not associated with chromosomal abnormalities alone (p=0.114; and p=0.095, respectively, Fisher's exact test); but, BRAF V600E expression was significantly associated with FISH abnormalities when p16 was retained (p=0.03, Fisher's exact test). When examined as a double-screen, p16-retained and BRAF-negative lesions had low rates of chromosomal abnormalities (5/32, 16%), while all other marker combinations had high rates of FISH positivity (70-80% of cases; $p < 0.001$).

Table 1. Characteristics of Spitzoid Lesions Evaluated with FISH

Factor †	All cases	FISH+	FISH-
Sex	n = 163	n = 57	n = 106
Male	54 (33%)	21 (36%)	33 (32%)
Female	109 (67%)	36 (64%)	73 (68%)
Age at diagnosis	n = 163	n = 57	n = 106
Average (SD)	30 (17)	29 (17)	30 (17)
Median (IQR)	28 (17-41)	25 (16-39)	31 (17-42)
Range	5 mo - 74 yrs	1 -74 yrs	5 mo - 67 yrs
Tumor site	n = 163	n = 57	n = 106
Extremities	75 (46%)	29 (51%)	46 (43%)
Head and neck	39 (24%)	12 (21%)	27 (25%)
Trunk	33 (20%)	11 (19%)	22 (21%)
Acral	8 (5%)	2 (4%)	6 (6%)
Special site (breast/genital)	8 (5%)	3 (5%)	5 (5%)
Dermal Mitotic Figures	n = 132	n = 56	n = 76
Average (SD)	1.2	1.6 (1.9)*	0.8 (1.3)*
Median (IQR)	1 (0-2)	1 (0-2)	0 (0-1)
Range	0-10	0-10	0-8
Diagnosis	n = 163	n = 57	n = 106
Spitz Nevus	20 (12%)	0	20 (19%)
Atypical Spitz Tumor	74 (45%)	6 (11%)	68 (64%)

Spitz Melanoma	2 (1%)	2 (4%)	0
Spitzoid Melanoma	52 (32%)	48 (84%)	4 (4%)
Dysplastic nevus, spitzoid	13 (8%)	1 (2%)	12 (11%)
BAP1-inactivated nevus	2 (1%)	0	2 (2%)
FISH Probe	n = 163	n = 57	n = 106
RREB1 > 2	45 (28%)	39 (68%)	6 (6%)‡ #
CCND1 > 2	32 (20%)	27 (47%)	5 (5%)‡
RREB1 > CEP6	10 (6%)	7 (12%)	3 (3%)‡
MYB < CEP6	20 (12%)	19 (34%)	0
	n = 93	n = 31	n = 62
MYC > 2	15 (16%)	14 (45%)	1 (2%)‡
CDKN2A homozygous del.	11 (12%)	11 (37%)	0
p16	n = 123	n = 43	n = 80
Retained	68 (56%)	13 (32%)**	55 (69%)**
Lost	53 (44%)	28 (68%)	25 (31%)
BRAF V600E	n = 77	n = 38	n = 39
Positive	12 (16%)	9 (23%)***	3 (8%)***
Negative	65 (84%)	30 (77%)	35 (92%)
PRAME	n = 37	n = 22	n = 15
Positive	7 (24%)	2 (9%)****	5 (38%)****
Negative			
0%	27	17	10
<25%	1	1	0
25-75%	2	2	0
SD, standard deviation; IQR, interquartile range;			
†means all cases where that feature was accessible; denominator varies between attributes. Percentages may not add to 100 due to rounding.			
‡These values reflect the five cases that were confirmed tetraploid			
#One case barely surpassed threshold and was called negative based on clinical judgment			
*p=0.007, Wilcoxon rank-sum test			
**p < 0.001, Fisher's exact test			
***p = 0.114, Fisher's exact test			
****p = 0.095, Fisher's exact test			

Conclusions: When used together, p16 and BRAF V600E IHC may predict the presence of chromosomal abnormalities as detected by FISH. p16 loss is associated with FISH abnormalities. In cases where p16 is retained, BRAF V600E mutant protein expression also predicts FISH abnormalities. PRAME appears to have limited utility in this setting.

315 The Routine Use of TRBC1 in Flow Cytometric Analysis of Skin Biopsy Specimens

Howard Meyerson[1], Aleksandar Krbanjevic[2]
[1]University Hospital Case Medical Center, Cleveland, OH, [2]Case Western Reserve University/University Hospitals Cleveland Medical Center, Cleveland, OH

Disclosures: Howard Meyerson: None; Aleksandar Krbanjevic: None

Background: Evaluation for T cell neoplasms in skin biopsy specimens by FCM is notoriously difficult due to low cell yields and small populations of clonal T cells. In the last few years, the introduction of the T cell receptor beta chain constant region 1 (TRBC1) antibody has facilitated the detection of clonal T cells in blood, bone marrow and tissue biopsy specimens. We therefore evaluated the utility TRBC1 to detect clonal T cell populations in skin biopsy specimens.

Design: Skin biopsies sent for FCM analysis with TRBC1 staining were identified based on review of the FCM records at UH Cleveland Medical Center. The following 6 color staining tube was employed: TRBC1-FITC, TCRgamma/delta-PE, CD4-PERCp-Cy5.5, CD8-APC, CD3-V450, CD45-V500. The percentage of TRBC1+ cells within the total CD4+ and CD8+ T cells was evaluated as well as gated subsets based on increased forward light scatter (FSC hi), side angle light scatter (SSC hi), increased CD45 (CD45 bright) and/ or decreased CD3 expression. A T cell clone was determined to be present if >95% of the cells were TRBC1+ or TRBC1- within the gated cell region. Clone size was the determined and correlation with TCR clonality determined by molecular methods was also performed.

Results: 40 samples were evaluated. A TRBC1 restricted clone was identified in 18. 1 sample was equivocal. The mean number of cells collected in clonal cases was 12600 (range 400-54000) vs 27860 (range 80-100000) in non-clonal samples, p = 0.06.

Average clone size was 29% (range 1-75%). A TRBC1 restricted population was detected in only 1/18 specimens when total CD4+ T cells or CD8+ T cells were gated (TRBC1 range 5-77%). TRBC1 clonality was identified in vast majority of cases after sub-gating on CD45bright/SSC hi, CD3dim, or FSC hi/SSC hi CD4+ or CD8+ T cells. A positive TCR gene rearrangement was identified in 11/12 TRBC1 clonal cases examined. Two cases were positive for a TCR gene rearrangement on a separate biopsy. The remaining samples (n= 4) were diagnostic morphologically. Four cases lacking a clonally-restricted TRBC1 population contained T cell lymphoma. Three of which were TCR gamma/delta clones. One case was an atypical lymphoid infiltrate with a positive TCR gene rearrangement. A repeat biopsy showed CTCL-MF type 7 months later.

Conclusions: Demonstration of clonality by TRBC1 via FCM is useful in skin biopsies but first requires recognition by the flow cytometrist of the presence of an atypical SSC hi, FSC hi, CD3dim or CD45bright T cell population.

316 Clinicopathologic Characterization of Cutaneous Adult T-cell leukemia/lymphoma (ATLL): A Single Tertiary Care-Center Experience in the United States

Mitul Modi[1], Jiani Chai[1], Ukuemi Edema[2], Shazia Khan[1], Yanhua Wang[3], Yang Shi[1]
[1]Albert Einstein College of Medicine, Montefiore Medical Center, Bronx, NY, [2]Montefiore Medical Center - Moses Division, Bronx, NY, [3]Albert Einstein College of Medicine, Bronx, NY

Disclosures: Mitul Modi: None; Jiani Chai: None; Ukuemi Edema: None; Shazia Khan: None; Yanhua Wang: None; Yang Shi: None

Background: ATLL is a rare mature T cell leukemia/lymphoma associated with human T lymphotropic virus (HTLV-1) infection. Patients may present with skin rash before/at/after diagnosis. The dermatopathological findings may vary in patients and can be diagnostically challenging. Here, we characterized the clinical, dermatopathological, immunophenotypic and molecular findings of ATLL patients with skin involvement in order to facilitate diagnosis.

Design: We retrospectively identified 110 patients with ATLL at one institution in a 19-year period (2003-2021). 19 patients had skin involvement by ATLL. Cases were further stratified into skin-first (initially diagnosed on skin biopsy) and skin-second (skin involvement after known diagnosis of ATLL). Clinical presentations, dermatological, immunophenotypic and molecular findings were studied.

Results: The cohort included 13 skin-first (5 acute, 2 chronic, 5 lymphomatous, 1 smoldering), 5 skin-second (1 smoldering, 4 acute), 1 without clinical information and 91 skin uninvolved patients. The mean age is 54.8 years (28-81); 12 (63%) were female. 14 patients were of Caribbean origin (73%), 3 were of Hispanic ethnicity. Skin manifestations at diagnosis include papular (5), erythroderma (1), nodulotumoral (3), plaques (1), patches (1), and 2 patients presented with combination of skin rashes (papular and erythrodermic; patches, plaques and papular). Histopathological findings included large pleomorphic cells, angiocentrism, epidermal infiltration with large pautrier-like microabscesses, and folliculotropism. Immunophenotypically, 78.9% (15/19) of cases showed CD4+/CD7-/CD25+, while other immunophenotypic patterns are described in table 1. Five patients had next generation sequencing performed, which demonstrating multiple variable mutations (Table 1).

Table 1: Clinicopathological characteristics of cutaneous Adult T Cell Leukemia/Lymphoma

Number of patients	19/110
Average Age (years)	54.8 (range 28-81)
Gender	Female: 12 (63%); Male: 7 (36%)
Skin-first (clinical variant)	13/18 (72.2%)
Acute	5
Lymphomatous	5
Chronic	2
Smoldering	1
Skin-second (clinical variant)	5/18 (27.8%)
Acute	4
Smoldering	1
Clinical skin manifestations	
nodulotumoral	3
Multipapular	5
plaques	1
patches	1
erythroderma	1
papular + erythroderma	1

patches+plaques+papular	1
Others	4
TCR gene rearrangement	100% (8/8) positive
Ethnicity	77.8% (14/18) Caribbean; 16.7% (3/18) Hispanic; 5.6 % (1/18) born in US with Caribbean parents
Immunophenotype	
CD4+/CD8-/CD7-/CD25+	78.9% (15/19)
CD4+/CD8+/CD7+/CD25+	10.5% (2/19)
CD4+/CD8+/CD7-/CD25+	5.3% (1/19)
CD4-/CD8+/CD7+/CD5-/CD25+	5.3% (1/19)
Next Generation Sequencing	
lymphomatous ATLL (1)	CDH1, EP300
acute ATLL (1)	BRAC2, CARD11, HIST1H1E, MSH2, PLCG2
lymphomatous ATLL (1)	NF1, NOTCH1, P2RY8
chronic ATLL (1)	ATM, CSF3R
smoldering ATLL (1)	ATM, BRCA1, CEBPA, PIK3CD, STAT3

Figure 1 - 316

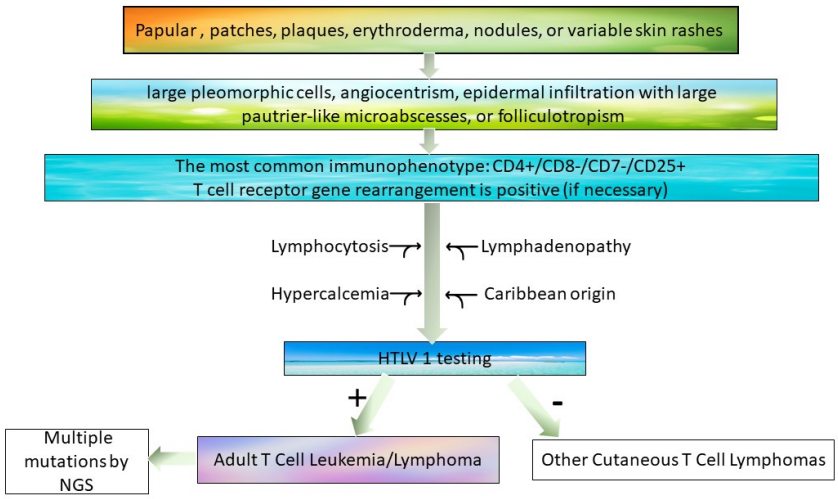

Figure 1 Diagnostic Flow Chart for Cutaneous Adult T Cell Leukemia/Lymphoma

Conclusions: Diagnosis of ATLL on skin biopsy can be initially challenging. Clinical manifestations are variable, ranging from papular to nodular lesions. Familiarity with clinicopathologic features with molecular ancillary testing may aid diagnosis. Pleomorphic large, atypical cells with CD4+/CD25+/CD7- immunophenotype in patients with Caribbean origin raise suspicion. If the patient has lymphocytosis, hypercalcemia, lymphadenopathy, then HTLV-1 testing is needed to confirm diagnosis. T cell receptor gene rearrangement is frequently positive, and neoplasms usually demonstrate multiple mutations in next generation sequencing study. A diagnostic flow chart is graphically demonstrated in Figure 1.

317 Evaluation of Performance and Impact of a Pathology Deep Learning System to Classify Skin Specimens Prior to Routine Pathology Review

Kiran Motaparthi[1], Michael Bonham[2], Julianna Ianni[2], Aysegul Ergin[2], Liren Zhu[2], Pratik Patel[2], Jason Lee[3]
[1]University of Florida College of Medicine, Gainesville, FL, [2]Proscia Inc, Philadelphia, PA, [3]Sidney Kimmel Medical College, Thomas Jefferson University, Philadelphia, PA

Disclosures: Kiran Motaparthi: *Grant or Research Support*, Proscia, Inc.; *Consultant*, Castle Biosciences; Michael Bonham: *Employee*, Proscia Inc; Julianna Ianni: *Employee*, Proscia Inc; Aysegul Ergin: *Employee*, Proscia Inc.; Liren Zhu: *Employee*, Proscia; Pratik Patel: None; Jason Lee: *Primary Investigator*, Proscia

Background: The adoption of digital pathology has enabled use of machine learning and artificial intelligence algorithms to improve accuracy and efficiency in the pathology lab. We deployed a pathology deep learning system (PDLS) which can classify whole slide images (WSIs) from any skin specimen into one of six morphological classes (melanocytic-high, melanocytic-suspect, melanocytic, basaloid, squamous, and other) to prioritize the pathologist's worklist before review (1). We used the PDLS to

prospectively assess performance at two different academic medical centers and measure the impact of the PDLS on the pathologist's diagnosis and review time.

Design: Our dataset consisted of WSIs from 1422 skin specimens prospectively collected over 14 weeks. Specimens were first diagnosed per routine using glass slides. Following sign out, slides were acquired as WSIs, uploaded to the PDLS, and reviewed digitally by a second dermatopathologist with or without the PDLS results. Accuracy of the PDLS compared to the glass diagnosis and the inter-pathologist concordance between glass and digital diagnoses were evaluated. Pathologist review efficiency was calculated by measuring the length of time between opening the first image for a specimen and generating a diagnosis.

Results: The PDLS provided a classification result on 84% of all specimens with an overall specimen level accuracy of 77%. Classification of specific diagnostic groups are listed in table 1. The inter-pathologist discordance rate for glass to digital review alone was 5.1% versus a discordance rate of 5.6% for glass to digital plus PDLS. Median pathology review time per case was 11.6 and 17.2% faster at the two laboratories using a digital plus PDLS workflow over a digital workflow alone.

Table 1: Diagnosis Specific Performance

Diagnosis	Sensitivity	Specificity
Melanoma/MIS/Severe Dysplastic Nevi (Melanocytic High/Suspect)	0.93	0.91
All benign nevi (Melanocytic)	0.73	0.97
Basal Cell Carcinoma (Basaloid)	0.83	0.98
Squamous Cell Carcinoma (Squamous)	0.74	0.94

Conclusions: We successfully demonstrated the capability of the PDLS to accurately classify skin specimens by morphology alone prior to pathology review within a routine laboratory workflow. The prospective performance of the PDLS is reproducible to a larger retrospective study (1) and was consistent over a period of 14 weeks. Use of the PDLS during review did not significantly increase the glass to digital discordance rate. With the ability to classify, sort and triage skin specimens, the PDLS has the potential to reduce digital pathology review times and improve the distribution of case workloads within a pathology laboratory without introducing significant bias in diagnosis.

1) Sankarapandian, S, et al. arXiv preprint arXiv:2109.07554 (2021).

318 Imaging Mass Spectrometry Aids in the Classification of Capsular Nevi Versus Metastatic Melanoma in Lymph Nodes

Caroline Mullins Underwood[1], Jessica Moore[2], Heath Patterson[3], Sarah Nicholson[4], Jeremy Norris[2], Maria Angelica Selim[5], Michelle Schneider[5], Ahmed Alomari[6], Rami Al-Rohil[7]
[1]Duke University Health System, Durham, NC, [2]Frontier Diagnostics, Nashville, TN, [3]Vanderbilt University, Nashville, TN, [4]Nashville, TN, [5]Duke University, Durham, NC, [6]Indiana University School of Medicine, Indianapolis, IN, [7]Duke University School of Medicine, Durham, NC

Disclosures: Caroline Mullins Underwood: None; Jessica Moore: *Employee*, Frontier Diagnostics; *Employee*, Frontier Diagnostics; Heath Patterson: *Employee*, Frontier Diagnostics; Sarah Nicholson: *Employee*, Frontier Diagnostics; Jeremy Norris: *Stock Ownership*, Frontier Diagnostics, LLC; Maria Angelica Selim: None; Michelle Schneider: None; Ahmed Alomari: None; Rami Al-Rohil: *Consultant*, Frontier Diagnostics; *Employee*, Foundation Medicine Inc.

Background: Distinguishing metastatic melanoma from capsular nevi in lymph nodes relies on histopathologic evaluation, but this classification can be difficult. Immunohistochemistry has shown utility in limited studies and few molecular studies have assessed capsular nevi. Matrix-Assisted Laser Desorption/Ionization Mass Spectrometry (MALDI MS) technology has ideal characteristics for *in situ* molecular analysis and compares mass spectra collected from tissues with known pathologic outcomes to discover unique molecular signatures. These signatures can aid in differentiating disease states in tissues of unknown pathology.

Design: We investigated the validity of MALDI MS in classifying capsular nevi verses metastatic melanoma deposits in lymph nodes. To prove the high-performance parameters of this platform relative to histopathologic evaluation, lymph nodes containing capsular nevi (13) and metastatic melanoma deposits (16) were both analyzed. The mean patient age was 64-years-old. Lymph nodes containing capsular nevi were axillary (11), cervical (1), and inguinal (1). Lymph nodes containing metastatic melanoma were axillary (7), inguinal (4), cervical (1), epitrochlear (1), retroperitoneal (1), post-auricular (1), and unknown (1). Regions of interest were annotated using a 50 µm spot tool, and the annotated slide image was registered to 6-micron thick serial section for mass spectrometry. Serial sections were antigen retrieved and digested using the enzyme trypsin to release peptides from the tissue. MALDI matrix was applied to extract peptides and mass spectra were obtained from annotated areas.

Results: Mass spectra were extracted and spectra normalized before peak-picking. Mass spectra were compared for metastatic melanoma and capsular nevi with analysis revealing several unique peaks for each entity. Figure 1A compares averaged spectra extracted from a sample containing metastatic melanoma (red) and a capsular nevus (blue). A peak unique to metastatic melanoma is shown in figure 1B and a peak unique to the capsular nevus is shown in figure 1C. Certain peaks (ex. m/z 816.4, 944.5) were present in all samples.

Figure 1 - 318

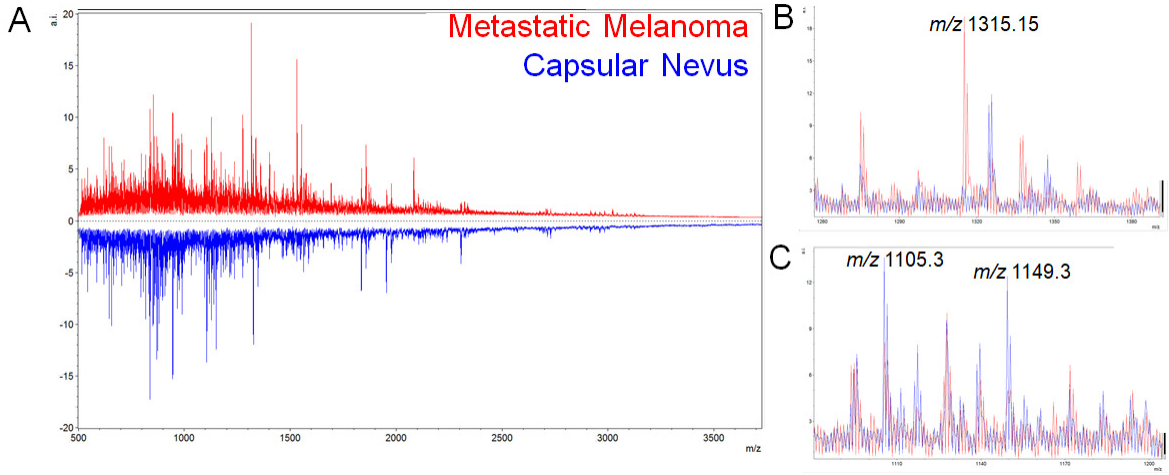

Conclusions: These findings support the utility of MALDI MS as an analytical tool for differentiating capsular nevi verses metastatic melanoma in lymph nodes, aiding in diagnosis while requiring minimal tissue. Additional studies, including larger sample sets, are needed to further develop and validate MALDI MS for the automatic classification of capsular nevi and metastatic melanoma.

319 Exploratory Analyses of Tumor-Infiltrating Inflammatory Cells in Male Genitourinary Melanoma

Priya Nagarajan[1], Frederico Gleber-Netto[1], Edwin Parra[1], Curtis Pickering[1], Michael Davies[1], Phyu Aung[1], Woo Cheal Cho[1], Carlos Torres-Cabala[1], Jonathan Curry[1], Doina Ivan[1], Victor Prieto[1], Curtis Pettaway[1]
[1]The University of Texas MD Anderson Cancer Center, Houston, TX

Disclosures: Priya Nagarajan: None; Frederico Gleber-Netto: None; Edwin Parra: None; Curtis Pickering: None; Michael Davies: *Consultant*, Roche/Genentech, Array, Pfizer, Novartis, BMS, Apexigen, Eisai; *Advisory Board Member*, ABM Therapeutics; Phyu Aung: None; Woo Cheal Cho: None; Carlos Torres-Cabala: None; Jonathan Curry: None; Doina Ivan: None; Victor Prieto: *Consultant*, Novartis, Orlucent; Curtis Pettaway: None

Background: Male genitourinary melanoma (MGUM) is the rarest type of anogenital melanoma with incidence of 0.14 to 0.19 cases/million men and may be of cutaneous (penile shaft, outer foreskin) and mucosal (glans, inner foreskin, meatus, urethra) origin. Immune features have been shown to correlate with clinical outcomes and responsiveness to immunotherapy in cutaneous melanomas, but little is known about the status and significance of tumor-infiltrating inflammatory cells (TILCs) in MGUM.

Design: We evaluated 10 cases of MGUM using 2 multiplex immunofluorescence mIF panels encompassing SOX10 CD3 CD8 PD1 PDL1 CD68 CD45RO FoxP3 and granzyme B to determine the density, distribution and composition of TILs and T-cell activation (Figure 1). A minimum area of 0.65mm^2 was evaluated for each case and the results were expressed as the average cell density/mm^2. One-way and Wilcoxon analyses were performed to determine associations with histological features and outcomes.

Results: Most patients were white (n=9) with median age of 71.5y (range 19-83y); anatomic site: 4 cutaneous, 6 mucosal (all urethral); 6 patients died, including 4 due to progression of MGUM; 1 of 4 surviving patients had melanoma, while 3 were free of disease at the last follow-up. Mucosal MGUMs had higher density of cytotoxic T-cells (p=0.07) and antigen-experienced T-cells (p=0.05), compared to cutaneous MGUMs, while presence of ulceration associated with lower density of tumor PDL1+ cytotoxic antigen-experienced T-cells (p=0.04). Spindled cytology correlated with lower density of T-cells (p=0.03), cytotoxic T-cells (p=0.01),

PD-L1-positive T-cells (p=0.9) and tumor-associated macrophages (p=0.05). In this small cohort, there was a trend for (**a**) shorter disease-specific survival with lower densities of cytotoxic T-cells (p=0.07), memory T-cells (p=0.07) and macrophages (p=0.08) (Figure 2), and (**b**) shorter overall survival with lower densities of T-cells (p=0.06), memory T-cells (p=0.03), PD-L1-positive T-cells (p=0.05) and antigen experienced T-cells (p=0.05).

Figure 1 - 319

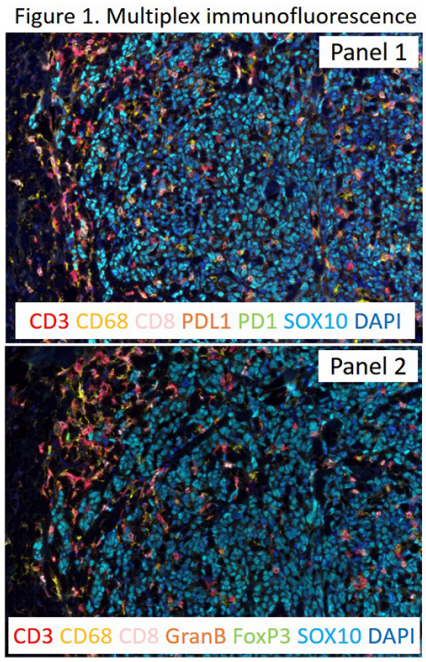

Figure 2 – 319

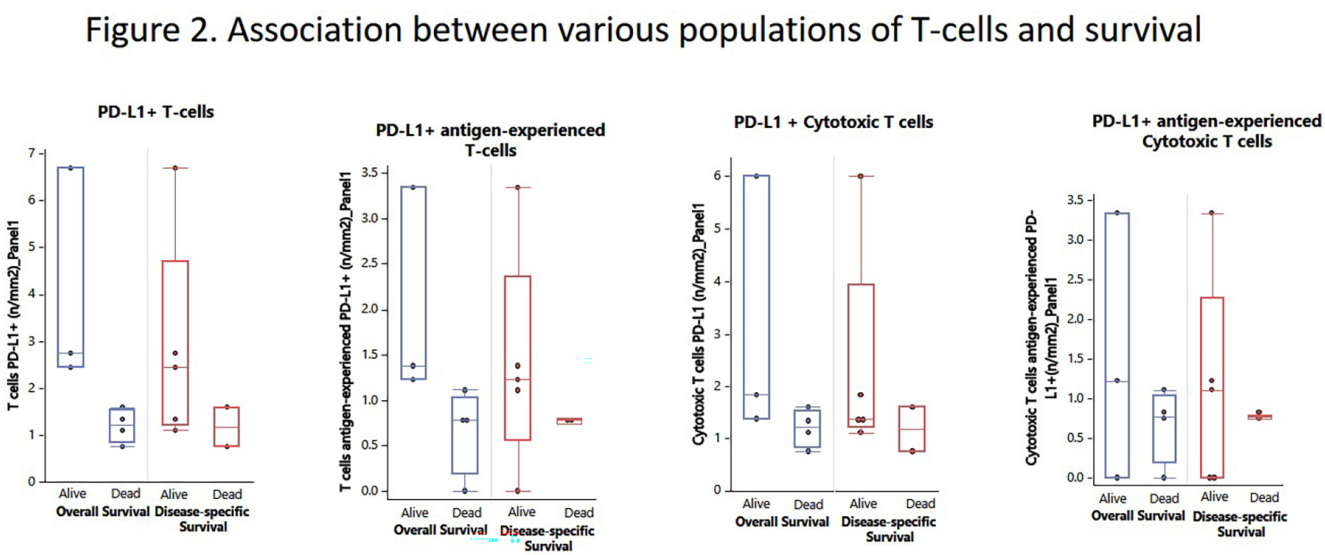

Conclusions: Our exploratory analysis suggests that the density and composition of TILs and macrophages may vary based on anatomic location, ulceration and spindled cytology in MGUM. Lower densities of various types of T cells may correlate with worse prognosis, thus, affect response to immunotherapy in MGUM patients. Studies using larger cohorts are necessary to validate these findings.

320 Quantifying Invasive Melanoma Volume by Deep Learning Segmentation at the Pixel-Level

Neil Neumann[1], Michael Wang[1], Amal Mehta[2], Aman Shah[2], Mara Olson[1], Wudi Fan[2], Anna Weier[3], Avideh Zakhor[2], Timothy McCalmont[1]

[1]University of California, San Francisco, San Francisco, CA, [2]University of California, Berkeley, Berkeley, CA, [3]University of California, Davis, Davis, CA

Disclosures: Neil Neumann: None; Michael Wang: *Consultant*, Singularity.ai; Amal Mehta: None; Aman Shah: None; Mara Olson: None; Wudi Fan: None; Anna Weier: None; Avideh Zakhor: *Primary Investigator*, University of California, Berkeley; Timothy McCalmont: None

Background: Melanoma is the deadliest skin cancer with the fastest rising incidence rate in the United States. The most important predictor of melanoma patient survival is the volume of invasive tumor. Currently there are no clinically robust artificial intelligence (AI) workflows that identify the invasive melanoma at the pixel-level with accuracy approaching practicing dermatopathologists. The current standard of care for outcome prediction is to manually measure a single-dimension tumor thickness, the Breslow thickness, as a proxy for volume (Fig 1A) or more recent work manually approximating tumor cross sectional area (Fig 1B). Neither of these methodologies takes advantage of modern digital pathology workflows (Fig 1C), and both depend on a host of subjectively defined measurements that can lead to incorrect risk assessment and management planning (Fig E-H). A current challenge in using AI to identify the invasive component is that the appearance of melanoma *in situ* and invasive melanoma is similar.

Design: We propose a novel two-stage method to both mitigate subjective measurements and identify invasive melanoma. 57 melanomas (pT1-pT4; 42 training, 15 test set) were identified from the UCSF Dermatopathology archive from 2004-2014, digitally scanned at 40x resolution on a Leica Aperio scanner (~3960 pixels per mm), and then annotated by two dermatopathologists. Next, deep learning separately computes segmentation maps for melanoma and epidermis. The second stage then combines melanoma and epidermis predictions to yield invasive melanoma predictions. Our method utilizes multiple resolutions and downscaling to increase information passed to the model and to improve model accuracy.

Results: Using HRNet+OCR model, a recently updated convolutional neural network algorithm, for both epidermis and melanoma segmentation (Fig 2) in our proposed system results in a marked improvement of F1 score (mIoU) to 0.44 (0.64) as compared to the current state-of-the-art of 0.14 (0.53) (Table 1).

#	Stage 1 Epidermis Model	Stage 1 Melanoma Model	mIoU	fwIoU	F1 Score	Sensitivity
1	HRNet+OCR 1576	HRNet+OCR (IM)	0.58	0.97	0.29	0.28
2	HRNet+OCR 1576	3-Branched HookNet (IM)	0.60	0.97	0.35	0.36
3	HRNet+OCR 1576	UNet (IM)	0.47	0.86	0.13	**0.74**
4	HRNet+OCR 1576	HRNet+OCR (IM ∪ E)	0.61	0.97	0.39	0.42
5	HRNet+OCR 1576	3-Branched HookNet (IM ∪ E)	0.58	0.97	0.32	0.50
6	HRNet+OCR 1576	UNet (IM ∪ E)	0.58	0.96	0.31	0.56
7	HRNet+OCR 3152	HRNet+OCR (IM)	0.56	0.97	0.24	0.22
8	HRNet+OCR 3152	3-Branched HookNet (IM)	0.62	**0.98**	0.41	0.37
9	HRNet+OCR 3152	UNet (IM)	0.49	0.89	0.15	0.18
10	HRNet+OCR 3152	HRNet+OCR (IM ∪ E)	**0.64**	**0.98**	**0.44**	0.39
11	HRNet+OCR 3152	3-Branched Hooknet (IM ∪ E)	0.62	0.97	0.41	0.37
12	HRNet+OCR 3152	UNet (IM ∪ E)	0.6	0.97	0.37	0.53
13	UNet	UNet (IM)	0.47	0.86	0.13	**0.74**
14	UNet	UNet (IM ∪ E)	0.57	0.97	0.27	0.29

IM, invasive melanoma; E, epidermis

Figure 1 - 320

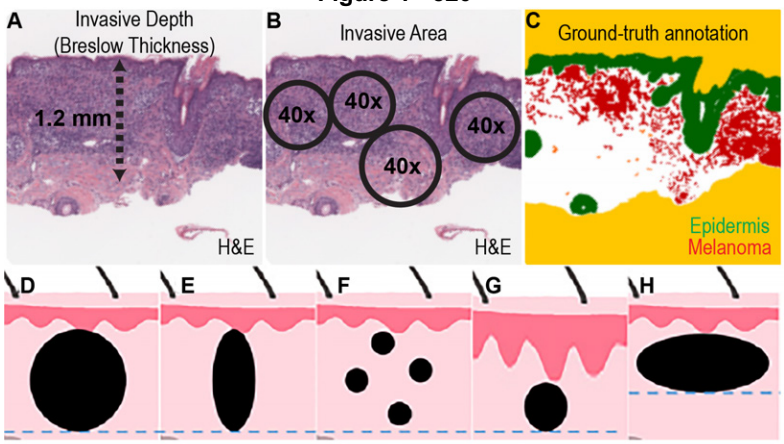

Figure 1. (A) H&E of melanoma with Breslow thickness measured from the granular layer to the deepest aspect of the cancer; (B) Manual area estimation method that counts the number of tumor-occupying microscopic fields combined with tumor density estimation; and (C) an example of dermatopathologist-annotated areas of invasive melanoma (red) with overlying epidermis (green). (D-H) Breslow thickness (blue line) is an inaccurate proxy for tumor volume. It overestimates the tumor volume in (E-G) compared to (D), and it under-estimates the tumor volume in (H).

Figure 2 – 320

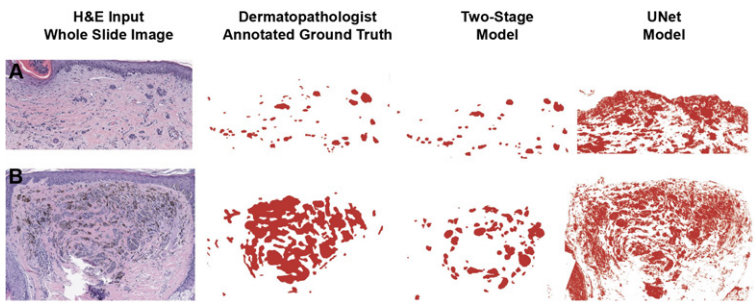

Figure 2. Two examples of predictions from our two-stage model compared to a 2 stage UNet. (A) model predictions on a WSI patch containing a hair follicle; (B) model predictions on a WSI patch of skin without adnexa. For the second row, the full WSI mIoUs of the two-stage approach, and 2 stage UNet are 0.630 and 0.528, respectively.

Conclusions: We propose a novel, two-stage pipeline to markedly improve segmentation of invasive melanoma at the pixel-level in whole slide pathology images. The performance of our models using a test set shows that our method produces superior segmentation results on most melanomas encountered clinically, including smaller tumors not included in previously published data. Future work will expand the training and test sets and correlate the invasive tumor area with clinical variables.

321 Diagnostic and Prognostic Value of PRAME in Cutaneous Melanocytic Lesions

Ourania Parra[1], Zhongze Li[2], Bryan Coffing[3], Konstantinos Linos[1], Shabnam Momtahen[1], Wendy Wells[1], Shaofeng Yan[1]
[1]Dartmouth-Hitchcock Medical Center, Lebanon, NH, [2]Dartmouth Geisel School of Medicine, Lebanon, NH, [3]Metropolitan Pathologists, Lakewood, CO

Disclosures: Ourania Parra: None; Zhongze Li: None; Bryan Coffing: None; Konstantinos Linos: None; Shabnam Momtahen: None; Wendy Wells: None; Shaofeng Yan: None

Background: PRAME is an antigen identified in specific cytotoxic T-cells in a patient with cutaneous melanoma. Its expression has been described in a variety of neoplasms and has been correlated with disease prognosis. PRAME immunohistochemistry is an important ancillary tool in the differential diagnosis between cutaneous benign and malignant melanocytic lesions; however, its prognostic value in melanocytic lesions has not been well studied. In this study, we evaluated PRAME in comparison to Ki67 as a diagnostic and prognostic marker in primary and metastatic melanomas as well as benign nevi.

Design: We analyzed 165 melanocytic lesions (92 primary melanomas, 19 melanoma metastases and 54 nevi) in a tissue microarray using PRAME and Ki67 immunohistochemistry. Nuclear staining of PRAME was scored based on percentage of positive nuclei as follows: 0 no staining, 1+ 1-25%, 2+ 26-50%, 3+ 51-75% and 4+ >75%. The percentage of positive Ki67 nuclei was used to calculate a proliferation index.

Results: The difference in PRAME expression between malignant melanomas and benign nevi was statistically significant ($p < 0.0001$). There was no significant difference in PRAME expression in primary versus metastatic melanomas, or in primary melanomas with versus without metastasis at follow-up. There was a significant association between PRAME expression and mitotic rate ($p=0.047$), as well as Ki67 proliferation index ($p=0.007$). High proliferation index also correlated with ulceration ($p<0.001$), tumor thickness ($P=0.001$) and mitotic rate ($p<0.0001$), but PRAME expression did not show significant correlation with the first two parameters. Neither PRAME nor Ki67 showed a prognostic significance in survival by Kaplan-Meier disease specific survival analyses ($p=0.4$ and 0.24 respectively). In multivariate analysis of patients with primary melanoma, shorter duration of survival was associated with thicker tumor, ulceration, and high mitotic rate ($P=0.002$, 0.01, and <0.001), indicating that these factors are independent predictors of survival. PRAME expression and Ki67 index were not predictive of survival ($P=0.39$ and 0.26).

Conclusions: PRAME is a useful ancillary tool for distinguishing benign from malignant melanocytic lesions. PRAME expression does not distinguish primary melanomas from metastases. Although increased PRAME expression correlates with Ki67 proliferation index and mitotic rate, PRAME is not an independent prognostic marker.

322 Preferentially Expressed Antigen in Melanoma Expression in Merkel Cell Carcinoma and Non-cutaneous High-grade Neuroendocrine Tumor

Neda Rezaee[1], Andrea Krajisnik[1], Bonnie Balzer[1], David Frishberg[2], Wonwoo Shon[1]
[1]Cedars-Sinai Medical Center, Los Angeles, CA, [2]Cedars-Sinai Medical Center, West Hollywood, CA

Disclosures: Neda Rezaee: None; Andrea Krajisnik: None; Bonnie Balzer: *Consultant*, Core Diagnostics; *Consultant*, Castle Biosciences; *Consultant*, PathologyWatch; David Frishberg: None; Wonwoo Shon: None

Background: Preferentially expressed antigen in melanoma (PRAME) is a member of the family of cancer-testis antigens. It is now widely accepted as a valuable diagnostic marker for melanocytic lesions. High levels of PRAME expression have also been found to correlate with shorter overall survival and poor clinical outcomes in various solid tumors. Recently, PRAME was reported to be expressed in a small number of Merkel cell carcinoma (MCC) cases. In this study, we investigated the frequency of PRAME expression in a large series of well-characterized MCC and non-cutaneous high-grade neuroendocrine tumors (HGNET).

Design: Formalin-fixed, paraffin-embedded whole and tissue microarray sections from 37 MCC and 147 non-cutaneous HGNET were obtained and immunostained for PRAME (E7I1B; Cell Signaling Technology, Danvers, MA). Only nuclear PRAME staining was considered to be “positive”. All slides were scanned using Aperio GT450 and Roche Ventana DP200 digital scanner at 40X. Quantitative digital image analysis was performed using QuPath version 0.3.0 and the H-score was generated. MCC PRAME results were further correlated with various clinicopathologic parameters, including MCPyV status, tumor size, morphology, lymph node status, tumor recurrence, and survival time, using Fisher’s exact, Wilcoxon-Mann-Whitney, Kaplan-Meier survival, and log-rank tests.

Results: 16 of 37 (43.2%, H-score range: 1.1-226, median 17.4) MCC, and 16 of 147 (10.9%, H-score range: 2-98, median 27.6) non-cutaneous HGNET expressed PRAME. There was no strong association between the percentage of positive cells and the intensity of PRAME expression. Furthermore, PRAME expression in MCC did not reveal any significant correlation with evaluated clinicopathological parameters.

Conclusions: In this study, we were able to demonstrate that PRAME is overexpressed in a subset of MCC and non-cutaneous HGNET. Thus, PRAME staining has no diagnostic role in distinguishing MCC from other HGNET, but the presence of PRAME expression further highlights the potential for exploring novel immune therapeutic strategies in MCC and other HGNET. Although we did not find a statistically significant relationship between MCC PRAME expression and overall survival or clinical outcomes, these issues should be investigated in a larger, prospective study.

323 Hematoxylin and Eosin (H&E) is Preferable to Double Staining (CD34/SOX10) for the Detection of Lymphovascular Invasion in Cutaneous Melanoma

Costantino Ricci[1], Stefano Chillotti[1], Francesca Ambrosi[2], Angelo Corradini[1], Martina Lambertini[1], Emi Dika[1], Michelangelo Fiorentino[2], Barbara Corti[1]
[1]S.Orsola-Malpighi Hospital, University of Bologna, Bologna, Italy, [2]Maggiore Hospital, University of Bologna, Bologna, Italy

Disclosures: Costantino Ricci: None; Stefano Chillotti: None; Francesca Ambrosi: None; Angelo Corradini: None; Martina Lambertini: None; Emi Dika: None; Michelangelo Fiorentino: None; Barbara Corti: None

Background: Lymphovascular invasion (LVI) is an unfavorable prognostic factor in cutaneous melanoma (CM), but its detection by hematoxylin and eosin (H&E) stain is rare and with not well-known levels of inter- (IrOA) and intra-observer agreement (IaOA). In a previous study of our group, we found that double staining for CD34/SOX10 could increase the detection rate of LVI but how H&E-detected LVI is associated with adverse clinical-pathologic features and improves the IrOA. Herein, we validated the superiority of H&E over CD34/SOX10 and evaluated the association with relevant clinical-pathological features and the effect on IrOA and IaOA.

Design: Five authors independently evaluated 92 consecutive and prospectively enrolled cases of CM. We compared the LVI assessment with H&E and CD34/SOX10, analyzing the association with other clinical-pathological features [χ^2 tests for dichotomous and categorical data; Student *t*-test (normal distribution) and Mann-Whitney *U*-test (non-normal distribution) for continuous data], the IrOA (*Fleiss's* Kappa/FK and intraclass correlation coefficient/ICC) and the IaOA (*Cohen's* Kappa/CK).

Results: LVI was detected in 10 (9.2%) and 11 (10.1%) cases with H&E and IHC, respectively (*McNamar=1.000*). Both H&E and IHC was significantly associated with vertical growth phase (H&E, *p: 0.014*; IHC, *p: 0.010*), mitosis ≥ 1/mm^2 (H&E, *p: 0.000*; IHC, *p: 0.004*), pT (H&E, *p: 0.000*; IHC, *p: 0.001*), pN (H&E, *p: 0.003*; IHC, *p: 0.003*) and Breslow thickness (H&E, *p: 0.000*; IHC, *p: 0.000*); only H&E was associated with ulceration (*p: 0.002*) and distant metastasis (*p: 0.000*). The IrOA was superimposable with H&E (KF=0.446; ICC=0.805) and IHC (KF=0.454; ICC=0.810); the IaOA was higher with H&E for Path2 (H&E: 0.809; IHC: 0.665) and with IHC for Path1 (H&E: 0.492; IHC: 0.563).

Conclusions: Our study proved that CD34/SOX10 does not significantly increase the detection rate of LVI, the IrOA and the IaOA in a routine set of CM. Besides, H&E is associated with a higher number of relevant clinical-pathological features (distant metastasis) and so more suitable than CD34/SOX10 for the prognostic stratification of these patients. These results are relevant because show as the application of CD34/SOX10 to a routine set would have no significant benefits on the prognostic characterization of CM

324 Cutaneous Rosai-Dorfman disease - A Clinicopathologic Study of 27 Cases

Shira Ronen[1], Anurag Sharma[2], Pablo Ortega[3], David Suster[4], Jennifer Ko[1], Steven Billings[5]
[1]Cleveland Clinic, Cleveland, OH, [2]Cleveland Clinic Foundation, Cleveland, OH, [3]Ortega Pathology Lab, Loja, Ecuador, [4]Rutgers New Jersey Medical School/Rutgers University, Newark, NJ, [5]Cleveland Clinic, Lerner College of Medicine, Cleveland, OH

Disclosures: Shira Ronen: None; Anurag Sharma: None; Pablo Ortega: None; David Suster: None; Jennifer Ko: None; Steven Billings: None

Background: Cutaneous Rosai-Dorfman (CRD) is a rare disease characterized by histiocytic proliferation in the skin. CRD restricted exclusively to the skin is even less common.

Design: 52 CRD cases were identified from our anatomic pathology database (2006-2021). Of which 47 were consultation cases. Clinical data and follow-up information were obtained, and histopathological features were evaluated.

Results: 27 cases had slides available for review: 16F;11M with a median age of 51 (range 21-88 years[y]). 11 occurred on the lower extremities (thigh, knee, leg, buttock), 7 cases on the upper extremities (arm, forearm, shoulder), 5 cases on the trunk and back, and 4 cases on the head (cheek and scalp). The clinical presentation varied widely and included nodules, plaques, and papules measuring from 0.5-9.4 cm with the impression of neoplasm, cyst, fixed drug eruption, infection, dermatofibroma, panniculitis, Sweet syndrome, and xanthogranuloma. 14 patients (pt) did not have lymphadenopathy and systemic evidence of disease (unknown status for other cases). 14/19 pt were treated with wide excision, 2/19 with steroids, 2/19 with methotrexate, and 1/19 with thalidomide and hydroxychloroquine. There was no evidence of recurrence or widespread disease in 8/10 pt with a follow-up period of 0.5-11y and 2 pt with cutaneous recurrence. Histologic examination revealed histiocytic proliferation involving

the superficial dermis only (9/27, entire dermis (13/27) and extension to the subcutis (14/27). 2 cases were localized predominantly to the subcutis. The lesions were relatively well circumscribed (14/22) and comprised of large histiocytes with abundant pale eosinophilic cytoplasm and prominent nucleoli. There was a background inflammatory infiltrate composed of lymphocytes (100%), plasma cells (PC) (81%), neutrophils (56%), and eosinophils (18%). Germinal centers were absent. Emperipolesis was a constant element in all the cases and was recognizable on H&E slides. 60% of cases showed fibrosis, mainly in the subcutis. Immunohistochemistry was used to confirm the diagnosis in all cases with S100+ (27/27), CD68+ (17/17), and CD1a- (0/7).

Conclusions: This represents the largest series of patients with CRD to date, a unique entity distinct from systemic RD. CRD is most common in middle age women and extremities. Clinically, they mimic other tumors, infections, and inflammatory disorders and have an indolent clinical course.

325 Extramammary Post-Radiation Atypical Vascular Lesions: A Clinicopathologic Study of Eight Cases

Shira Ronen[1], Steven Billings[2], Jennifer Mcniff[3], Carlos Torres-Cabala[4], Saira George[4], Meghan Heberton[4], Valencia Thomas[4], Phyu Aung[4], Jonathan Curry[4], Woo Cheal Cho[4], Doina Ivan[4], Victor Prieto[4], Priya Nagarajan[4]
[1]Cleveland Clinic, Cleveland, OH, [2]Cleveland Clinic, Lerner College of Medicine, Cleveland, OH, [3]Yale School of Medicine, New Haven, CT, [4]The University of Texas MD Anderson Cancer Center, Houston, TX

Disclosures: Shira Ronen: None; Steven Billings: None; Jennifer Mcniff: None; Carlos Torres-Cabala: None; Saira George: None; Meghan Heberton: None; Valencia Thomas: None; Phyu Aung: None; Jonathan Curry: None; Woo Cheal Cho: None; Doina Ivan: None; Victor Prieto: *Consultant*, Novartis, Orlucent; Priya Nagarajan: None

Background: Atypical vascular lesions (AVL) are well-known complications of radiation and have been reported almost exclusively in the breast after radiation therapy (RT) for breast cancer. Rarely, AVLs have been described in the scalp and larynx following RT. We present unique cases of cutaneous AVLs arising in anatomic sites other than breast or chest wall following RT.

Design: Cutaneous AVL located in sites other than the chest diagnosed between 2010-2020 were retrieved from pathology archives of 3 tertiary medical centers, including 5 consultations from outside institutions and 3 in-house cases. Demographic information, clinical data, and histopathologic features were collected.

Results: 8 patients diagnosed with AVL were found (Table 1), with F=M and a median age of 68.5 years (range 32-86). The most common anatomic site was the neck (n=3), followed by the head (n=2), and calf, forearm, and abdomen (n=1 each). The patients had been treated with adjuvant radiation for squamous cell carcinoma (n=3) and metastatic breast carcinoma, brain cancer, Kaposi sarcoma, Merkel cell carcinoma, and uterine cancer (n=1 each). Where available, the cumulative radiation dose was at least 50 Gy and latency to onset of skin lesions after RT was 0.67-6 years (mean 3.1). Clinical presentations varied widely including macules, ulcerated papules, nodules and plaques. Histologic sections revealed variably sized ectatic lymphovascular spaces lined by a single layer of small, monomorphic, slightly plump endothelial cells. . The lesions were located primarily in the superficial and mid-reticular dermis and lacked significant cytologic atypia, mitotic activity, necrosis or infiltrative growth. Some biopsies showed background features of radiation dermatitis. cMYC immunostains revealed lack of strong and diffuse positivity in endothelial cells in 6/6 cases. The patients were treated conservatively with observation and topical therapies.

Table 1: Atypical vascular lesions presenting in skin locations other than the chest.

Case #	Age(y)/ sex	Tumor type	Prior non-surgical therapy	Anatomic site	Clinical information/impression	Latency interval (years)
1	69/M	Oropharyneal squamous cell carcinoma	Chemoradiation	Bilateral neck	Irregular erythematous coalescing crusted papules and plaques	4
2	79/M	Metastatic squamous cell carcinoma	Chemoradiation	Left posterolateral neck	3 cm eczematous scaly indurated plaque	6
3	66/F	Merkel cell carcinoma	Chemoradiation	Submental/chin	2 cm erythematous nodule	0.67
4	51/F	Metastatic breast carcinoma	Radiation	Right neck	N/A	N/A
5	32/F	Brain cancer	Radiation	Vertex scalp	Nevus sebaceous versus radiation changes	N/A
6	72/M	Classic Kaposi sarcoma (HIV negative)	Radiation	Right calf	Dark macules within the prior radiation field	1
7	68/M	Cutaneous squamous cell carcinoma	Radiation	Right forearm	Persistent, focally ulcerated papule	4
8	86/F	Uterine cancer	Radiation	Right lower abdomen	Thick edematous skin, simulating p'eau d'orange	N/A

Figure 1 - 325

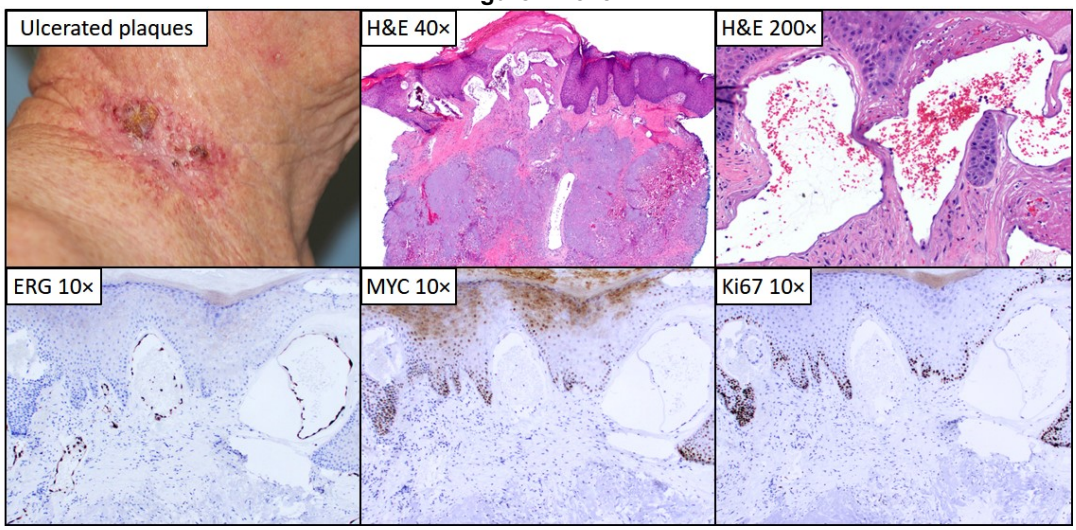

Conclusions: This case series describes the clinical and histopathologic attributes of cutaneous AVL arising in anatomic sites other than the breast. Although rare, these cases emphasize the importance of considering the possibility of AVL and other RT-associated vascular proliferations when evaluating persistent lesions within radiation field. Awareness of this entity is crucial to avoid potential misdiagnosis of such lesions as post-radiation angiosarcoma and for appropriate patient management.

326 Diagnostic Utility of PRAME Immunohistochemistry in Subungual and Acral Melanocytic Lesions

Aimi Rothrock[1], Woo Cheal Cho[1], Priya Nagarajan[1], Jonathan Curry[1], Kaitlin Vanderbeck[1], Doina Ivan[1], Victor Prieto[1], Carlos Torres-Cabala[1], Phyu Aung[1]
[1]The University of Texas MD Anderson Cancer Center, Houston, TX

Disclosures: Aimi Rothrock: None; Woo Cheal Cho: None; Priya Nagarajan: None; Jonathan Curry: None; Kaitlin Vanderbeck: None; Doina Ivan: None; Victor Prieto: *Consultant*, Novartis; *Consultant*, Orlucent; Carlos Torres-Cabala: None; Phyu Aung: None

Background: The novel immunohistochemical (IHC) marker PRAME, or PReferentially expressed Antigen in MElanoma, has had increasing popularity due to its utility as a diagnostic, prognostic and immunotherapeutic marker of various melanomas. Although more studies are warranted to uncover its full potential, its diagnostic utility in helping distinguish banal and dysplastic nevi from their malignant counterpart is promising and exciting, especially in dermatopathology.

Acral melanomas, especially including those of subungual origin, are rare and harbor molecular signatures distinct from those of cutaneous melanomas arising in non-acral sites. To date, only a few studies have investigated PRAME IHC expression in acral melanomas, and expression in subungual melanomas remains largely unknown. Herein, we evaluate the diagnostic utility of PRAME in distinguishing acral and subungual melanomas from their benign counterparts, acral nevi.

Design: After obtaining institutional review board approval, cases of acral nevi and invasive acral melanomas, including those arising in the subungual site, were searched using our institutional pathology database. Ten subungual melanomas, eleven non-subungual acral melanomas, and ten acral nevi with sufficient tissue material for IHC analysis were identified. IHC studies using anti-PRAME antibody (rabbit monoclonal, Abcam, Cambridge, UK) were performed on unstained slides prepared from selected paraffin blocks. The percentage of lesional cells with PRAME expression in our cohort was recorded. Patients' demographics and other relevant clinicopathologic parameters were also documented.

Results: In the subungual melanoma group (Figure 1), 40% (4/10) of subungual melanomas showed diffuse (4+) PRAME expression, while 20% (2/10) lacked immunoreactivity with anti-PRAME (Figure 2). 64% (7/11) of non-subungual acral melanomas exhibited diffuse (4+) PRAME expression; there was one case (9%, 1/11) that completely lacked PRAME expression. In contrast,

none (0%, 0/10) of the acral nevi showed PRAME expression. Overall, the presence of PRAME expression, even focally (1-3+), showed high sensitivity for both non-subungual acral (91.7%) and subungual (83.3%) melanomas, with 100% specificity for melanomas.

Figure 1 - 326

Figure 1: Summary of patients' demographics and clinicopathologic characteristics and PRAME expression

Case #	Lesion#	PRAME expression*	Age at diagnosis	Sex	Location of Primary	Type of specimen$	Clark level	Breslow thickness (mm)	Mitotic count	Ulceration!	Regression (PF = present & focal (<75%))	Lympho-vascular invasion	Perineural invasion	Microscopic satellitosis	Tumor-infiltrating lymphocytes (NB = non-brisk, M = minimal)	Associated melanocytic nevus	Predominant cytology (E = epithelioid, N = nevoid, S = spindled)	Lymph node metastases
1	SUM	0	60	M	Toenail	M (soft tissue of leg)	IV	1.2	<1	P, 0.5	NI	NI	NI	NI	NB	NI	E	N/A
2	SUM	0	27	F	Fingernail	Bx (shave)	III	0.25	<1	NI	PF	NI	NI	NI	NB	NI	E	0/3
3	SUM	2	74	M	Fingernail	Bx (shave)	IV	2.0	1	NI	NI	NI	NI	NI	NB	NI	E, N, S	0/2
4	SUM	4	57	F	Thumbnail	E	IV	1.95	8	NI	NI	P	NI	NI	NB	NI	E	2/4
5	SUM	3	55	M	Thumbnail	M (chest)	V	4.5	3	P, 2.0	NI	NI	P	NI	NB	NI	S/E	0/1
6	SUM	4	83	F	Fingernail	Bx	IV	N/A	6	P, 0.05	NI	NI	NI	NI	NB	NI	E	0/6
7	SUM	1	46	M	Toenail	E	V	4.73	11	P, 12	NI	NI	P	NI	NB	NI	S	0/2
8	SUM	3	41	M	Thumbnail	M (LN)	V	7.0	14	P, 20	NI	NI	NI	NI	NB	NI	E	6/41
9	SUM	4	66	F	Fingernail	E	IV	3.6	1	NI	NI	NI	NI	NI	M	NI	E	0/6
10	SUM	4	37	F	Thumbnail	M (LN)	IV	3.95	7	NI	NI	P	NI	NI	NB	NI	E	3/19
11	ALM	4	55	F	Great toe	M (great toe)	IV	3.5	6	P, 3.0	NI	NI	NI	NI	NB	NI	E	1/2
12	ALM	1	61	M	Fourth toe	E	V	35.0	67	P, 18	NI	P	NI	NI	NB	NI	E	3/3
13	ALM	4	46	F	Heel	E	V	3.2	8	NI	NI	NI	NI	NI	NI	NI	E	2/2
14	ALM	4	78	M	Great toe	E	IV	7.2	25	P, 12	NI	NI	NI	NI	NB	NI	E	3/10
15	ALM	2	76	M	Foot	E	IV	1.6	<1	NI	NI	NI	NI	NI	NB	NI	E	N/A
16	ALM	4	48	F	Middle finger	Bx (shave)	V	4.8	2	P, 6.2	NI	P	NI	NI	NB	NI	E	2/3
17	ALM	4	37	F	Foot	E	IV	3.0	15	P, 2.0	NI	NI	P	NI	NB	NI	E	2/13
18	ALM	0	64	M	Foot	Bx (punch)	IV	2.75	2	NI	NI	P	NI	NI	NB	NI	E	N/A
19	ALM	2	82	F	Foot	E	IV	3.5	9	P	NI	NI	NI	NI	NB	NI	E, S	0/1
20	ALM	4	81	M	Foot	E	V	5.5	4	P, 3.1	NI	NI	NI	P	NB	NI	E	N/A
21	ALM	4	66	M	Foot	E	IV	2.6	2	NI	NI	P	NI	NI	NB	NI	E, N	1/2
22	AN	0	54	F	Toe	E	-	-	-	-	-	-	-	-	-	-	-	-
23	AN	0	38	M	Foot	Bx (shave)	-	-	-	-	-	-	-	-	-	-	-	-
24	AN	0	27	F	Foot	E	-	-	-	-	-	-	-	-	-	-	-	-
25	AN	0	64	F	Foot	Bx (shave)	-	-	-	-	-	-	-	-	-	-	-	-
26	AN	0	36	M	Toe	Bx (shave)	-	-	-	-	-	-	-	-	-	-	-	-
27	AN	0	30	M	Toe	Bx (punch)	-	-	-	-	-	-	-	-	-	-	-	-
28	AN	0	63	F	Foot	Bx (shave)	-	-	-	-	-	-	-	-	-	-	-	-
29	AN	0	49	M	Heel	Bx (punch)	-	-	-	-	-	-	-	-	-	-	-	-
30	AN	0	58	F	Foot/sole	Bx (shave)	-	-	-	-	-	-	-	-	-	-	-	-
31	AN	0	45	M	Foot	Bx (shave)	-	-	-	-	-	-	-	-	-	-	-	-

NI = not identified, P = present
# (SUM = subungual melanoma, ALM = acral lentiginous melanoma, AN = acral nevus)
* PRAME expression based on percentage scores (0 = 0%, 1 = 1-25%, 2 = 26-50%, 3 = 51-75%, 4 = >76%)
$ E = excision, Bx = biopsy (shave vs. punch), M = metastasis (LN or other sites)
! width of ulceration in mm

Figure 2 – 326

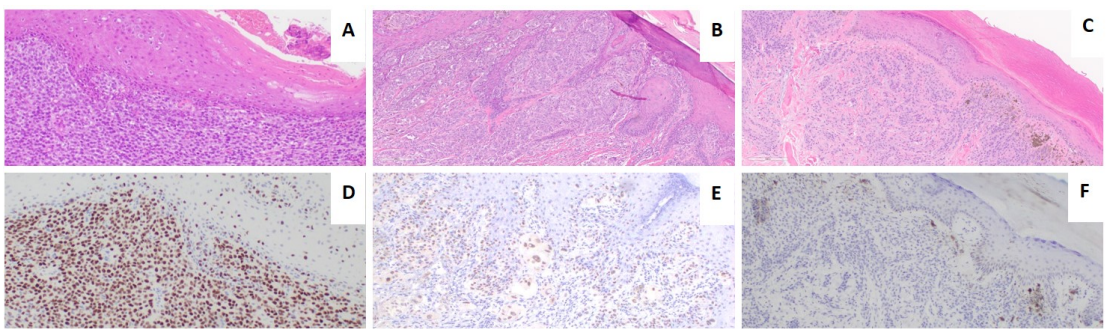

Figure 2: Representative figures of melanoma and nevus from acral site: A-C: H&E (x100) figures of subungual melanoma (SUM) (A), melanoma from non-nail acral site (ALM) (B) and acral nevus (AN) (C). D-F: Immunohistochemical study (x100) with PRAME showing 4+ positive expression SUM (D) and ALM (E), but negative expression in AN (F).

Conclusions: In our study, PRAME served as a sensitive and specific IHC marker for acral melanomas, even of subungual origin. These findings further support that PRAME is a useful discriminatory IHC marker that aids in differentiating melanomas at acral sites from benign nevi.

327 PRAME Expression in Merkel Cell Carcinoma and Clinicopathologic Correlation

Mario Saab Chalhoub[1], Geoffrey Chen[2], Frances Akwuole[2], Muhlbauer Aaron[1], Jodi Speiser[1], Kumaran Mudaliar[1]
[1]Loyola University Medical Center, Maywood, IL, [2]Loyola University Chicago Stritch School of Medicine, Maywood, IL

Disclosures: Mario Saab Chalhoub: None; Geoffrey Chen: None; Frances Akwuole: None; Muhlbauer Aaron: None; Jodi Speiser: None; Kumaran Mudaliar: None

Background: PRAME immunohistochemistry (IHC) is often positive in melanoma. Also, positivity in other malignancies (such as breast carcinoma or leukemia) can be seen with prognostic associations. After noticing PRAME positivity in a subset of Merkel cell carcinoma (MCC) cases, we aimed to assess PRAME expression in a larger cohort of MCCs and correlate the findings with the clinicopathologic data.

Design: After IRB approval, PRAME IHC was performed on 42 MCC and the clinicopathologic data were gathered. For PRAME positive cases, both the intensity of expression and percentage of positive tumor cells were noted (see figure 1). For statistical analysis, a Fisher Exact probability test was used for frequency data and a two sample t-test was used for continuous variables.

Results: 26 (61.9%) cases were positive for PRAME, and percentage of positive tumor cells ranged from 10 to 100%. Intensity was 1+ in 13 cases, 2+ in 9 cases, and 3+ in 2 cases. No statistically significant clinical (including demographics, immune status, radiation exposure, treatment received, prognosis) or histopathologic (including solar elastosis, tumor size and depth, borders, tumor infiltrating lymphocytes, lymphovascular invasion, and mitotic rate) differences were identified between PRAME positive and PRAME negative MCC cases (see Table 1).

	Overall	PRAME Pos	PRAME Neg	p-value
Sample size	42	26	16	
Age median	78	80	78	NS
Gender				
Male	31	20 (76.9%)	11 (68.7%)	NS
Female	11	6 (23.1%	5 (31.3%)	
Race				
White	39	24 (92.3%)	15 (93.7%)	
Asian	1	0 (0%)	1 (6.3%)	
Hispanic	2	2 (7.7%)	0 (0%)	
Immunocompromised				
Yes	5	3 (11.5%)	2 (12.5%)	NS
No	37	23 (88.5%)	14 (87.5%)	
Radiation exposure				
Yes	2	0 (0%)	2 (12.5%)	NS
No	40	26 (100%)	14 (87.5%)	
Location of tumor				
Head and Neck	31	18 (69.2%)	13 (81.2%)	
Upper Extremity	5	4 (15.4%)	1 (6.3%)	
Lower Extremity	4	2 (7.7%)	2 (12.5%)	
Trunk	2	2 (7.7%)	0 (0%)	
Procedure				
Excision	34	20 (76.9%)	14 (87.5%)	
Biopsy	8	6 (23.1%)	2 (12.5%)	
Median Follow Up (months)	17.5	25	10.5	
F/U results				
NED	28	18 (69.2%)	10 (62.5%)	NS*
AWD	5	1 (3.8%)	4 (25.0%)	
DOD	6	5 (19.2%)	1 (6.3%)	
DFOC	3	2 (7.7%)	1 (6.3%)	
Treatment				
Surgery alone	23	14 (53.8%)	9 (56.3%)	
Surgery with radiation and/or chemotherapy	19	12 (46.2%)	7 (43.8%)	
Solar elastosis				
Mild	17	11 (47.8%)	6 (37.5%)	NS
Moderate to severe	22	12 (52.2%)	10 (62.5%)	
Median tumor thickness (mm)	6	5	8	NS
Size (mm)	10.5	10	13	NS
Borders				
Nodular	16	9 (40.9%)	7 (46.7%)	NS
Infiltrative	21	13 (59.1%)	8 (53.3%)	
TIL				

Non-Brisk	25	14 (60.9%)	11 (68.8%)	NS
Brisk	5	3 (13.0%)	2 (12.5%)	
Not identified	9	6 (26.1%)	3 (18.8%)	
Epidermal connection				
Present	9	7 (30.4%)	2 (13.3%)	NS
Not present	29	16 (69.6%)	13 (86.7%)	
level involved				
Dermis	10	6 (26.1%)	4 (25.0%)	NS
Subcutaneous tissue	29	17 (73.9%	12 (75.0%)	
LVI				
Present	17	10 (43.5%)	7 (46.7%)	NS
Absent	21	13 (56.5%)	8 (53.3%)	
Mitotic rate/4HPF=1mm2 hot spot	71	73	69	

Table 1: Clinical, demographic and histopathologic characteristics of MCC cases. Abbreviations: Pos=positive. Neg=negative. NS=not statistically significant. NED=no evidence of disease. AWD=alive with disease. DOD=dead of disease. DFOC=dead from other causes. *: AWD, DOD, DFOC were grouped into one entry and compared with NED for p-value calculations due to small sample size.

Figure 1 - 327

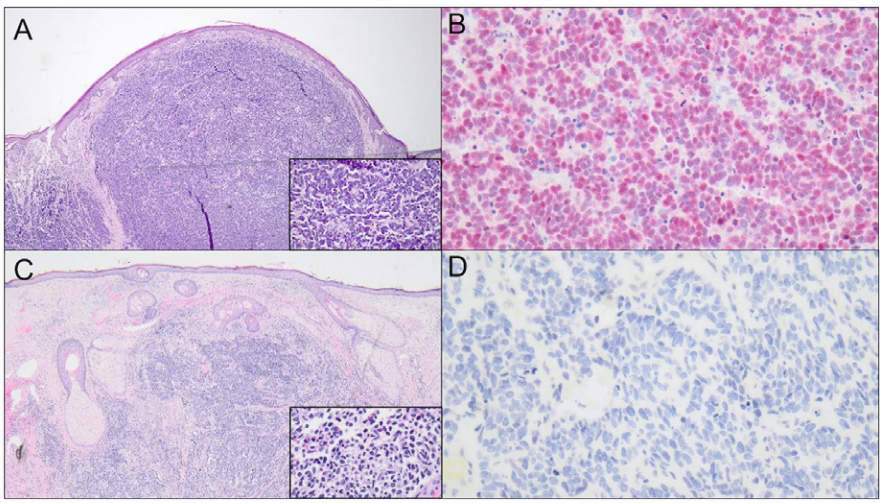

Figure 1: A: Low power magnification of MCC (H&E, inset: 40x). B: Same tumor as figure A showing 3+ PRAME staining in 80% of cells (40x). C: Low power magnification another case of MCC (H&E, inset: 40x). D: Same tumor as figure C showing no PRAME staining (40x).

Conclusions: PRAME positivity is seen in a significant proportion of MCC and pathologists should be aware of such positivity to avoid misdiagnosing MCC as melanoma. In our cohort of cases, no statistically significant clinicopathologic differences were identified between PRAME positive and PRAME negative cases.

328 High Expression of Nectin-4 in a Subset of Adnexal Carcinomas: A Potential Target for Enfortumab Vedotin Therapy

Rayan Saade[1], Woo Cheal Cho[1], Priya Nagarajan[1], Phyu Aung[1], Mario Marques-Piubelli[1], Courtney Hudgens[1], Debora Ledesma[1], Kelly Nelson[1], Meghan Heberton[1], Doina Ivan[1], Miao Zhang[1], Carlos Torres-Cabala[1], Matthew Campbell[1], Victor Prieto[1], Ignacio Wistuba[1], Bita Esmaeli[1], Jonathan Curry[1]
[1]The University of Texas MD Anderson Cancer Center, Houston, TX

Disclosures: Rayan Saade: None; Woo Cheal Cho: None; Priya Nagarajan: None; Phyu Aung: None; Mario Marques-Piubelli: None; Courtney Hudgens: None; Debora Ledesma: None; Kelly Nelson: None; Meghan Heberton: None; Doina Ivan: None; Miao Zhang: None; Carlos Torres-Cabala: None; Matthew Campbell: *Advisory Board Member*, Astellas, Seagen; *Grant or Research Support*, Exelixis; *Consultant*, Exelixis; *Grant or Research Support*, Janssen, ApricityHealth, AstraZeneca; *Advisory Board Member*, Pfizer; *Grant or Research Support*, Pfizer; *Advisory Board Member*, Eisai; Victor Prieto: *Consultant*, Novartis, Orlucent; Ignacio Wistuba: *Advisory Board Member*, Genentech/Roche, Bayer, Bristol-Myers Squibb, AstraZeneca, Pfizer, HTG Molecular,

Merck, GlaxoSmithKline; *Consultant*, Flame; *Advisory Board Member*, Novartis, Sanofi, Daiichi Sankyo, Amgen, Oncocyte; *Speaker*, Platform Health, AstraZeneca, Genentech/Roche; *Grant or Research Support*, Genentech, HTG Molecular, Merck, Bristol-Myers Squibb, Medimmune/Astra Zeneca, Adaptimmune, Adaptive, EMD Serono, Pfizer, Takeda, Amgen, Karus, Johnson & Johnson, Bayer, Iovance, 4D, Novartis, Akoya; Bita Esmaeli: None; Jonathan Curry: None

Background: Adnexal carcinomas (ACs) are a heterogeneous group of rare tumors with variable biological behaviors, which may carry a poor prognosis. Nectin-4 is a cell adhesion molecule belonging to the Nectin family of immunoglobulin-like proteins. Nectin-4 regulates cell-cell adhesion and can also interact with receptor tyrosine kinases to promote cell migration, proliferation, and survival. Nectin-4 is naturally expressed in the skin and hair follicles and have been shown to be upregulated in several cancers including urothelial carcinoma. Enfortumab vedotin (EV) is an antibody-drug conjugate directed at Nectin-4, delivering a potent, antimitotic monomethyl auristatin E payload. EV is an FDA-approved treatment for locally advanced or metastatic urothelial carcinomas, with documented successes in early clinical trials. The availability of novel anticancer therapy for ACs is limited. We sought to examine Nectin-4 expression in a series of AC to identify potentially EV-targetable malignancies.

Design: Twenty-four ACs (8 digital papillary adenocarcinomas [DPAs], 7 squamoid eccrine ductal carcinomas [SEDCs], and 9 sebaceous carcinomas [SCs]) were included in the study. Formalin-fixed paraffin-embedded tissues of ACs were subjected to immunohistochemical staining using anti-Nectin-4 rabbit polyclonal antibodies. Nectin-4 intensity (0-3+) and percent of positive cells (0-100%) were recorded and H score was calculated. H score values were categorized as: negative (0–14), low (15–99), moderate (100–199), and high (200–300). Nectin-4 expression was compared between the diagnostic categories using ANOVA.

Results: Cytoplasmic/membranous expression of Nectin-4 was detected in 22/24 (92%) of ACs (Figure 1). Two cases of SEDC were negative for Nectin-4 expression. SEDCs exhibited fewest number of cases (2/7, 29%) with high Nectin-4 expression and had the lowest mean H-score of 131.4 ±105.6. DPAs displayed moderate (4/8, 50%) and high (4/8, 50%) Nectin-4 expression with a mean H-score of 197.5 ±49.1. High expression of Nectin-4 was frequently observed in 7/9 (78%) of SCs. Nectin-4 expression was significantly higher in SCs (mean H-score 241.7 ±69.4) when compared with those of DPAs and SEDCs (p = 0.04, Table 1).

Table 1. Immunohistochemical expression of Nectin-4 in adnexal carcinomas

Type of Tumors	No. of Lesions	Age in yrs (Range)	M:F	Site of Involvement, n (%)	Nectin-4 Expression, n (%)				H-Score ± SD
					Negative	Low	Moderate	High	
Digital papillary adenocarcinoma (DPA)	8	49 (32-71)	3:1	Foot = 4 (50%)			4 (50%)	4 (50%)	197.5 ± 49.1
				Hand = 3 (38%)					
				LN = 1 (12 %)					
Squamoid eccrine ducal carcinoma (SEDC)	7	69 (53-79)	6:1	H&N = 4 (57%)	2 (28.5%)	1 (14.5%)	2 (28.5%)	2 (28.5%)	131.4 ±105.6
				UE =1 (14%)					
				LE = 1 (14%)					
				Back =1 (14%)					
Sebaceous carcinoma (SC)	9†	73 (57-88)	5:4	Eyelid = 4 (44%)			2 (22%)	7 (78%)	241.7 ±69.4*
				Orbit = 3 (33%)					
				LN = 2 (22 %)					

†Include lesion of lymph node metastasis for one patient. *Analysis of variance (ANOVA) p = 0.04. Abbreviations: No., number; yrs, years; M, male; F, female; SD, standard deviation; H&N, head and neck; UE, upper extremity; LE, lower extremity; LN, lymph node.

Figure 1 - 328

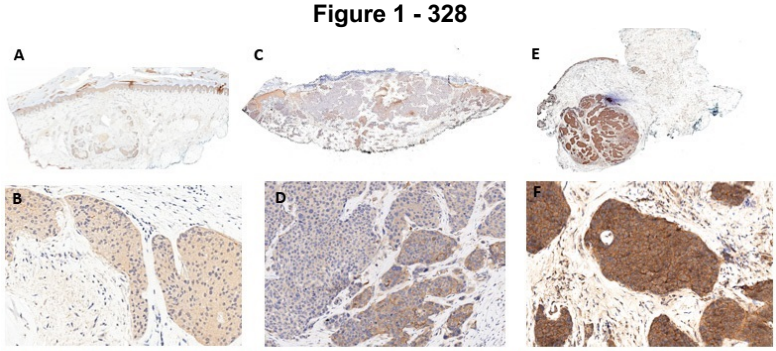

A, B. Low and high magnifications of digital papillary adenocarcinoma; representative case of 2+ diffuse staining intensity (H-score = 210). **C, D.** Low and high magnifications of squamoid eccrine ductal carcinoma; representative case of 0-3+ variable staining intensity (H-score = 120). **E, F.** Low and high magnifications of sebaceous carcinoma; representative case of 3+ diffuse staining intensity (H-score = 300).

Conclusions: High expression of Nectin-4 was observed in a subset of DPAs, SEDCs, and SCs. The frequent expression of Nectin-4 in ACs, particularly in SCs, is a novel finding; Nectin-4 directed EV therapy may serve as a potential therapeutic neoadjuvant option in advanced stage disease.

329 Graft Invasion by Melanoma Cells in Acral Sites: A Retrospective Integrated Clinicopathological and Immunohistochemical Analysis of a Single-Center Case Series

Giacomo Santandrea[1], Moira Ragazzi[1], Riccardo Valli[1], Eleonora Zanetti[1], Riccardo Pampena[1], Michela Lai[1], Caterina Longo[1], Anna Maria Cesinaro[2], Simonetta Piana[1]

[1]Azienda Unità Sanitaria Locale - IRCCS di Reggio Emilia, Reggio Emilia, Italy, [2]Policlinico of Modena, Modena, Italy

Disclosures: Giacomo Santandrea: None; Moira Ragazzi: None; Riccardo Valli: None; Eleonora Zanetti: None; Riccardo Pampena: None; Michela Lai: None; Caterina Longo: None; Anna Maria Cesinaro: None; Simonetta Piana: None

Background: Melanoma recurrence in skin graft is an ominous but relatively frequent event in acral site. This is mostly due to the underdiagnosis of the excision completeness, as the deceiving histological features of melanomas in acral sites, often in contrast with their clinical worrisome appearance, elude a careful evaluation of the margins. This study aims to analyze morphologically a series of acral melanomas recurring on skin grafts, with the aid of PRAME immunostaining, a recently introduced tool.

Design: The databases of the Skin Cancer Unit and of the Pathology Unit were retrospectively searched to identify all patients who developed a melanoma recurrence on a graft. Complete clinical, surgical data and follow up were collected. The slides were reviewed by an experienced dermatopathologist and PRAME staining was performed both on primary tumor and tumor recurrences.

Results: Six patients were identified, all Caucasians, three males and three females, with a median age at diagnosis of 71 (range 56-88). Five out of six lesions were located on the soles, one on the palm. After a diagnostic punch biopsy, all tumors were surgically excised and followed by a graft implant. Histologically, four cases were in situ melanoma (MIS) and two invasive melanomas (IM). Both primary and recurring MIS showed poor cellularity, bland nuclear atypia, scattered distribution of melanocytes at the dermo-epidermal junction and irregular, vanishing, tumor margins. One IM showed a well-defined, neoplastic melanocytic proliferation both in the primary and in the graft recurrence, while the second IM recurred locally as MIS but subsequently developed lymph node metastases. PRAME was diffusely and strongly expressed in all cases, and resulted helpful in highlighting the waning margins of MIS. At follow-up, two patients (both diagnosed with IM) died with disease.

Table 1. Clinicopathological Data of Acral Sites Melanoma Recurrence.

Case n°	Age at diagnosis (Y)	Tumor site	Histology (primary tumor)	Histology (recurrence)	Time to first recurrence	PRAME expression in tumor cells (1+ = 0-25%, 2+ 25-50%, 3+ 50-75%, 4+ >75%)	PRAME intensity (1+ = weak, 2+ = moderate, 3+ = strong)	Duration of follow-up (months)	Outcome
1	61	Foot	In situ melanoma	In situ melanoma	72 months	4+	3+	19	Alive, no evidence of disease
2	56	Foot	In situ melanoma	In situ melanoma	6 months	4+	3+	3	Alive, no evidence of disease
3	81	Foot	Invasive melanoma	Invasive melanoma	29 months	4+	3+	67	Dead of disease
4	67	Foot	Invasive melanoma	In situ melanoma	42 months	4+	3+	29	Dead of disease
5	76	Foot	In situ melanoma	In situ melanoma	28 months	4+	3+	39	Dead of other cause
6	81	Hand	In situ melanoma	In situ melanoma	83 months	4+	3+	48	Dead of other cause

Figure 1 - 329

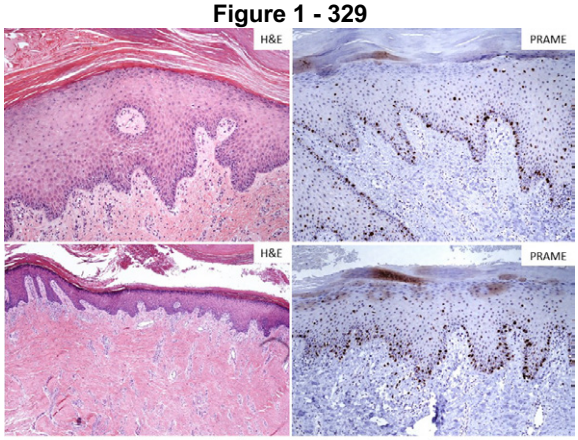

Figure 1. Two examples of recurrent melanoma in situ on skin grafts.

Conclusions: Herein, we presented a unique series of acral melanoma recurring on graft implants. These events are characterized by a peculiar deceptive morphology at histological examination, representing a diagnostic challenge, especially for unexperienced pathologists. PRAME staining demonstrated a strong and diffuse positivity in all cases, supporting its role as a promising diagnostic tool. Careful examination of the whole specimen, in particular tumor margins, is essential to establish a correct diagnosis to avoid a potential underdiagnosis.

330 MALDI Imaging Mass Spectrometry Differentiates Basal Cell Carcinoma from Trichoblastoma and Trichoepithelioma

Ashley Rose Scholl[1], Jessica Moore[2], Heath Patterson[3], Sarah Nicholson[4], Jeremy Norris[2], Jason Robbins[2], Rami Al-Rohil[5]

[1]Duke University Health System, Durham, NC, [2]Frontier Diagnostics, Nashville, TN, [3]Vanderbilt University, Nashville, TN, [4]Nashville, TN, [5]Duke University School of Medicine, Durham, NC

Disclosures: Ashley Rose Scholl: None; Jessica Moore: *Employee*, Frontier Diagnostics; *Employee*, Frontier Diagnostics; Heath Patterson: *Employee*, Frontier Diagnostics; Sarah Nicholson: *Employee*, Frontier Diagnostics; Jeremy Norris: *Stock Ownership*, Frontier Diagnostics, LLC; Jason Robbins: *Stock Ownership*, Frontier Diagnostics; Rami Al-Rohil: *Consultant*, Frontier Diagnostics; *Employee*, Foundation Medicine Inc.

Background: Basal cell carcinoma (BCC) and trichoblastoma/trichoepithelioma (TB/TE) often appear clinically similar and comprise a large portion of dermatopathology specimens. Because the management for these two basaloid neoplasms differs, it is of the utmost importance that dermatopathologists distinguish these entities. Traditional diagnosis has relied on histological and immunohistochemical interpretation, but newly developed tools can predict outcomes more accurately via molecular analysis. Matrix-Assisted Laser Desorption/Ionization Mass Spectrometry (MALDI MS) can be used to perform in situ molecular/proteomic analysis by collecting mass spectra directly from areas of interest within tissue sections. Spectra from tissue with known pathologic diagnoses can be used to train machine learning classification models. Tissues of unknown pathology can be analyzed and then classified using the models to provide a score on both per spectra and per sample level.

Design: Two board-certified dermatopathologists reviewed 69 specimens of BCC and TB/TE and only those specimens with concordant diagnoses were included to control for histologic variability. Pathologists used an online annotation platform and digital whole slide images to annotate tissue regions of interest, annotating epithelial and stromal elements separately. A serial section was prepared for MALDI IMS by paraffin removal, antigen retrieval, tryptic digestion, and matrix application. Mass spectra were collected from regions of interest. The 69 specimens were divided into a training set (n=56) and a validation set (n=13.) A linear support vector machine (SVM) model was used for classifying the mass spectra.

Results: In this study, mass spectra were collected from 44 BCC samples, resulting in 5,652 spectra from BCC and 2,711 spectra from stroma. Mass spectra were also collected from 27 TB/TE samples, resulting in 685 spectra from diseased regions and 880 spectra from adjacent stroma. The platform predicted BCC over TB/TE with a sensitivity of 94% and a specificity of 95% at the spectral level. All test set samples had >90% of individual spectra classified correctly in the validation set (BCC n=8, TB/TE n=5.)

Conclusions: MALDI IMS is an emerging analytical tool in the field of dermatopathology. Here we present a SVM model capable of differentiating basal cell carcinoma from trichoblastoma/trichoepithelioma with a sensitivity and specificity of >94%.

331 Correlation Between Gene Expression Profiling, Sentinel Lymph Node Biopsy Status, and Metastatic Risk in Primary Cutaneous Melanoma Cases – A Series of 206 Cases

Anurag Sharma[1], Gabriel Oaxaca[2], Eleanor Cook[1], Lauren Duckworth[1], Derek Frew[2], John McAfee[2], Pauline Funchain[2], Steven Billings[3], Shira Ronen[2], Jennifer Ko[2]
[1]Cleveland Clinic Foundation, Cleveland, OH, [2]Cleveland Clinic, Cleveland, OH, [3]Cleveland Clinic, Lerner College of Medicine, Cleveland, OH

Disclosures: Anurag Sharma: None; Gabriel Oaxaca: None; Eleanor Cook: None; Lauren Duckworth: None; Derek Frew: None; John McAfee: None; Pauline Funchain: *Primary Investigator*, Pfizer; *Primary Investigator*, Bristol Myers Squibb; *Consultant*, Eisai; Steven Billings: None; Shira Ronen: None; Jennifer Ko: None

Background: 31-gene expression profile (31-GEP) test (DecisionDx-Melanoma, Castle Biosciences Inc, Friendswood, TX, USA) predicts metastatic risk in melanoma by categorizing cutaneous tumors as Class 1 (low risk) or Class 2 (high risk). We examined the correlation between 31-GEP class, sentinel lymph node biopsy (SLNBx) status, and metastasis.

Design: Melanoma cases (2015-2021) where 31-GEP testing was performed, were identified from our archives. Cases with available sentinel lymph node (LN) status and follow-up data were included. Clinicopathologic characteristics were compared between the two classes.

Results: 206 cases were included (age range 21-92 years[y], mean=62.2; M:F ratio = 1.5). 157/206 (76%) were 31-GEP Class 1 and 49/206 (24%) were Class 2. Among Class 1 cases, 2.5% (4/157) showed SLNBx+ (3 Class 1A and 1 Class 1B). None of the 4 Class 1/SLNBx+ patients experienced disease recurrence or melanoma specific mortality (MSM). Of 153 Class 1/SLNBx- patients, 2 experienced recurrences, and both were Class 1B [1 local and one distant/hematogenous (lung, liver, brain)]. The mean follow-up period in Class 1 patients was 28 months (mo). 4/49 (8%) Class 2 cases had SLNBx+. Although there was a trend toward increased SLNBx positivity in Class 2 cases, this was not statistically significant (p=0.07). 1 of 4 (25%) Class 2 patients with SLNBx+ developed metastatic disease (4y after definitive surgery) and died of disease (DOD); the other 3 did not recur. 9/45 (20%) patients with Class 2 scores and SLNBx- developed distant hematogenous metastases (n=8, lung, liver, brain, bone) and lymphatic metastasis (n=1, draining LN basin). 2/9 DOD, 2/9 died of other causes, and 5/9 are alive without disease. The mean follow-up for Class 2 cases was 20 mo.

Conclusions: Our data confirm the overall excellent outcome for Class 1 melanoma patients; SLNBx+ in this setting did not have prognostic significance in our cohort. There is a possible increased risk of SLNBx+ in Class 2 patients (p-value = 0.07). Importantly, our data support previous findings demonstrating increased risk for distant *hematogenous* metastasis in Class 2 patients, in the presence *or* absence of a SLNBx+. Melanoma specific mortality did not significantly differ in Class 2 patients according to SLNBx status. Identifying Class 2 patients most likely to benefit from adjuvant systemic therapy remains essential.

332 Long Non-Coding RNA MALAT1 and PD-L1 Expression in Merkel Cell Carcinomas

Oyewale Shiyanbola[1], Heather Hardin[1], Darya Buehler[2], Ricardo Lloyd[1]
[1]University of Wisconsin, Madison, WI, [2]University of Wisconsin-Madison, Madison, WI

Disclosures: Oyewale Shiyanbola: None; Heather Hardin: None; Darya Buehler: None; Ricardo Lloyd: None

Background: Long non-coding RNA (lncRNA) participate in transcription, epigenetic or post-transcriptional regulation of gene expression and may contribute to carcinogenesis. Programmed cell Death Ligand-1(PD-L1) inhibitors may be useful neoadjuvant immunotherapy agents for the treatment of Merkel Cell Carcinomas (MCCs). In this study we analyzed expression of lncRNA metastatic-associated lung adenocarcinoma transcript 1(*MALAT1*) and its correlation with PD-L1 expression in carcinoma cells of Merkel Cell Polyoma virus (MCPyV)-positive and MCPyV-negative MCCs cases.

Design: Tissue microarrays (TMAs) were constructed with duplicate cores of 51 cases of formalin-fixed, paraffin-embedded MCCs. TMA sections were analyzed by in situ hybridization (ISH) using RNAscope technology with *MALAT1* probe (Advanced Cell

Diagnostics). Immunohistochemical (IHC) stains for MCPyV, PD-L1, chromogranin, synaptophysin, INSM1, CK20, and neurofilament were performed. The results of ISH were analyzed with Vectra imaging technology, Nuance® and inForm® software.

Results: *MALAT1* was expressed mainly in the tumor cell nuclei. More MCPyV-positive cases (n=28) expressed *MALAT1* compared to MCPyV-negative cases (n=23), although the differences were not statistically significant. PD-L1 on tumor cells were evaluated as <1%,1-50% and >50%. *MALAT1* expression was significantly higher in cases with PDL-1>50% compared to PDL-1<1% (p< 0.01) and in PDL-1 cases1-50% compared to PDL-1 <1% (p<0.01). As expected, all MCCs expressed neuroendocrine markers and most expressed CK20.

Conclusions: MCC cases with PD-L1 expression are more likely to express *MALAT1*. suggesting that LncRNAs may influence the immunogenic evolution of MCCs. Further investigation is underway.

333 Patterns of Cutaneous Metastases of Renal Cell Carcinoma: A Clinicopathologic Study of 70 Cases

David Suster[1], Huy Nguyen[2], Pablo Ortega[3], Jose Plaza[4], Phyu Aung[2], Jennifer Ko[5], Steven Billings[6], Shira Ronen[5]
[1]Rutgers New Jersey Medical School/Rutgers University, Newark, NJ, [2]The University of Texas MD Anderson Cancer Center, Houston, TX, [3]Ortega Pathology Lab, Loja, Ecuador, [4]The Ohio State University Wexner Medical Center, Columbus, OH, [5]Cleveland Clinic, Cleveland, OH, [6]Cleveland Clinic, Lerner College of Medicine, Cleveland, OH

Disclosures: David Suster: None; Huy Nguyen: None; Pablo Ortega: None; Jose Plaza: None; Phyu Aung: None; Jennifer Ko: None; Steven Billings: None; Shira Ronen: None

Background: A rare percentage of renal cell carcinoma (RCC), approximately ~3%, may occur as a cutaneous metastasis, with the distribution of metastasis following an unpredictable pattern of spread. Clinically cutaneous metastasis may mimic various benign and malignant processes including melanoma, vascular tumors and benign reactive conditions.

Design: 70 cases of cutaneous metastasis of renal cell carcinoma were collected from multiple institutions. Clinical data including age, sex, clinical diagnosis, time to metastasis, and metastatic site was collected and histologic evaluation of level of dermal involvement, epidermal changes, morphology, architecture, tumor differentiation, immunohistochemical expression, and mitotic activity was undertaken.

Results: The patients were 61 males and 9 females with an average of 63 years (range: 23 – 84 years). 44 cases occurred on the scalp, 11 cases the face (cheek, lip, nose, eyelids), 10 cases the trunk (chest, abdomen, back), 2 cases neck, 1 case each on the ear, ankle and upper arm. The average time from initial diagnosis was 4.9 years, with 12 cases occurring after 9.5 years. The longest interval between initial diagnosis and metastasis was 30 years. In 4 cases the metastasis was the initial presentation. The clinical differential included mimics such as pyogenic granuloma (5 cases), hemangioma (2 cases), angiosarcoma (2 cases), and melanoma (2 cases). Immunohistochemistry was used to confirm the diagnosis in 50/70 cases and included cytokeratins, PAX8, as well as vascular and melanocytic markers. Histologically 68 cases were conventional clear cell RCC, 26 of which had prominent oncocytic cytoplasm. 1 case was papillary type RCC and one case was a renal medullary carcinoma. 61 cases demonstrated a nodular lesion; often involving the entire dermis (32 cases) with intact grenz zone. 9 cases demonstrated an infiltrative pattern, often with poorly differentiated cells without obvious clear cytoplasm. The subcutis was involved in 34 cases. 14 cases demonstrated epidermal ulceration with a neutrophilic crust. 60 cases demonstrated <1 mitosis/2 mm^2. Rare findings included epithelioid hemangioendothelioma-like histology, melanoma-like architecture, and neuroendocrine-like architecture.

Figure 1 - 333

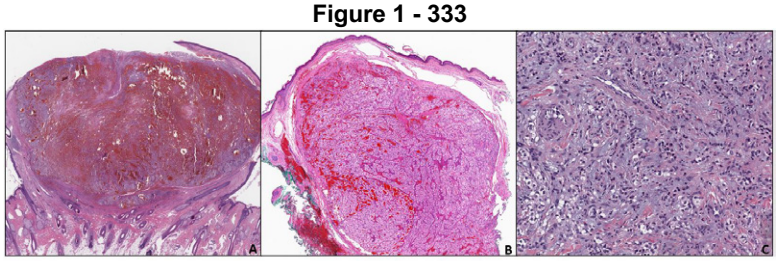

A) Low power magnification shows a nodular renal cell carcinoma of the upper dermis growing in a polypoid manner with central hemorrhagic changes and a focal dermal collaret. B) Metastatic renal cell carcinoma involving the entire dermis with a prominent grenz zone and the classic features of renal cell carcinoma with nests and trabeculae of clear cells with hemorrhagic changes. C) Infiltrative pattern of renal cell clear cell carcinoma shows an irregular pattern of infiltration in a myxoid stroma; focal areas of cytoplasmic clearing are present, helping with identification.

Figure 2 – 333

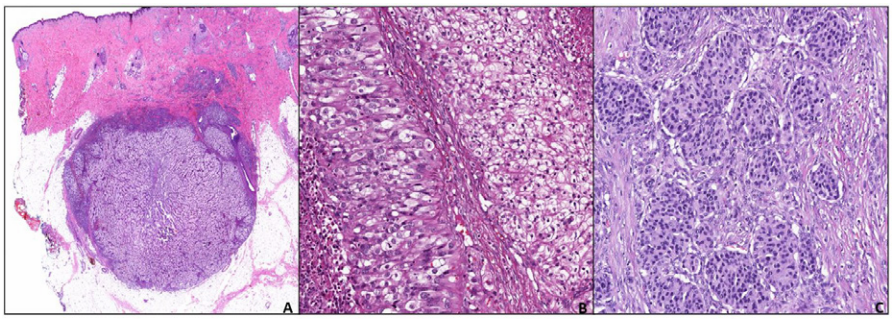

A) Low power magnification shows a nodular renal cell carcinoma seated in the deep dermis involving predominantly the subcutaneous tissue. B) Metastatic lesion of renal cell carcinoma showing low grade clear cell features (right) adjacent to higher grade oncocytic features (left), patchy necrosis is present. C) Unusual case of renal cell carcinoma without clear cytoplasm growing in small nests mimicking a neuroendocrine tumor (PAX8+, TTF1/thyroglobulin-).

Conclusions: A small percentage of cutaneous metastatic RCC may present with unusual histologic features or poorly differentiated morphology that may cause diagnostic difficulty. Lesions may mimic other tumor types and require a clinical history to achieve an accurate diagnosis.

334 Expression of SATB2 in Cutaneous Sarcomatoid Neoplasms: A Potential Diagnostic Pitfall

Julianne Szczepanski[1], Javed Siddiqui[1], Paul Harms[1], Steven Hrycaj[1], May Chan[1]
[1]University of Michigan, Ann Arbor, MI

Disclosures: Julianne Szczepanski: None; Javed Siddiqui: None; Paul Harms: *Other*, Q32 Bio; Steven Hrycaj: None; May Chan: None

Background: Immunohistochemistry for special AT-rich sequence-binding protein 2 (SATB2) is most frequently used as a gastrointestinal epithelial marker, but also as a marker for osteoblastic differentiation in benign and malignant mesenchymal tumors. Sarcomatoid neoplasms of the skin are potential mimickers of osteosarcoma, yet SATB2 expression in cutaneous sarcomatoid neoplasms has not been studied.

Design: Sections of tissue microarrays consisting of atypical fibroxanthoma (AFX; n=23), pleomorphic dermal sarcoma (PDS; n=20), sarcomatoid squamous cell carcinoma (SCC; n=14), sarcomatoid melanoma (n=39), high-grade cutaneous angiosarcoma (n=14), high-grade cutaneous leiomyosarcoma (n=17), and osteosarcoma controls (n=8) were immunostained with SATB2 (clone EP281). H-score was calculated for each case by multiplying intensity (0=negative, 1=weak, 2=moderate, 3=strong) and extent (0-100) of staining. Results were classified as negative (h-score <20), low-positive (h-score of 20-50), or high-positive (h-score >50). Average h-scores were calculated and compared between groups by two-tailed t-tests.

Results: Nearly half (62/127, 49%) of cutaneous sarcomatoid cases expressed SATB2. Average h-scores for all cutaneous entities ranged from 9 (angiosarcoma) to 71 (AFX), compared to an average h-score of 133 for osteosarcoma (Figure 1). The difference between AFX and osteosarcoma did not reach statistical significance (p=0.07). The remaining cutaneous sarcomatoid neoplasms showed significantly lower average h-scores compared to osteosarcoma. Of the cutaneous entities, AFX showed the highest percentage (48%) of high-positive cases, followed by PDS (40%) and sarcomatoid melanoma (33%) (Figure 2).

Figure 1 - 334

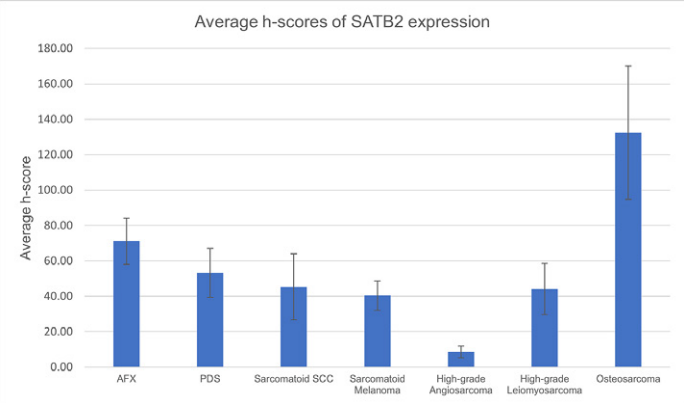

Figure 2 - 334

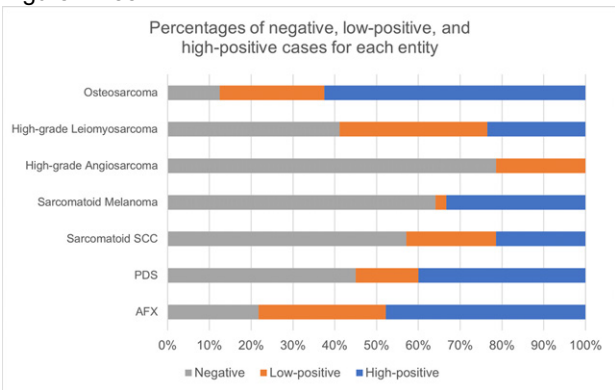

Conclusions: Expression of SATB2 is common in cutaneous sarcomatoid neoplasms, with the highest degree of staining in AFX and PDS, likely reflecting the undifferentiated nature of these neoplasms. Awareness of these findings is important when evaluating patients with a history of osteosarcoma, as positive SATB2 staining alone is insufficient for diagnosing cutaneous involvement by osteosarcoma.

335 Diffuse Mucocutaneous Melanocytoses with Unusual Clinicopathologic Features: Case Series with Emphasis on Single Nucleotide Polymorphism Microarray Findings and Melanoma Development

Burak Tekin[1], Katherine Geiersbach[1], William Sukov[1], Patricia Greipp[1], Ruifeng (Ray) Guo[1]
[1]Mayo Clinic, Rochester, MN

Disclosures: Burak Tekin: None; Katherine Geiersbach: None; William Sukov: None; Patricia Greipp: None; Ruifeng (Ray) Guo: None

Background: Mucocutaneous melanocytoses are a heterogeneous group of congenital or acquired lesions characterized by a spindled and dendritic melanocytic population in the dermis or stroma of mucosal site with frequent deep soft tissue involvement. Many dermal melanocytoses are categorized into well-defined entities such as blue nevus (BN) or nevus of Ota. However, classification remains challenging for cases with poorly demarcated diffuse clinical and pathological features. Some authors proposed the term “large plaque-type BN with subcutaneous cellular nodules” in a subset of cases. Based on the few reported cases, this variant was associated with a high risk of melanoma transformation.

Design: This study is a case series with a descriptive design, encompassing 8 diffuse melanocytosis cases with unusual clinicopathologic features, ranging from unusual location, extensive clinical involvement, to challenging cellular proliferations. Single nucleotide polymorphism microarray (SNP array) was performed on 4/8 cases.

Results: At presentation, ages of the patients ranged from 14 to 65 years. The most common localization was the scalp (*n*=2), followed by the back, flank, elbow, buttock, periorbital area, and ovarian teratoma in one case each.

One patient (case 1) underwent total mastectomy for solid papillary carcinoma, with the specimen exhibiting dermal and subcutaneous involvement by melanocytes with variable cellularity, extending to and largely effacing a sentinel lymph node.

Four patients (cases 2–5) had new-onset nodules suspicious for melanoma. SNP array did not support melanoma in case 2 (normal pattern), supported congenital proliferative nodule (PN) in case 3 (multiple gains of whole chromosomes), and confirmed sarcomatoid melanoma in case 4 (complex aneuploidy pattern). Case 5 developed 3 tumors undergoing SNP array with different results, which supported 2 melanomas and 1 congenital PN in this patient. All tumors in this patient shared *GNAQ* mutation.

Cases 6–8 only demonstrated diffuse dermal melanocytosis (plaque-type BN). Among them, case 8 represented a congenital-type lesion arising in the skin tissue of a mature ovarian teratoma.

Figure 1 - 335

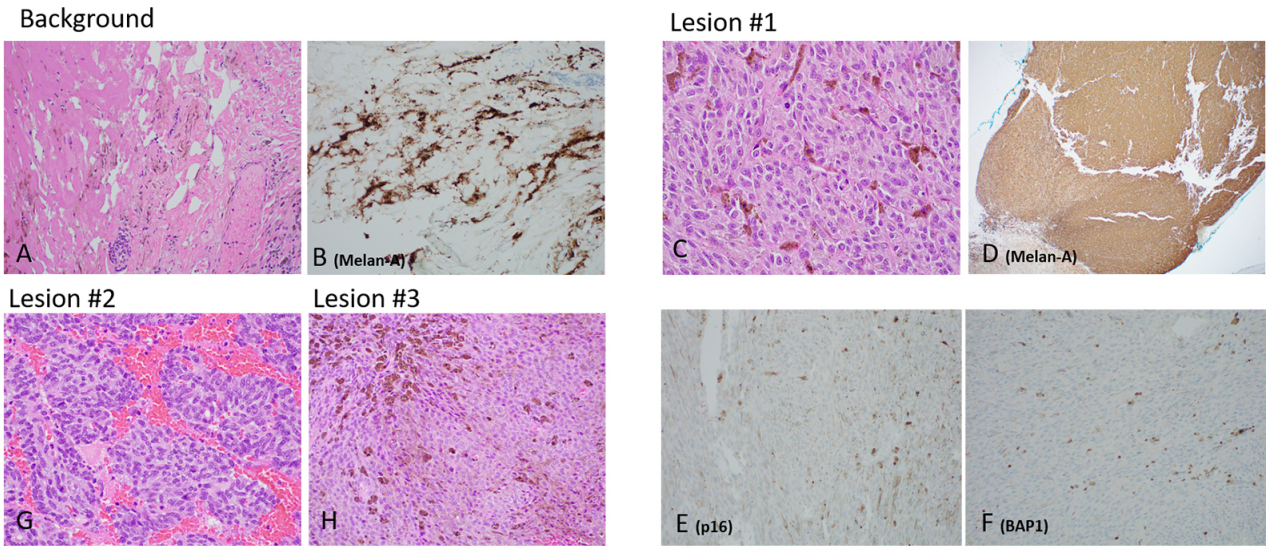

Conclusions: Histological evaluation of diffuse melanocytosis can be challenging. Ancillary SNP array sheds light on genetic findings in these cases that are potentially critical for better classification. High risk of melanoma development is noted in diffuse melanocytosis, and unusual proliferation such as congenital PN can be a diagnostic pitfall.

336 Utility of Aberrant p53 Expression in the Differentiation of Atypical Fibroxanthoma From Atypical Fibrous Histiocytoma

Gisele Toumi[1], Jeffrey Cloutier[2], Greg Charville[1], Ryanne Brown[1]
[1]Stanford Medicine/Stanford University, Stanford, CA, [2]The University of Texas MD Anderson Cancer Center, Houston, TX

Disclosures: Gisele Toumi: None; Jeffrey Cloutier: None; Greg Charville: None; Ryanne Brown: None

Background: Atypical fibrous histiocytoma (AFH) and atypical fibroxanthoma (AFX) are dermal fibrohistiocytic proliferations characterized by atypical, pleomorphic cells, mitotic activity, and diffuse CD10 expression. The histologic and immunohistochemical overlap can make these entities difficult to distinguish, especially on superficial biopsy. Ultraviolet radiation-induced TP53 mutations have been implicated in the development of AFX and pleomorphic dermal sarcoma (PDS), but not in benign fibrous histiocytomas. In this study, we evaluated the utility of p53 immunohistochemical staining in discriminating AFH and AFX.

Design: A total of 65 skin samples, including 40 benign fibrous histiocytomas (7 atypical, 20 conventional, 12 cellular, and 1 hemosiderotic) and 25 AFX/PDS, were subject to immunohistochemical staining for p53. Expression was classified as wild type or aberrant (null or overexpressed) according to previously described criteria.

Results: Twenty-one AFX/PDS showed aberrant immunohistochemical expression of p53 (84%), with 19% showing a null pattern and 81% showing overexpression. By contrast, benign fibrous histiocytomas consistently showed wildtype expression of p53 (n=39/40, 97.5%). Overall, aberrant p53 expression was 97.5% specific for diagnosis of AFX/PDS, with a positive predictive value (PPV) of 95.4%. Wildtype p53 expression had a negative predictive value (NPV) of 90.7% for a diagnosis of AFX/PDS. When considering the differential diagnosis of AFH and AFX/PDS, aberrant p53 expression had a specificity and PPV of 100% for a diagnosis of AFX/PDS in our study.

Conclusions: Aberrant p53 staining is common in AFX/PDS but rare in benign fibrous histiocytomas. Immunohistochemical staining for p53 may be particularly useful for distinguishing AFH from AFX on superficial biopsies.

337 SOX11 Serves as an Effective Discriminatory Marker, When Used in Conjunction with CK20 and TTF1, for Merkel Cell Carcinoma: A Comparative Analysis of SOX11, CK20, PAX5, and TTF1 Expressions in Merkel Cell Carcinomas and Pulmonary Small Cell Carcinomas

Kaitlin Vanderbeck[1], Denai Milton[1], Priya Nagarajan[1], Aimi Rothrock[1], Wei-Lien (Billy) Wang[1], Jonathan Curry[1], Carlos Torres-Cabala[1], Doina Ivan[1], Victor Prieto[1], Phyu Aung[1], Woo Cheal Cho[1]
[1]The University of Texas MD Anderson Cancer Center, Houston, TX

Disclosures: Kaitlin Vanderbeck: None; Denai Milton: None; Priya Nagarajan: None; Aimi Rothrock: None; Wei-Lien (Billy) Wang: None; Jonathan Curry: None; Carlos Torres-Cabala: None; Doina Ivan: None; Victor Prieto: *Consultant*, Novartis; *Consultant*, Orlucent; Phyu Aung: None; Woo Cheal Cho: None

Background: The distinction between Merkel cell carcinoma (MCC), a rare aggressive primary cutaneous neuroendocrine carcinoma (NEC), and cutaneous metastases of other NECs, particularly of pulmonary origin, is challenging on histologic grounds alone. This holds true even with the aid of widely used immunohistochemical studies, including CK20 and TTF1, as aberrant expression patterns (e.g., lack of CK20 expression in MCCs) often do arise. Herein, we evaluate the utility of SOX11 and PAX5 immunohistochemistry (IHC) as potential discriminatory markers for MCCs compared with their close histologic mimic, pulmonary small cell carcinomas (PSmCCs).

Design: Immunohistochemical studies with anti-SOX11, -PAX5, -CK20, and -TTF1 were performed on selected cases of primary (n = 31) and metastatic (n = 13) MCCs and primary (n = 16) and metastatic (n = 6) PSmCCs, respectively. The pattern, intensity and proportion of IHC expression for each antibody among the four groups were evaluated and compared using Fisher's exact test.

Results: The IHC expression pattern, intensity and proportion by group type and polyomavirus status are summarized in Table 1. Overall, when compared to those in PSmCCs, the expression of both SOX11 and CK20 (Fig. 1B-C) in MCCs was predominantly diffuse ($p < 0.001$) and strong in intensity ($p < 0.001$). PAX5 expression (Fig. 1D) tended to be more diffuse in MCCs than in PSmCCs ($p = 0.003$); however, there was no statistically significant difference in intensity of PAX5 expression. TTF1 expression was predominantly diffuse ($p < 0.001$) and strong in intensity ($p < 0.001$) in PSmCCs when compared to that of MCCs, although a subset (9%, 2/22) of PSmCCs lacked TTF1 immunoreactivity. Additionally, the presence of SOX11 expression in at least 25% of tumor cells (≥ 3), with an at least moderate (≥ 2) intensity, favored the diagnosis of MCCs over PSmCCs ($p < 0.001$) in our cohort. Moreover, when SOX11 expression was present, the presence of CK20 expression, regardless of its intensity and proportion, and the lack of TTF1 immunoreactivity in the tumor cells invariably supported the diagnosis of MCCs.

Table 1: The expression intensity, proportion, and pattern of SOX11, PAX5, CK20, and TTF1 in MCCs and PSmCCs

IHC Type	Pattern*	Primary MCC	Primary PSmCC	*p*-value	Pattern*	Combined MCC	Combined PSmCC	*p*-value	Pattern*	Polyoma-virus Status#: ABSENT (n=10) n (%)	Polyoma-virus Status#: PRESENT (n=31) n (%)	*p*-value
SOX11	0	0	4(25)	0.01	0	0	6(27)	<0.001	0	0	0	n/a
	1	0	0		1	0	0		1	0	0	
	2	31 (100)	12(75)		2	44(100)	16(73)		2	10(100)	31(100)	
	3	0	0		3	0	0		3	0	0	
PAX5	0	16(52)	12(75)	0.21	0	21(48)	17(77)	0.034	0	7(70)	11(35)	0.08
	1	0	0		1	0	0		1	0	0	
	2	15(48)	4(25)		2	23(52)	5(23)		2	3(30)	20(65)	
	3	0	0		3	0	0		3	0	0	
CK20	0	3(10)	16(100)	<0.001	0	5(11)	22(100)	<0.001	0	0	4(13)	0.81
	1	26(84)	0		1	34(77)	0		1	9(90)	23(74)	
	2	0	0		2	0	0		2	0	0	
	3	2(6)	0		3	5(11)	0		3	1(10)	4(13)	
TTF1	0	31(100)	2(13)	<0.001	0	43(98)	2(9)	<0.001	0	9(90)	31(100)	0.24
	1	0	0		1	0	0		1	0	0	
	2	0	14(88)		2	1(2)	20(91)		2	1(10)	0	
	3	0	0		3	0	0		3	0	0	
IHC Type	**Intensity***	**Primary MCC (n=31) n (%)**	**Primary PSmCC (n=16) n (%)**	***p*-value**	**Intensity***	**Combined MCC (n=44) n (%)**	**Combined PSmCC (n=22) n (%)**	***p*-value**	**Intensity***	**Polyoma-virus Status#: ABSENT (n=10) n (%)**	**Polyoma-virus Status#: PRESENT (n=31) n (%)**	***p*-value**
SOX11	0	0	4(25)	<0.001	0	0	6(27)	<0.001	0	0	0	0.14
	1	0	7(44)		1	0	7(23)		1	0	0	
	2	9(29)	5(31)		2	9(20)	8(36)		2	3(30)	3(10)	
	3	22(71)	0		3	35(80)	1(5)		3	7(70)	28(90)	
PAX 5	0	16(52)	12(75)	0.18	0	21(48)	17(77)	0.09	0	7(70)	11(35)	0.17
	1	10(32)	4(25)		1	0	0		1	2(20)	15(48)	
	2	5(16)	0		2	23(52)	5(23)		2	1(10)	5(16)	
	3	0	0		3	0	0		3	0	0	
CK20	0	3(10)	16(100)	<0.001	0	5(11)	22(100)	<0.001	0	0	4(13)	<0.001
	1	1(3)	0		1	1(2)	0		1	1(10)	0	
	2	13(42)	0		2	16(36)	0		2	8(80)	6(19)	
	3	14(45)	0		3	22(50)	0		3	1(10)	21(68)	
TTF-1	0	31(100)	2(13)	<0.001	0	43(8)	2(9)	<0.001	0	9(90)	31(100)	0.24
	1	0	2(13)		1	0	2(9)		1	0	0	
	2	0	3(19)		2	0	5(23)		2	1(10)	0	
	3	0	9(56)		3	1(2)	13(59)		3	0	0	
IHC Type	**Proportion#**	**Primary MCC**	**Primary PSmCC**	***p*-value**	**Proportion#**	**Combined MCC**	**Combined PSmCC**	***p*-value**	**Proportion#**	**Polyoma-virus Status#: ABSENT (n=10) n (%)**	**Polyoma-virus Status#: PRESENT (n=31) n (%)**	***p*-value**
SOX11	0	0	4(25)	<0.001	0	0	6(27)	<0.001	0	0	0	n/a
	1	0	1(6)		1	0	1(5)		1	0	0	
	2	0	3(19)		2	0	3(14)		2	0	0	
	3	1(3)	4(25)		3	1(2)	6(27)		3	0	0	
	4	30(97)	4(25)		4	43(98)	6(27)		4	10(100)	31(100)	
PAX 5	0	16(52)	12(75)	0.026	0	21(48)	17(77)	0.003	0	7(70)	11(35)	0.23
	1	0	1(6)		1	0	1(5)		1	0	0	
	2	0	1(6)		2	0	1(5)		2	0	0	
	3	9(29)	2(13)		3	13(30)	3(14)		3	2(20)	11(35)	
	4	6(19)	0		4	10(23)	0		4	1(10)	9(29)	
CK20	0	3(10)	16(100)	<0.001	0	5(11)	22(100)	<0.001	0	0	4(13)	0.006
	1	2(6)	0		1	3(7)	0		1	2(20)	0	
	2	3(10)	0		2	3(7)	0		2	2(20)	0	
	3	10(32)	0		3	11(25)	0		3	3(30)	8(26)	
	4	13(42)	0		4	22(50)	0		4	3(30)	19(61)	
TTF-1	0	31(100)	2(13)	<0.001	0	43(98)	2(9)	<0.001	0	9(90)	31(100)	0.24
	1	0	1(6)		1	1(2)	1(5)		1	1(10)	0	
	2	0	1(6)		2	0	1(5)		2	0	0	
	3	0	3(19)		3	0	3(14)		3	0	0	
	4	0	9(56)		4	0	15(68)		4	0	0	

*Intensity: 0 = none; 1= weak; 2=moderate; 3 =strong
#Proportion: 0=none; 1= 1-5% ; 2 = 6-25% ; 3 = 26-75%; 4= 76-100%
^Pattern: 0 = none; 1= perinuclear dot-like; 2 = nuclear; 3 = membranous and focal perinuclear dot-like
+Documented Polyomavirus Status in all MCC patients

Figure 1 - 337

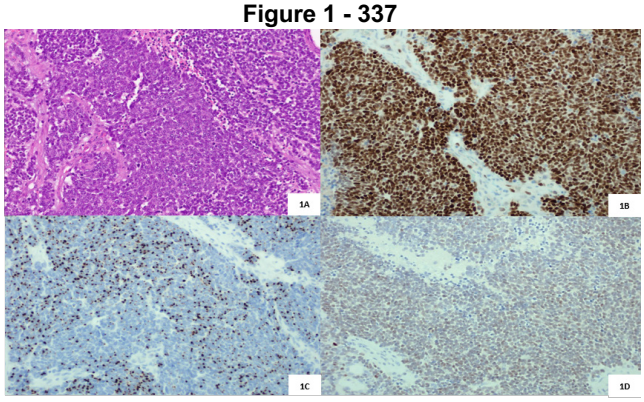

Figure 1. Representative figure showing MCC: 1A (H&E, x100) and 1B-1D (IHC, x100): SOX11 (B), CK20 (C, perinuclear dot like) and PAX5 (D)

Conclusions: Our results indicate that SOX11 is a powerful discriminatory marker for MCCs, especially when used in conjunction with other conventional IHC markers like CK20 and TTF1. We believe this combinatorial panel of IHCs will serve as an additional armamentarium for pathologists that helps distinguish MCCs from PSmCCs in difficult cases.

338 Cutaneous Syncytial Myoepithelioma: Multi-Institutional Study of Seven Cases with Keys to Recognition from Histologic Mimics

Sintawat Wangsiricharoen[1], Jorge Torres-Mora[2], Daniel Anderson[3], John Gross[4]
[1]Johns Hopkins University School of Medicine, Baltimore, MD, [2]Mayo Clinic, Rochester, MN, [3]United Hospital Center, Bridgeport, WV, [4]The Johns Hopkins Medical Institution, Baltimore, MD

Disclosures: Sintawat Wangsiricharoen: None; Jorge Torres-Mora: None; Daniel Anderson: None; John Gross: None

Background: Cutaneous syncytial myoepithelioma (CSM) is a recently described and underrecognized myoepithelioma variant which poses significant diagnostic challenges mimicking various carcinomas as well as melanocytic and other mesenchymal neoplasms, respectively.

Design: We retrieved cases from our institutional and consultation archives coded as myoepithelioma from 2000 to 2021 and retrospectively reviewed for the CSM variant.

Results: We identified 7 cases of the CSM variant. Our study cohort included 3 men and 4 women in patients ranging from 13 to 68 years of age (median: 17 years). Sites included toe (2), foot (1), knee (1), thigh (1), wrist (1), and shoulder (1), with tumor sizes varying from 0.4 cm to 0.9 cm (median: 0.6 cm). Histologically, CSM consists of a relatively well-demarcated (Fig 1A) solid sheet of spindled, ovoid to histiocytoid cells with fine chromatin and small nucleoli growing in a syncytial pattern with variably prominent lymphoplasmacytic inflammation which is most pronounced in a perivascular distribution (7/7) (Fig 1B). A subset showed adipocytic metaplasia (1/7) (Fig 1C). Mitotic activity was low and ranged from 0 to 1 per 10 HPF; 5/7 cases showed no mitotic activity. Cytologic atypia was minimal to absent in 6 cases with one case showing focal mild to moderate nuclear atypia (Fig 1D). All tumors were positive for EMA (5/5), S100 (diffuse 6/7, focal 1/7), SMA (diffuse 6/7, rare 1/7), and p63 (rare 1/1). While all cases were positive for EMA, most were negative for pancytokeratin (6/7, rare 1/7). All cases were negative for CD34 (0/4), desmin (0/5), and SOX10 (0/5). INI1 expression was retained in all cases (4/4). Six of seven cases (6/7) had genetic analysis; all cases tested showed *EWSR1* rearrangements (6/6); 5 cases showed *EWSR1-PBX3* fusions. Follow-up information was available for 3 patients (mean follow-up: 21 months) and all were without evidence of disease.

Case #	Age (years)	Sex	Site	Perivascular lymphoplasmacytic infiltrate	Cytologic atypia	Mitotic activity	EMA	S100	SMA	Pankeratin	CD34	Desmin	SOX10	INI1	p63	Molecular findings
1	16	M	Shoulder	Present	Absent	Absent	Pos	Pos	Pos	Neg	Neg	Neg	N/A	Retained	N/A	N/A
2	17	M	Toe	Present	Absent	Absent	Pos	Pos	Pos	Neg	N/A	N/A	N/A	Retained	N/A	FISH: *EWSR1* rearrangement
3	35	F	Toe	Present	Mild to moderate	1/10 HPF	Pos	Pos	Rare	Rare	N/A	Neg	Neg	N/A	Rare	Fusion panel: *EWSR1-PBX3* fusion
4	15	F	Foot	Present	Absent	Absent	N/A	Pos	Pos	Neg	Neg	Neg	Neg	Retained	N/A	Fusion panel: *EWSR1-PBX3* fusion
5	68	F	Knee	Present	Absent	Absent	Pos	Pos	Pos	Neg	Neg	N/A	Neg	N/A	N/A	Fusion panel: *EWSR1-PBX3* fusion
6	44	F	Wrist	Present	Absent	Absent	N/A	Pos (focal)	Pos	Neg	N/A	Neg	Neg	N/A	N/A	Fusion panel: *EWSR1-PBX3* fusion
7	13	M	Thigh	Present	Absent	1/10 HPF	Pos	Pos	Pos	Neg	Neg	Neg	Neg	Retained	N/A	Fusion panel: *EWSR1-PBX3* fusion

N/A, not available

Figure 1 - 338

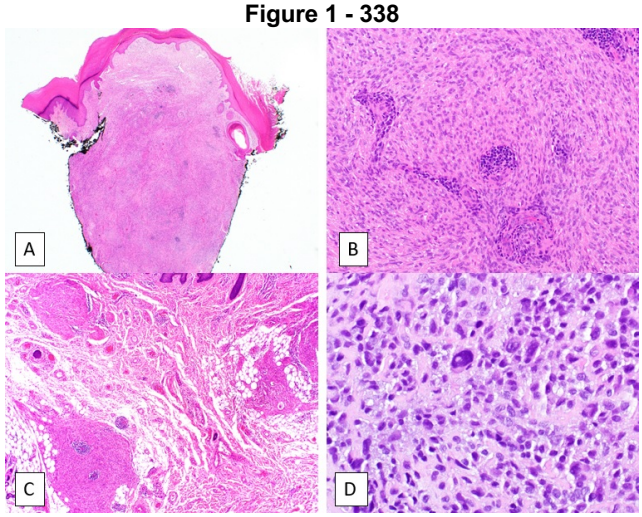

Conclusions: CSM is a rare but distinctive variant of myoepithelioma often mimicking other mesenchymal and non-mesenchymal neoplasms. An important diagnosis clue in CSM is the unique perivascular lymphoplasmacytic infiltrate. Increased pathologist awareness of the unique morphologic features of CSM and judicious application of a broad panel of immunohistochemistry to include EMA, SMA, and S100 and, when appropriate, molecular genetics should lead to the correct diagnosis in nearly all cases. Proper recognition of this variant is important as CSM tends to behave in a relatively benign/indolent fashion.

339 Non-Langerhans Cell Histiocytosis: Comprehensive Genomic Profiling Reveals Novel and Potentially Actionable FLT3 Gene Fusions

Erik Williams[1], Douglas Mata[2], Dean Pavlick[2], Helena Crowley[3], Julie Tse[4]
[1]University of California San Francisco, San Francisco, CA, [2]Foundation Medicine, Inc., Cambridge, MA, [3]University of Maryland Medical Center, Baltimore, MD, [4]Foundation Medicine, Inc., Boston, MA

Disclosures: Erik Williams: *Employee*, Foundation Medicine, Inc.; *Employee*, Foundation Medicine, Inc.; Douglas Mata: *Employee*, Foundation Medicine, Inc.; *Speaker*, Astellas Pharma, Inc.; Dean Pavlick: *Employee*, Foundation Medicine; *Stock Ownership*, Roche; Helena Crowley: None; Julie Tse: *Employee*, Foundation Medicine, Inc.

Background: Non-Langerhans cell histiocytoses (non-LCH) represent a family of a neoplasms that may be histopathologically indistinguishable. Patients may require systemic therapy in the setting of invasive or recurrent disease not amenable to surgery alone, validating the search for actionable molecular targets. Activating mutations in diverse kinase genes with clinical responses to targeted molecular therapy have previously been reported in non-LCH. Given this exciting precedent, we examined the genomic landscape of non-LCH to identify previously unreported molecular targets.

Design: Our archive of 93 cases, including 39 Rosai-Dorfman disease (RDD), 24 non-LCH not otherwise specified, 16 Erdheim-Chester disease (ECD), 7 juvenile xanthogranuloma (JXG), 4 ALK-positive histiocytosis, 2 xanthoma disseminatum, and 1 progressive mucinous histiocytosis, underwent hybrid-capture-based DNA and RNA sequencing during routine clinical care. Disease classifications were based on the diagnoses submitted by the clinician, pathology reports, and histology.

Results: The median age was 48 years (range: <1y - 74y) and 56% were female. Overall, 65 cases exhibited pathogenic alterations in previously reported genes,
including *BRAF* (n=20), *KRAS* (n=16), *MAP2K1* (n=11), *ALK* (n=6), *NRAS* (n=6), *CSF1R* (n=2), *NF1* (n=2), *FGFR1* (n=1), *MAP2K2* (n=1), *NTRK1* (n=1), *PTPN11* (n=2), and *RAF1* (n=1). Some cases harbored more than one pathogenic alteration in these genes. Of the remaining cases, three exhibited novel *FLT3* fusions with preserved kinase domains. *FLT3* fusion cases occurred at skin and subcutaneous sites in a wide range of ages (< 1y to 30 y) and had similar histology: sheets of cells with uniformly sized round-to-oval nuclei and vacuolated-to-foamy cytoplasm, with occasional Touton giant cells. Immunohistochemistry was typical for non-LCH such as JXG and ECD, except the cases had variable S100 positivity, raising the possibility of RDD.

Conclusions: We identified novel fusions in *FLT3* tyrosine kinase in a subset of non-LCH that were wildtype for previously reported alterations. Given that activating *FLT3* fusions have been identified in myeloid and lymphoid neoplasms with

eosinophilia and *in vitro* studies have shown responses to targeted inhibition, our findings offer exciting insight into a potential novel molecular therapy for aggressive non-LCH.

340 Deep Learning-Based Discrimination of Benign Naevi and Melanoma from Pigmented Lesions

Yufei Zhou[1], Ian Katz[2], Anant Madabhushi[1]
[1]*Case Western Reserve University, Cleveland, OH,* [2]*Southern Sun Pathology, Westmead, Australia*

Disclosures: Yufei Zhou: None; Ian Katz: None; Anant Madabhushi: None

Background: Melanoma (MEL) is the most lethal form of all skin cancers; however, early diagnosis and distinction from benign naevi (BN) and treatment lead to a five-year survival rate of > 99%. An automated approach to identify MEL from BN may assist pathologists' diagnostic speed and potentially accuracy. Herein, we present a deep learning-based (DL) approach employing a deep neural network for the automated discrimination of MEL from BN.

Design: A cohort of 77 patients was curated for the study comprising 99 digitized H&E stained WSIs at 20x magnification. Fifty patients had MEL (including invasive and in situ), and 37 patients had BN in which all cases were evaluated by a single experienced dermatopathologist. The occurrence of MEL and BN in the specimens were not mutually exclusive – there was BN observed in 10 MEL cases. 5185 ROIs identified by the pathologist were extracted from the WSIs. We used HistoQC (Janowczyk et al, 2019) to remove regions with artifacts (e.g. understaining, pen-markings, etc). Patients were randomly split into training and testing sets at a ratio of 4:1. A total of 61,119 non-overlapping tiles (40,205 in the training set and 20,914 in the testing set) of size 256x256 pixels were extracted from all ROIs in the cohort. **Table 1** describes the detailed composition of lesions in the training and testing tile data. The tiles were used to train and test the ResNet-50 model (He et al., 2015) to distinguish MEL from BN. We trained the ResNet-50 model for 250 epochs with a learning rate of 0.0001 and the ADAM optimizer (Kingma et al, 2014). The model was employed to predict the probability of a tile being malignant. The heat map of the tile-level probability was overlaid on the ROIs for visualization of the localization of melanoma as predicted by the network.

Results: The areas under the receiver operating characteristic curve (AUC) obtained from the ResNet-50 model were 0.995 and 0.901 for the training (S_t) and testing (S_v) sets, respectively. We further elaborated the prediction performance of each class (MEL or BN) in S_v in the confusion matrix in **Fig. 1** and the heat map in **Fig. 2**. A tile was predicted as MEL if the output probability score obtained by the ResNet-50 model was greater than 0.5.

Table 1. Composition of tiles in S_t and S_v. 23,730 (59%) are MEL and 16475 (41%) are BN of 40,205 S_t tiles. The 20,914 tiles from S_v are comprised of 18,848 (90%) MEL tiles and 2,066 (10%) BN tiles.

Tile Composition	MEL	BN
Training	23,730	16,475
Testing	18,848	2,066

Figure 1 - 340

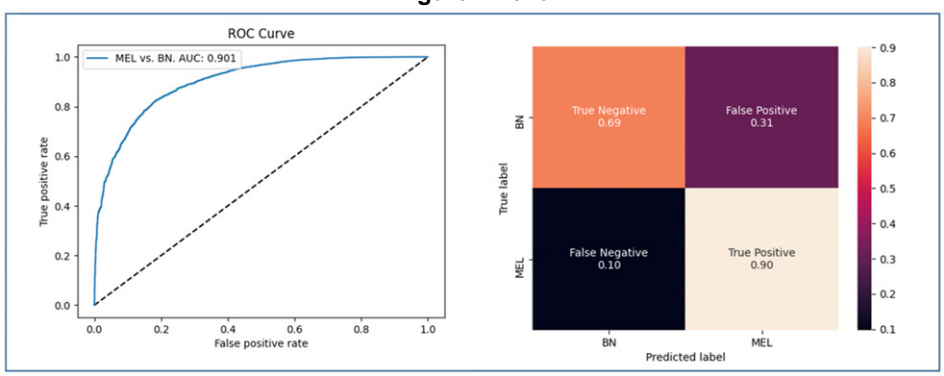

Fig. 1. The numerical analysis results for S_v. The confusion matrix indicates that while the model has a higher false-positive rate in identifying BN, the model performs well in capturing malignant regions from the input specimens.

Figure 2 – 340

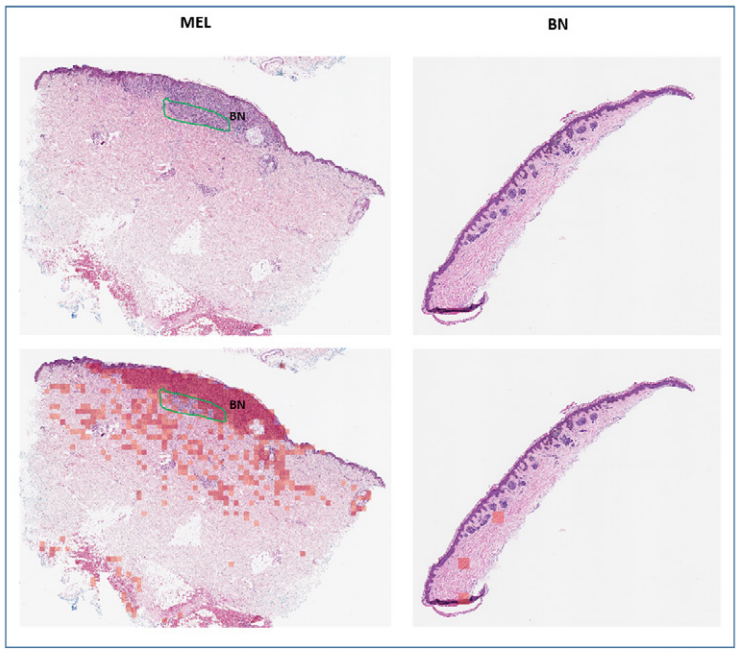

Fig. 2. The heat maps of malignant regions on the WSIs. The heatmap map overlaid on ROIs highlighting locations where the DL model predicts regions as MEL. Red color over a block of tile demarks the probability of that tile containing MEL. The green line highlights a BN area adjacent to the MEL, a region that the model was able to successfully distinguish from MEL regions.

Conclusions: The experiments suggest that our DL model is capable of distinguishing MEL from BN. Further independent multi-site validation is warranted.